The Use of Radionuclides to Identify Vulnerable Fractured and Karst Bedrock Aquifers in Eastern Ontario

Alex Harrison

Thesis submitted to the University of Ottawa in partial fulfillment of the requirements for the degree of Master of Science in Earth Sciences

Department of Earth Sciences
Faculty of Science
University of Ottawa

© Alex Harrison, Ottawa, Canada, 2023

Abstract

Domestic water wells in Eastern Ontario were identified in potentially vulnerable fractured and karst bedrock aquifers using geologic and geochemical data. A novel methodology is presented that evaluates ^{137}Cs and $^{210}Pb_{Ex}$ as local indicators of groundwater vulnerability. The method is designed to determine the vulnerability of a specific well. Suspended sediment samples and well-bottom sediment samples were collected from both potentially vulnerable and non-vulnerable wells. Surface soil samples were also collected from West Rural Ottawa and the Township of Alfred & Plantagenet in Ontario, Canada. Gamma spectroscopy was used to analyze the samples and quantify the presence of the radionuclides in cps and cps/g. The spectral data indicate no significant difference in the activities of $^{210}Pb_{Ex}$ among samples, but a significant difference in the activities of ^{137}Cs was observed between surface soil samples and well-bottom sediment samples collected from vulnerable wells. The data suggest that $^{210}Pb_{Ex}$ does not act as a good indicator of vulnerable aquifers because of its geogenic origin. The anthropogenic origin of ^{137}Cs precludes this issue, and while ^{137}Cs was detected in measurable quantities at the surface, its use as an indicator of vulnerable aquifers is limited by hydrologic and geologic controls that prevent infiltration in vulnerable terrains.

Acknowledgements

I would like to thank my supervisors. Tom Al, your scientific rigour and attention to detail have been invaluable throughout this project and instrumental in my growth as a scientist. Your knowledge and experience have compelled me to become a better problem solver and raised the standard to which I hold myself. Stew Hamilton, your passion for and expertise in groundwater and geochemistry is astounding and inspiring. Thank you for sharing what I can imagine is only a fraction of your knowledge through all of your thoughtful contributions.

I am most appreciative of the organizations that have supported this project. Financial support, field training, and resources were provided by the Ontario Geological Survey, the Eastern Ontario Water Resources Program, and the City of Ottawa. In particular, I would like to extend an enormous thank you to Tessa Di Iorio for her dedication to the project and her ongoing and unwavering encouragement of my work. Thank you also to Angie Bischoff, Kevin Mackey, and Colin Matassa for comprising the better portion of the best field team I could be a part of. I would also like to thank other City of Ottawa staff and members of the Eastern Ontario Geoscience Consortium Group that collaborated on this project and nourished my interest in hydrogeology: Michel Kearny, Sharon Lee, Claire Milloy, and Mike Ziebell.

I would like to thank the members of the uOttawa staff without whom this project would not have been possible. Thanks to Soroush Fard, Barbara Francisco, Alain Mauviel, and Ian Nandram for your insight, patience, and accommodation during my laboratory work. Thanks also to Magda Celejewski and Kirsten Smythe for your continual willingness and ability to help me in any capacity that you could.

I would also like to thank all of the volunteers who welcomed us into their homes for the 2019 West Ottawa Groundwater Study and follow-up testing. Your kindness and enthusiasm have driven this project from the beginning and continue to motivate my future endeavours.

Finally, I am extremely thankful to my family and friends for your relentless encouragement throughout this project. Your unconditional belief in me is what assured me to carry on, even in the face of what seemed insurmountable. Words cannot express my gratitude.

Forward ever.

Project Partnerships

The field work related to this thesis was conducted as part of provincial and municipal groundwater sampling programs. The Ontario Ambient Groundwater Geochemistry Program (OAGGP) is funded by the OGS and directed by Dr. Stewart Hamilton, with the objective to use water samples from domestic wells to characterize and map the natural geochemistry of groundwater throughout the province of Ontario. The Aquifer Capability Screening Tool is funded by the City of Ottawa and directed by Ms. Tessa Di Iorio, with the objective to characterize groundwater quality for resource use and protection.

Table of Contents

List of Figures

List of Tables

List of Appendices

1. Introduction

The protection of groundwater resources to ensure access to clean drinking water is paramount for all communities. In Canada, approximately 30% of the population is reliant on groundwater as the sole source of potable water (Environment Canada, 2013). However, a wide range of human activities including agriculture, industry, and land development put groundwater at risk. Protection of groundwater resources is particularly challenging in rural areas where residents depend on domestic wells, that are not subject to the same regulations regarding water testing and quality standards that municipal systems are. These unregulated private water systems can unknowingly become compromised when harmful pathogens and contaminants are introduced into the groundwater.

Groundwater in karst and fractured bedrock aquifers is particularly vulnerable to contamination. In these environments there may be high permeability connections between the surface and the sub-surface that can facilitate rapid recharge and infiltration. The fractures, channels, and conduits that characterize these systems can quickly transport surface-sourced contaminants into the aquifers (Hamilton et al., 2017; Iqbal & Krothe, 1995). Overburden cover on bedrock can protect karst and fractured bedrock aquifers by removing or reducing the risk of contamination (Allen & Morrison, 1973; Conboy & Goss, 2000), so groundwater vulnerability is heightened in areas of thin overburden cover. It is essential to identify hydrogeologically vulnerable aquifers in order to protect groundwater resources and reduce or mitigate the risk to human health.

Previous investigations have studied how vulnerable aquifers store and transmit water. Tracer tests are commonly used to gain understanding of the physical, chemical, and biological processes that control transport from a point of input to a point of output. Tracers can be artificially injected into an aquifer and may include dyes (Levison & Novakowski, 2012), salts (Goldscheider et al., 2008), or bacteriophages (Rossi et al., 1998) or tracers may naturally occur such as specific conductance (Ravbar et al., 2011), suspended sediment (Massei et al., 2002), or

stable water isotopes (Abbott et al., 2000). Artificial and natural tracers have also been used together to enhance physical characterization of groundwater systems (Auckenthaler et al., 2002; Einsiedl, 2005; Mudarra et al., 2014). Groundwater vulnerability models have been developed with Geographic Information Systems using spatial information to systematically quantify the intrinsic vulnerability of an aquifer. Groundwater vulnerability models such as DRASTIC (Aller et al., 1987) and GOD (Foster, 1987) use physical parameters to characterize the hydrogeological setting and to assess the vulnerability of an aquifer. These models have been expanded to account for the distinct hydrogeological behaviour and properties of karst aquifers in specific models such as EPIK (Doerfliger et al., 1999), PI (Goldscheider et al., 2000) and KAVI (van Beynen et al., 2012).

In the coming years, growing populations are likely to stress aquifers with mounting demands for withdrawals. Expanding human activity will also increase the risk of groundwater contamination. It is necessary to develop practical and reliable methods to characterize and understand the complexity of vulnerable environments (Levison & Novakowski, 2012) and guide decisions regarding development and land use (Foster et al., 2013), while maintaining safe drinking water supplies. It is particularly important to improve vulnerability assessment methods in fractured bedrock and karst aquifers because of the unique challenges that accompany the heterogeneity and anisotropy of these systems (Catani et al., 2020; Machiwal et al., 2018).

1.1 Background and Literature Review

1.1.1. Characterization of Fractured Bedrock and Karst Aquifers

Low permeability crystalline and sedimentary rocks are present on every continent and cover approximately 30 million km^2 of Earth's land-surface (Krásný & Sharp, 2007). In many of these hydrogeological environments, the rock matrix has insufficient connected primary porosity and hydraulic conductivity to allow for groundwater utilization (Gustafsson, 1994). However, substantial groundwater flow can occur in bedrock aquifers along secondary porosity features

that offer preferential flow paths (Sudicky & Frind, 1982). These features – including joints, fissures, shear zones, bedding planes, faults, and other discontinuities – occur at a variety of scales and herein are collectively referred to as fractures.

Early hydrogeological investigations revealed marked differences between porous and fractured media. Pirson (1953) addressed these differences by presenting the concept of two domains within fractured media – (1) intergranular porosity between mineral grains in the matrix blocks; and (2) relatively permeable fractures. In general, a porous medium that exhibits both domains is referred to as a dual-porosity or dual-permeability system (Krasny and Sharp, 2007). Depending upon the relative hydraulic properties of the matrix blocks and fractures, the medium can be further classified into one of four gradational categories (Figure 1-1).

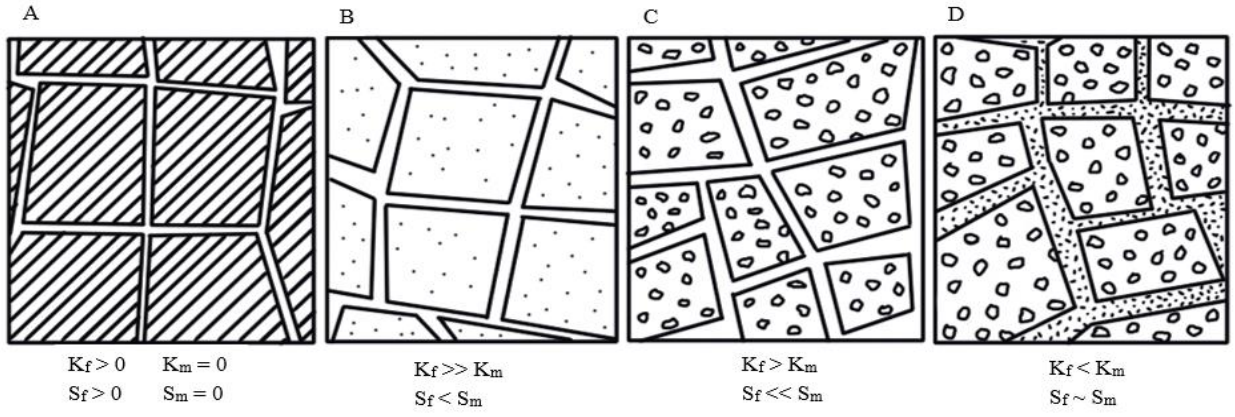

Figure 1-1. Gradational hydrogeological classification of fractured media (modified from Streltsova, 1976; Krasny & Sharp, 2007). (A) Purely fractured media; (B) Fractured media; (C) Doubly porous media; (D) Heterogeneous media. K_f and K_m are the hydraulic conductivities and S_f and S_m are the storativities of the fractures and matrix, respectively.

In purely fractured media the matrix has nearly negligible porosity and permeability, leaving hydraulic conductivity and fluid storage to occur almost completely in the fractures. In fractured media, the matrix is responsible for fluid storage, but again flow is dominant in the fractures. In a doubly porous media, the matrix permeability can be relatively similar to fracture permeability, but storage continues to occur predominantly in the matrix. Finally, formations

termed heterogeneous can occur in media where fractures become filled with material that has a different permeability than the matrix rock. This distributes fluid storage more evenly between the matrix and the fractures and restricts flow through the fractures, while promoting flow through the matrix. It is important to understand the specific conditions in a given aquifer, as variable hydraulic characteristics between matrix blocks and fractures affects transport properties.

In carbonate rocks, karst weathering features may develop where there is extensive chemical dissolution along secondary porosity features. The majority of karst aquifers form in soluble carbonate rocks such as limestone, composed primarily of the mineral calcite ($CaCO_3$), and dolostone, composed primarily of the mineral dolomite ($CaMg(CO_3)_2$) (Klimchouk et al., 2000). These carbonate rocks are exposed over approximately 10% of the ice-free continental regions on Earth and are believed to underly significantly more (Ford & Williams, 2007). As shown in equations 1 and 2 below, both calcite and dolomite undergo chemical dissolution in the presence of acidic water. In the natural carbonate geochemical system, these reactions are primarily driven by carbon dioxide (CO_2), which dissolves to form a weak acid that is introduced with meteoric water that percolates through the soil cover (Plummer et al., 1976).

(1) $$H_2O + CO_2 + CaCO_3 \longleftrightarrow Ca^{2+} + 2HCO_3^-$$

(2) $$2H_2O + 2CO_2 + CaMg(CO_3)_2 \longleftrightarrow Ca^{2+} + Mg^{2+} + 4HCO_3^-$$

As groundwater travels along preferential flow paths established by pre-existing secondary porosity features, the very act of flow causes progressive chemical dissolution and the enlargement of void space (Ford and Williams, 2007). This dissolution is the most important process in the development of a karst aquifer, as it creates an interconnected network of fractures through which groundwater flow can occur (Freeze & Cherry, 1979; Kresic, 2013). This network is closely tied to other karst features such as sinking streams, caves, springs, and sinkholes, creating a strong hydraulic connection between the surface and the sub-surface

(Vesper et al., 2013). As such, in addition to movement through fractures and matrix domains, conceptualizations of groundwater flow in karst aquifers must also consider flow through dissolution features. This distinction commonly results in karst aquifers being described as a triple permeability or triple porosity system (Singhal & Gupta, 2010; White, 2017).

The nature of fractured crystalline bedrock and karst aquifers yield highly complex heterogenous and anisotropic hydrogeological environments (Figure 1-2). In these aquifers, substantial groundwater movement can occur rapidly and over large distances because of high permeability preferential flow paths (Allen & Morrison, 1973; Personne et al., 1998). Transport times can vary dramatically based on flow conditions, as it is typical for peak flow velocities to be up to 100 times greater than base flow velocities (Vesper et al., 2013). Further, under a given set of flow conditions groundwater movement in the matrix blocks and fractures may occur independently, but under a separate set of conditions groundwater movement in the matrix blocks and fractures may be closely linked. This complexity can be especially problematic when a contaminant is introduced into the aquifer, as it may result in irregular and unpredictable distribution of the contaminant (Malard et al., 1994).

Extensive hydrogeological characterization of the abundance, development, and connectivity of fractures, channels, and conduits is needed to understand groundwater flow. This requires data collection related to individual fracture properties such as orientation, density, aperture (width), roughness, and length (Berkowitz, 2002; Singhal & Gupta, 2010). Moreover, at the scale of hydrogeologic interest, factors such as in situ fluid distribution, changing stress conditions, and geologic heterogeneity must also be considered in characterization (Neuman, 2005). However, the inaccessible nature of buried fractured and karst aquifers prevents this type of comprehensive analysis. Consequently, field techniques are typically developed to measure a response to the presence of fractures, instead of the physical aspects of the fractures themselves (Berkowitz, 2002). This can make it difficult to obtain accurate data, which may limit our ability to predict the occurrence and interconnectivity of fractures, and our understanding of flow within the fracture network.

(A)

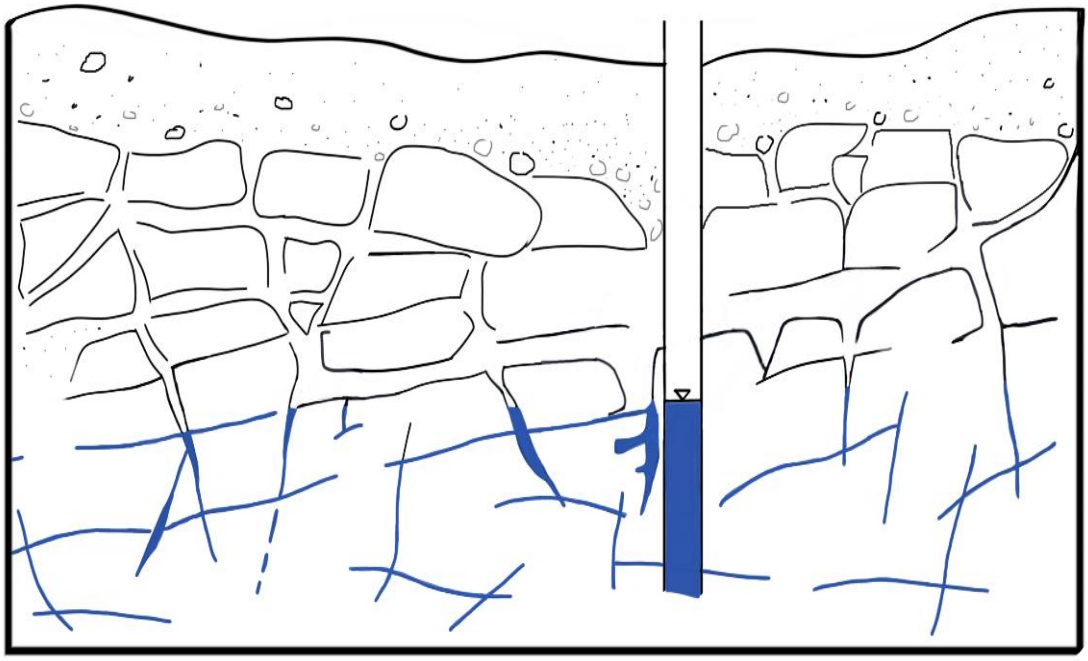

(B)

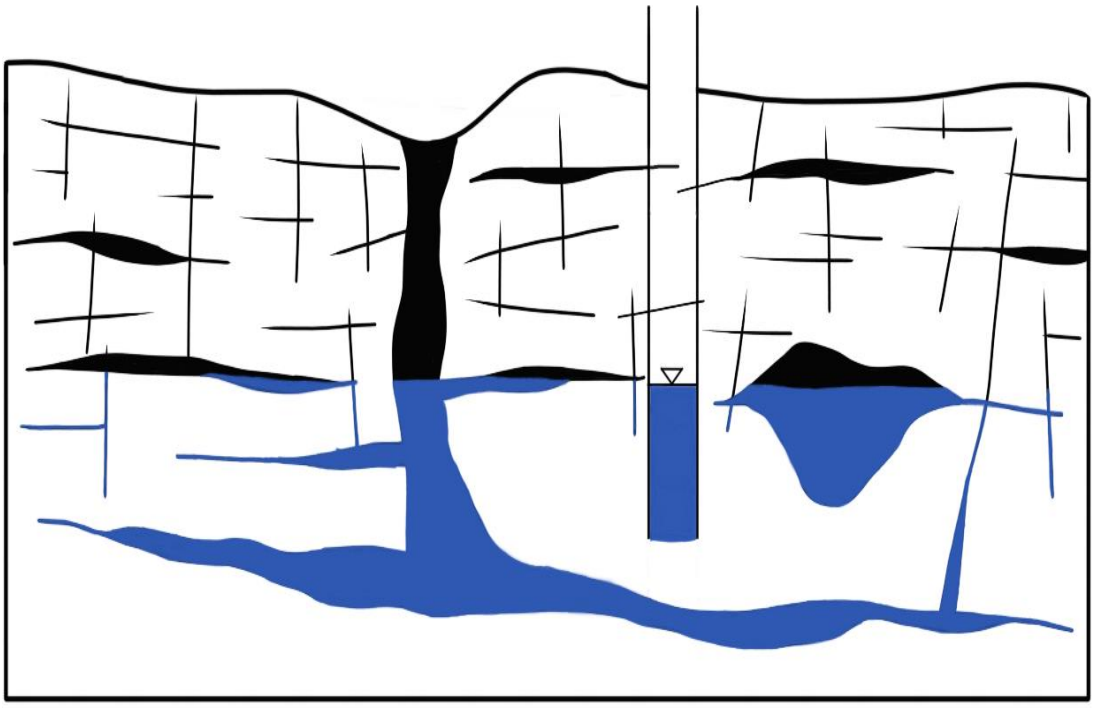

Figure 1-2. Conceptual diagrams depicting the high permeability connection between the surface and sub-surface in two aquifer systems. (A) A fractured bedrock aquifer. (B) A karst aquifer where the black infilled regions represent dissolution-enlarged secondary porosity features. Diagrams are not to scale.

It is thus well established that fractured crystalline bedrock and karst aquifers, particularly with thin overburden cover, are vulnerable to contamination (Ford & Williams, 2007; Lapcevic et al., 2017; Singhal & Gupta, 2010; Vesper et al., 2013; White, 2017). Additional and varied methodologies are necessary to aid in understanding the complexity that accompanies these systems and in determining the vulnerability of a specific well or aquifer.

1.1.2. Behaviour and Applications of ^{137}Cs and ^{210}Pb

The attenuation and transport of natural and anthropogenic radionuclides has been studied over the past 50 years following an increase in global nuclear activity. In particular, the particulate-reactive radionuclides ^{137}Cs and ^{210}Pb have been used extensively in tracer studies concerned with the deposition, erosion, and transport of soil particles in the unsaturated zone (Davis et al., 1984; Mizugaki et al., 2006; Putyrskaya et al., 2020; Wallbrink & Murray, 1993; Walling & He, 1999; Y. Zhang et al., 2014). Other research focuses on ^{137}Cs and ^{210}Pb as environmental contaminants and examines their fate and transport in saturated media (Ohtsuka et al., 1988; Sidle, 2009; Turner et al., 2006).

Cesium-137 is a relatively long-lived anthropogenic radioisotope with a half-life of 30.17 years. It was produced primarily as a result of thermonuclear weapons testing, from the 1950s to the 1970s, that released plumes of radioactive debris into the lower stratosphere (Kiss et al., 1988; Yan et al., 2012). Atmospheric currents facilitated widespread global circulation of ^{137}Cs, though this dispersion remained largely confined to the latitude belt of the test site (Di Stefano et al., 2019). More recently, ^{137}Cs has been released into the atmosphere as a result of the nuclear accidents at Chernobyl (1986) and Fukushima (2011). However, the low altitude of the emission plumes has restricted the impact of these events to a local scale (Di Stefano et al., 2019; Ritchie & McHenry, 1990). In all cases, the movement of ^{137}Cs from the atmosphere to the ground surface (i.e., fallout) occurs largely with precipitation (Davis et al., 1963; Kiss et al., 1988; Yan et al., 2012). Yearly fallout records indicate a distinct maximum deposition peak in 1963, prior to the Test Ban Treaty, with generally decreasing fallout rates thereafter (Hirose et al., 2008; Ritchie & McHenry, 1990).

Lead-210 is a naturally occurring radioisotope that also has a relatively long half-life of 22.6 years. It is one of the radioactive daughter nuclides of the ^{238}U decay series and is derived from the decay of ^{226}Ra, via ^{222}Rn, and a series of short-lived nuclides (Figure 1-3). Radium-226 is found ubiquitously in soils and rocks and acts as a source for the continuous production of ^{210}Pb (Walling and He, 1999; Sidle, 2009). The ^{210}Pb that is generated in situ by the decay of ^{226}Ra is called supported ^{210}Pb and is in equilibrium with the parent ^{226}Ra (Figure 1-4). However, ^{222}Rn can outgas to the atmosphere from soils and rocks where it decays to ^{210}Pb that then adsorbs onto aerosols and is returned to Earth's surface with precipitation as fallout ^{210}Pb (Lewis, 1977; Wallbrink & Murray, 1993; Y. Zhang et al., 2014). This is referred to as unsupported or excess ^{210}Pb and it is not in equilibrium with the parent ^{226}Ra (Figure 1-4).

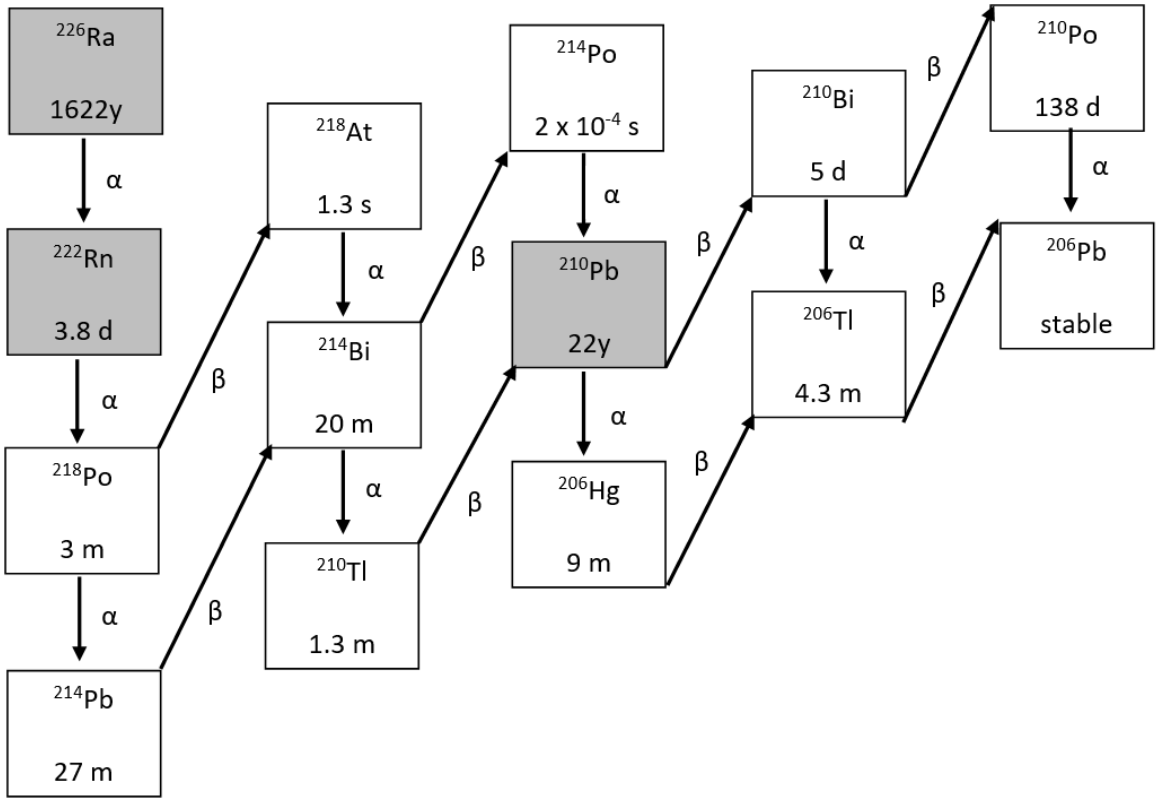

Figure 1-3. Portion of the ^{238}U decay series with various radioactive decay modes and nuclide half-lives. The ^{226}Ra, ^{222}Rn, and ^{210}Pb isotopes are highlighted (modified from Sidle, 2009).

Once in contact with soil at the surface, both ^{210}Pb and ^{137}Cs adsorb strongly and rapidly to cation exchange sites on clay minerals and organic material (Sankar et al., 2018; Sidle, 2009; Spezzano et al., 1994). It is generally accepted that this tendency renders both nuclides essentially non-exchangeable and immobile (Kiss et al., 1988; Ritchie et al., 1973; Zapata & Nguyen, 2009). As such, loss by biological uptake or natural chemical processes can be assumed to be negligible (Dalham et al., 1975; Karamanos et al., 1975; Ritchie & McHenry, 1990). This behaviour also limits downward infiltration into the soil profile, which results in an exponential decrease in concentration with depth. It has been shown that ^{137}Cs remains concentrated in the upper 5cm to 10cm of the soil profile, even decades after initial deposition (Koarashi et al., 2019; Ritchie et al., 1973). Similarly, it has been shown that ^{210}Pb tends to accumulate in the upper organic-rich fraction of the soil profile (Benninger et al., 1975; Zapata & Nguyen, 2009). Long-term mobility of both ^{137}Cs and ^{210}Pb within the environment is therefore predominantly associated with physical redistribution of soil particles (Kiss et al., 1988; Walling and He, 1999; Sankar et al., 2018).

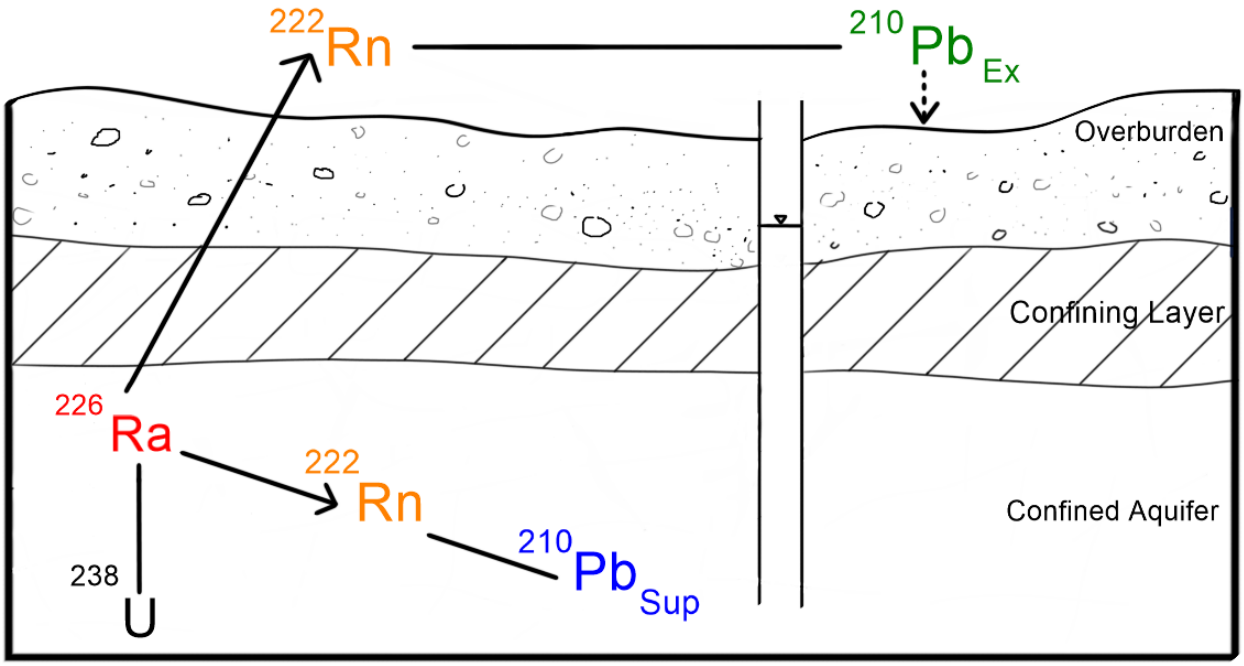

Figure 1-4. Representation of ^{226}Ra decay to supported ($^{210}Pb_{Sup}$) or excess ($^{210}Pb_{Ex}$) ^{210}Pb.

Early transport models assumed that because of the strong tendency for particulate-reactive radionuclides like ^{137}Cs and ^{210}Pb to adsorb to mineral surfaces, they were essentially immobile (Buddemeier & Hunt, 1988). However, testing at contaminated sites indicated that these radionuclides tend to be associated with the mobile colloidal and particulate fractions of groundwater (Flury et al., 2002; Kersting et al., 1999; Penrose et al., 1990). Field and laboratory evidence suggests that strongly adsorbed radionuclides can be transported by fine particulates (Grolimund et al., 1996; Saiers & Hornberger, 1996; Vilks & Baik, 2001), as they are generally smaller than pores in permeable and fractured media. A majority of these studies focus on migration in saturated porous media, largely in the context of radioactive waste management and groundwater contamination.

Research related to particulate-facilitated transport of radionuclides in fractured media is far less extensive and conclusive (W. Zhang et al., 2012). In particular, the irreversibility of radionuclide sorption (Rumynin & Nikulenkov, 2016; Tran et al., 2018) and the main mechanisms of transport (Froidevaux et al., 2010; W. Zhang et al., 2012) remain uncertain. These unknowns are both discussed by (Smith & Degueldre, 1993) in their presentation of two transport models specific to radionuclide transport at the high-level waste repository in the crystalline basement of northern Switzerland. More recently, Tang and Weisbrod (2010) presented the reversibility of radionuclide adsorption and variable means of transport in their comparison of cesium and lead transport in a natural chalk fracture. Most notably, Sidle (2009) proposed that high hydraulically conductive units transporting clay and colloid sized particles with adsorbed radionuclides may be responsible for the elevated concentrations of ^{137}Cs and excess ^{10}Pb in the shallow groundwater wells in the Shaker Valley Catchment, Maine, USA. These findings are particularly relevant to the present investigation as Sidle (2009) suggests that rapid colloidal transport and fracture flow may facilitate the accumulation of ^{137}Cs and excess ^{210}Pb at depth in media with high hydraulic conductivity.

1.2. Hypothesis and Research Objectives

It is proposed that elevated levels of ^{137}Cs and ^{210}Pb will occur in surface soils and consequently will be detected at elevated levels in sediment-laden samples taken from vulnerable wells. In contrast, it is proposed that ^{137}Cs and ^{210}Pb will be detected at very low levels in sediment-laden samples taken from non-vulnerable wells.

The primary objective of this research was to develop a novel geochemical method using ^{137}Cs and excess ^{210}Pb to assess aquifer vulnerability in fractured bedrock and karst geologic settings. The approach was to:

1) characterize the distribution of known parameters of hydrogeological vulnerability in the study areas to identify potentially vulnerable and non-vulnerable locations
2) determine if a qualitative difference could be identified between the radionuclide indicators in potentially vulnerable and non-vulnerable locations, and
3) determine if a quantitative difference could be measured between the radionuclide indicators in potentially vulnerable and non-vulnerable locations

1.3. Study Areas

This research was conducted in two regions of southeastern Ontario. The first of these areas, the Township of Alfred and Plantagenet, is located 60km to the east of the City of Ottawa along the southern shore of the Ottawa River. The second area, West Rural Ottawa, extends from the City's western most limit to the urban serviced boundary in the east (Figure 1-5). The West Rural Ottawa study area is bounded in the north by the Ottawa River and the southern boundary was determined by practical financial and time constraints on the sampling activities for the 2019 West Ottawa Groundwater Study. Within the study areas, villages are primarily serviced by water treatment plants pumping water from the Ottawa River. Outside of serviced zones, homeowners rely on private water wells for potable water.

Both areas are located in a mixed wood plains ecozone with cold winters and warm summers. The coldest month is January and the warmest month is July, with average temperatures of -10.2°C and 21.2°C, respectively (Environment Canada, 2021). Data collected from the Ottawa weather station from 1981 to 2010 indicates that annual precipitation averaged 919.5mm/yr. Approximately 19% of this precipitation fell as snow and 81% fell as rain (Environment Canada, 2021). The majority of groundwater recharge in southeastern Ontario occurs from mid-March to early May as the snowpack melts, temperatures rise, evapotranspiration is low, and soil moisture is close to saturation (Armstrong & Dodge, 2007; Singer et al., 2003). It is estimated by Natural Resources Canada that in the Ottawa area only 10% of the precipitation that falls infiltrates into the ground, with the balance lost to evapotranspiration or runoff (City of Ottawa, 2011).

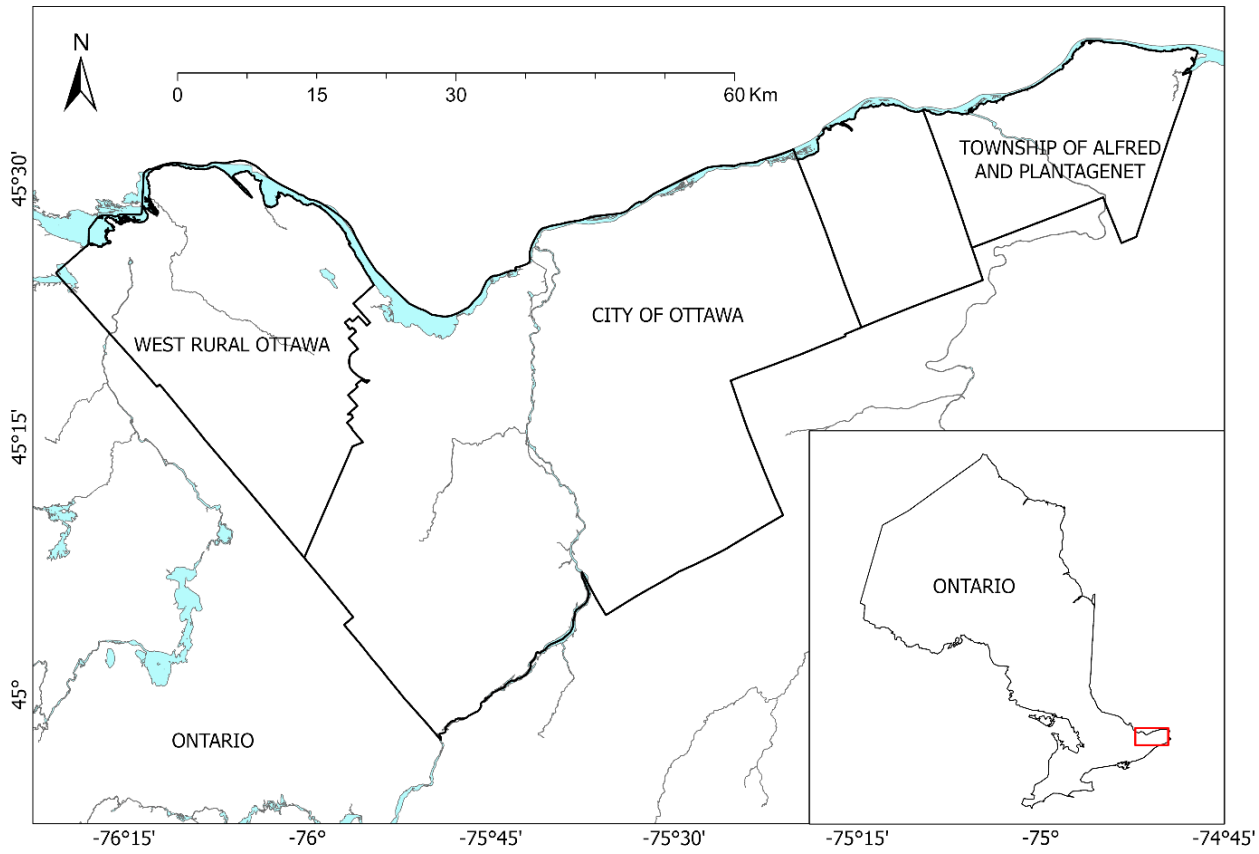

Figure 1-5. Location of the study areas in Eastern Ontario, Canada. Universal Transverse Mercator (UTM) co-ordinates provided using North American Datum 1983 (NAD83) in Zone 18N.

1.3.1. Bedrock and Surficial Geology

Both study areas are located within the limits of the former Ottawa Embayment, a former sedimentary basin that experienced a marine incursion persisting from the Late Cambrian to Upper Ordovician periods. Within this basin, Paleozoic sedimentary rocks were deposited unconformably over Precambrian Canadian Shield crystalline basement rocks. These basement rocks, such as metamorphic gneiss and marble with igneous intrusions of pegmatitic syenite, were formed during the Grenville Orogeny that occurred from 1.3 to 1.0 Ga. Tectonic activity and physical/chemical erosion in eastern Ontario has resulted in pervasive fracturing of the Precambrian and Paleozoic bedrock (Brunton and Dodge, 2008). Outcrops of bedrock are found with irregular distribution across the West Rural Ottawa study area and in the northeastern region of the Alfred and Plantagenet study area.

The Paleozoic sedimentary rocks found in the study areas can be broadly described as transitioning from sandstone and dolostones in the Upper Cambrian and Lower Ordovician to interbedded limestones, shales, and siltstones in the Middle to Upper Ordovician. Figure 1-6 and Figure 1-7 show the Paleozoic units in the study areas in ascending order of deposition, beginning with the Nepean Formation in the Late Cambrian and ending with the Billings and Carlsbad Formations in the Upper Ordovician. The Nepean Formation is predominantly quartzose sandstone with some conglomerates (Armstrong & Dodge, 2007). It is disconformably overlain by shallow marine carbonate rocks of the Beekmantown Group, made up of the Lower Ordovician March and Oxford formations. The March Formation is composed of interbedded sandstones and dolostones, while the conformable Oxford Formation is composed of some sandstone, fine-grained dolostone, and shaly dolostone (Johnson et al., 1992).

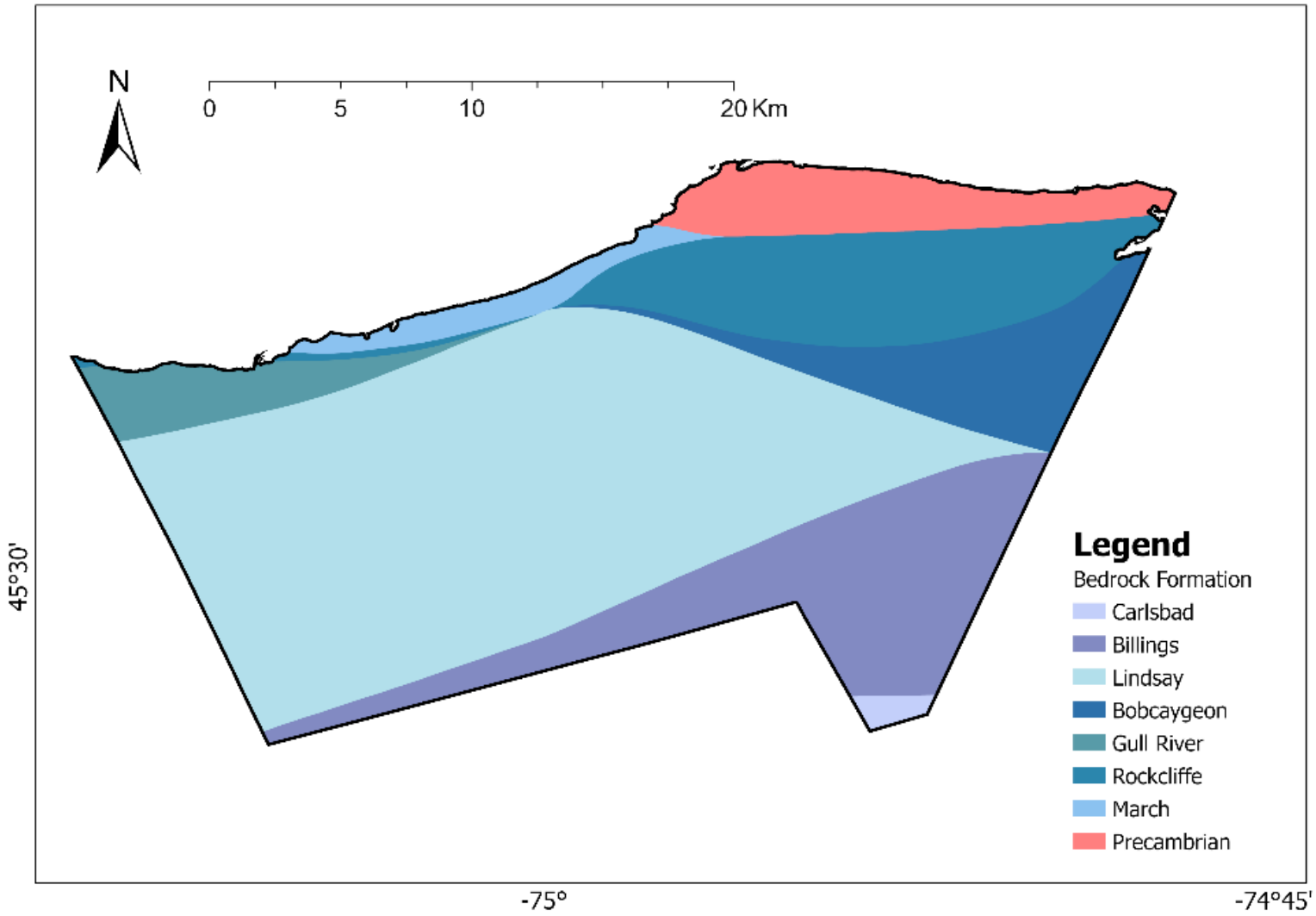

Figure 1-6. Bedrock geology in the Township of Alfred & Plantagenet. Universal Transverse Mercator (UTM) co-ordinates provided using North American Datum 1983 (NAD83) in Zone 18N. Data obtained from OGS Miscellaneous Data Release 219.

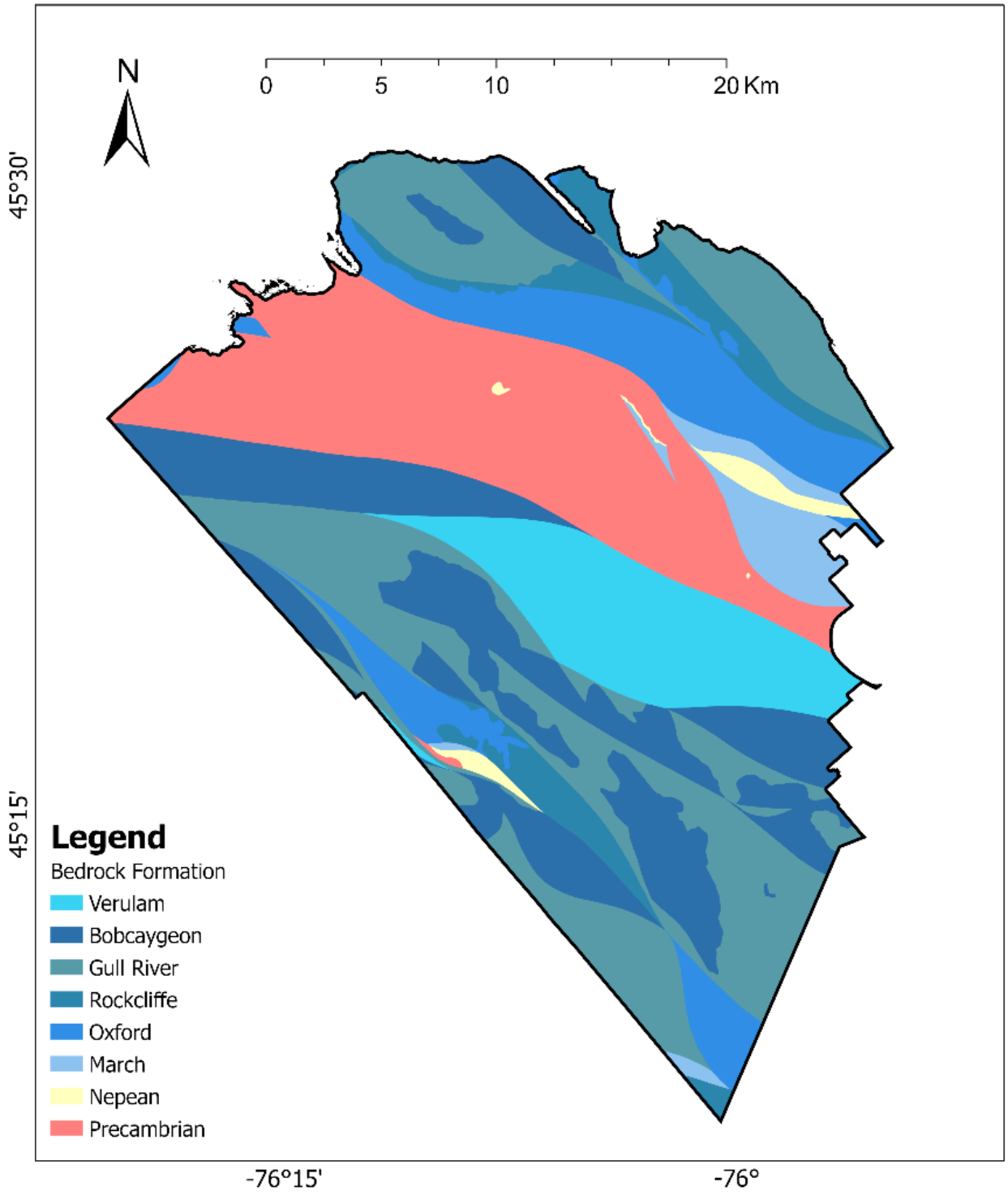

Figure 1-7. Bedrock geology in West Rural Ottawa. Universal Transverse Mercator (UTM) co-ordinates provided using North American Datum 1983 (NAD83) in Zone 18N. Data obtained from OGS Miscellaneous Data Release 219.

The Rockcliffe Formation was deposited unconformably above the Oxford Formation during the Middle Ordovician, following the progression of basin development (Johnson et al., 1992). It is composed of interbedded quartz sandstone and shale, with some limestone present in the upper portion of the formation (Johnson et al., 1992). The Ottawa Group, also deposited in the Middle Ordovician, lies disconformably above the Rockcliffe Formation (Armstrong and Dodge, 2007). This group is made up of the Gull River, Bobcaygeon, Verulam, and Lindsay Formations, all of which are observed in the study area. The Shadow Lake Formation is also found in the Ottawa Group, but it does not crop out in southeastern Ontario. These formations are difficult to distinguish due to repeating beds of highly fossiliferous interbedded limestone and shale units, which indicates constant deposition in a deepening marine environment (Johnson et al., 1992). Finally, under continually depressed basin conditions in the Upper Ordovician, the Billings and Carlsbad formation shales were deposited. The Billings Formation is characterized as a dark blue to black shale with interbeds of limestone and calcareous siltstone, while the Carlsbad Formation is described as a grey shale with interbeds of fossiliferous siltstone and bioclastic limestone (Armstrong and Dodge, 2007).

The sequence of Paleozoic sedimentary rocks is generally flat and relatively undeformed compared to the underlying Precambrian basement rocks (Johnson et al., 1992). However, during the Late Mesozoic, rifting activity occurred in association with the breakup of Pangaea and the opening of the Atlantic Ocean. The tensional forces likely reactivated the failed triple junction of the St. Lawrence rift system in addition to creating new fault lines. This resulted in block faulting, which formed the Ottawa-Bonnechere Graben and produced complex regional stratigraphy. The areas exhibiting the most extreme faulting are located near the shore of the modern-day Ottawa River.

During much of the Quaternary Period, eastern Ontario was affected by multiple glacial advances, the latest being the Wisconsinan glaciation (~75 to 11 ka). The physiography of the region determined the patterns of ice flow during glacial advance, which eroded underlying Precambrian and Paleozoic bedrock. Glaciation resulted in the widespread deposition of glacial

till. The texture and composition of both the shield-derived and carbonate-derived silty to sandy till was affected by the bedrock geology from which the unconsolidated sediments were eroded. After deposition, the till was subsequently reworked in estuarine, lacustrine, and fluvial environments (McCormack and Therrien, 2014).

Following the last glacial maximum at 18 ka, the Laurentide Ice Sheet began to melt, revealing an isostatically depressed basin. This allowed for the incursion of the Atlantic Ocean through the St. Lawrence Gulf, which formed the Champlain Sea (Figure 1-8). This marine water body occupied the St. Lawrence Lowlands from approximately 12 ka to 9.5 ka, with conditions becoming progressively shallower as isostatic rebound of the crust occurred. By 9.5 ka the Champlain Sea had drained, conditions had shifted from marine to alluvial, and the proto-Ottawa River was formed.

The Champlain Sea deposited massive grey to brown silty clays with lenses of silt and sand (Quigley et al., 1983), known as the Champlain Sea mud. The sediments are very fine-grained rock "flour" generated from glacial abrasion of the underlying bedrock. Mineralogically, the non clay minerals consist of quartz, feldspar, amphiboles, and carbonates, while the clay minerals are reported as predominantly illite and chlorite, with some smectite and vermiculite (Quigley et al., 1983). The Champlain Sea mud is also reported to contain abundant organic carbon (Fulton, 1987). Additionally, O'Shaughnessy and Garga (1994) report a high cation retention for divalent cations such as Mg^{2+} and Ca^{2+} on the solid phase clays, with a much lower cation retention for monovalent cations such as Na^{+}. The Champlain Sea mud is expected to act as a confining layer, which affects the recharge and infiltration of surface water into underlying aquifers.

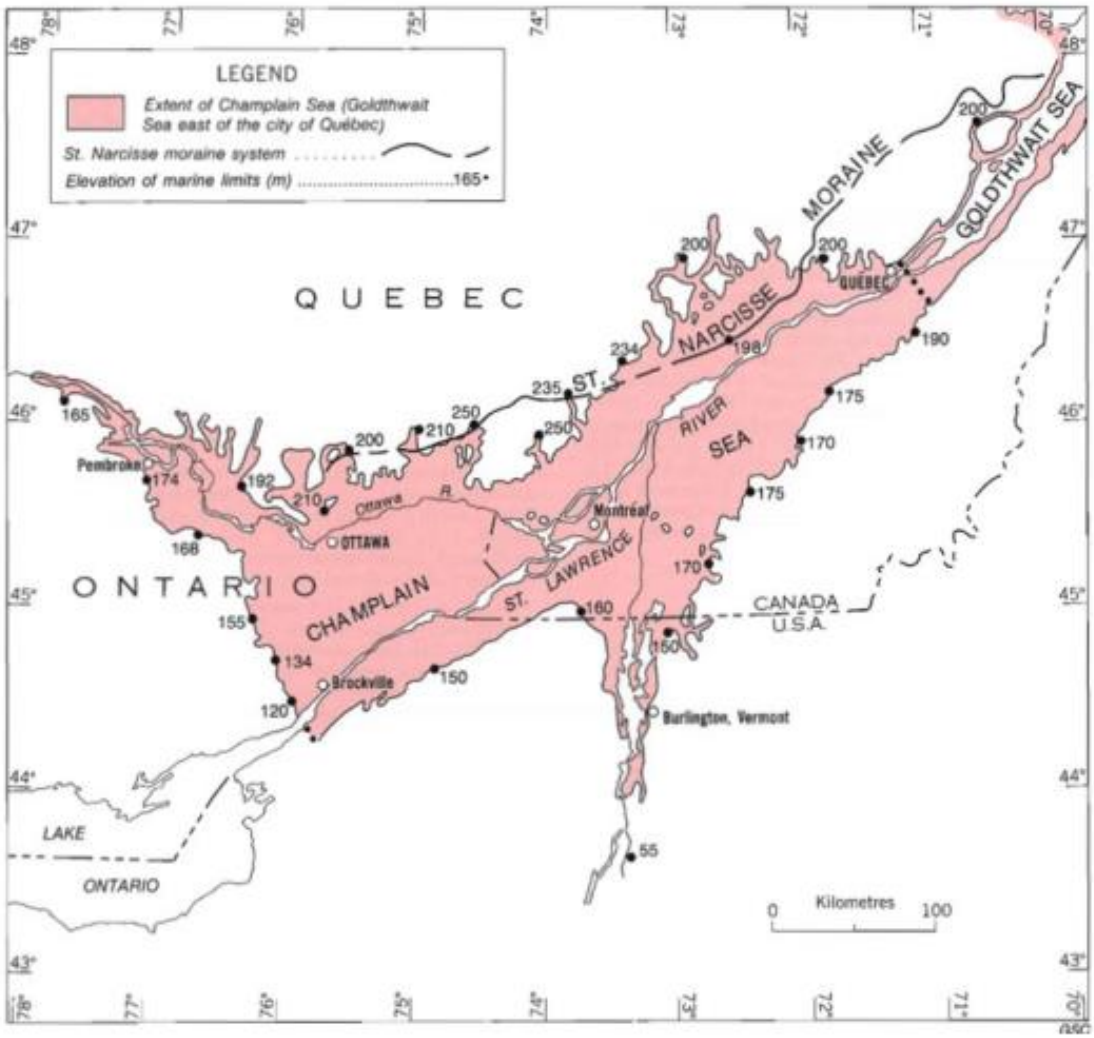

Figure 1-8. Maximum geographic extent of the Champlain Sea at 12 ka (from Sanford 1993 based on Occhietti 1989).

The distribution of Quaternary surficial deposits across the study areas are shown in Figure 1-9 and Figure 1-10. Based on the nature of the surficial deposits, Chapman and Putnam (1984) identified nine physiographic regions in eastern Ontario. Two of these physiographic regions are found within the Township of Alfred and Plantagenet. The low-lying Winchester Clay Plains are found in the eastern portion of the Township and consist of fine-grained glaciomarine deposits interspersed with ridges of rock, till, and sand. The Russell and Prescott Sand Plains are found in the western portion of the Township and are dominated by coarse grained glaciomarine and glaciofluvial deposits, intermixed with clays. An additional two physiographic regions identified

by Chapman and Putnam (1984) occur within the West Rural Ottawa study area. The Ottawa Valley Clay Flats, consisting of fine-grained glaciomarine deposits, interrupted by till deposits and Paleozoic bedrock, are found along the shore of the Ottawa River. Finally, the Smiths Falls Limestone Plain is found in the southern portion of the study area, where overburden is thin and discontinuous, exposing the bedrock.

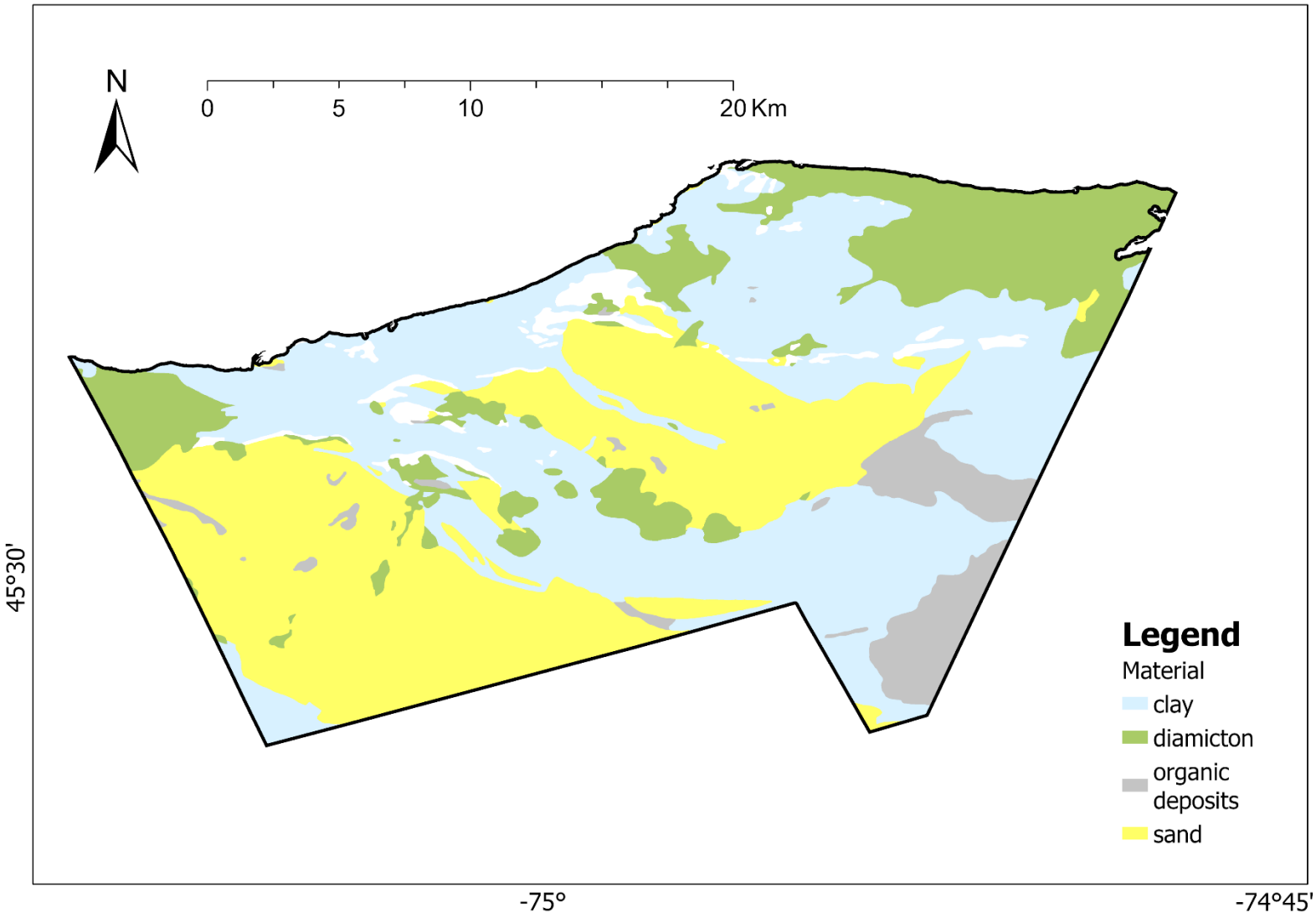

Figure 1-9. Surficial geology in the Township of Alfred & Plantagenet. Universal Transverse Mercator (UTM) co-ordinates provided using North American Datum 1983 (NAD83) in Zone 18N. Data obtained from OGS Miscellaneous Data Release 128.

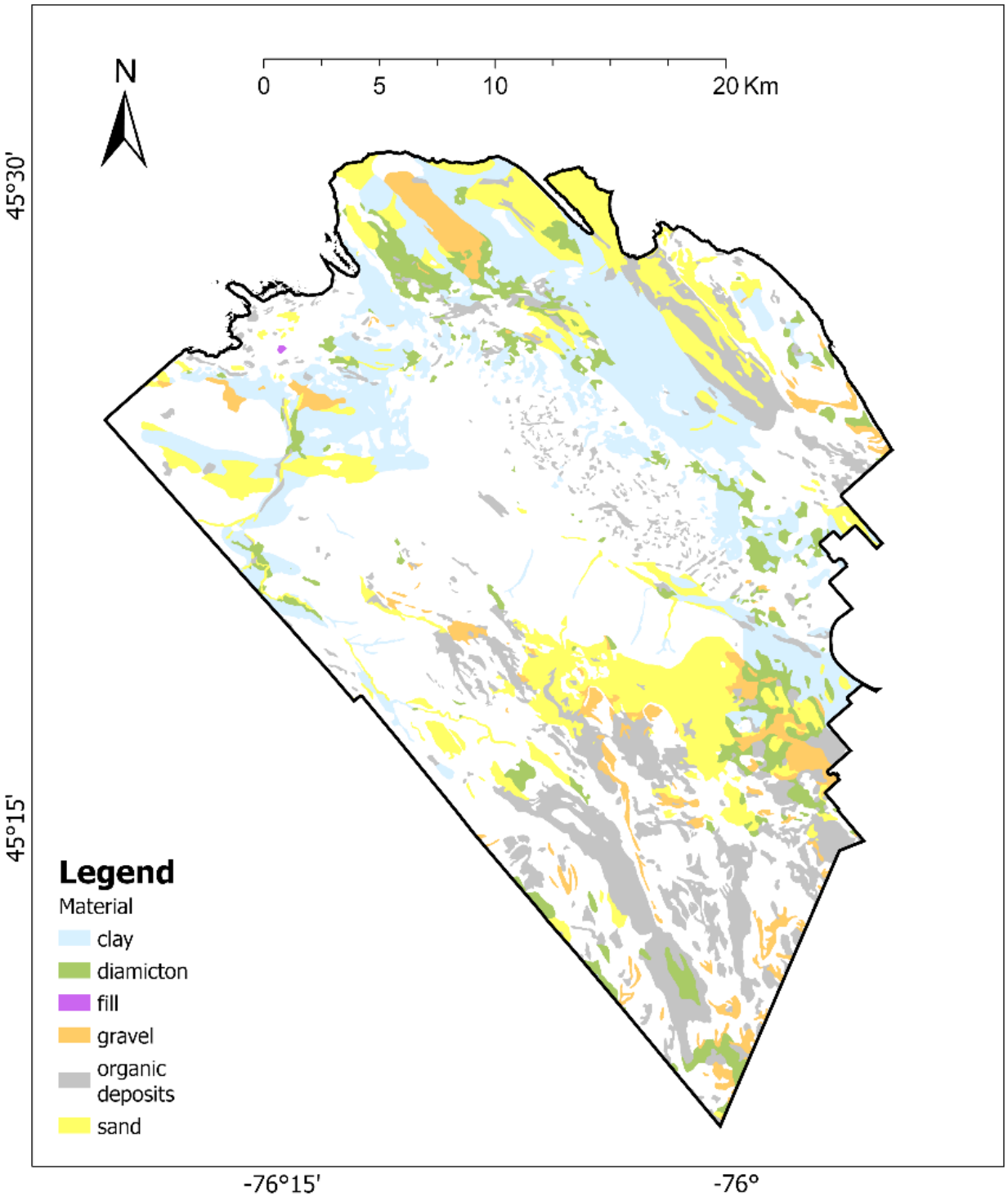

Figure 1-10. Surficial geology in West Rural Ottawa. Universal Transverse Mercator (UTM) co-ordinates provided using North American Datum 1983 (NAD83) in Zone 18N. Data obtained from OGS Miscellaneous Data Release 128.

1.3.2. Previous Indications of Groundwater Vulnerability

The Jessup's Falls Escarpment outcrops with an east-west orientation in the Township of Alfred and Plantagenet. This feature was produced during the rifting of the Ottawa-Bonnechere Graben in the Late Mesozoic and has been subject to extensive chemical dissolution (Brunton and Dodge, 2008). There are several well-known karst features and landforms that occur along the escarpment. Limestone pavement with near vertical fractures, bedding-plane joints, and solution enlarged voids are all observed (Dyck et al., 2019). Taken together, these features indicate that a direct high-permeability connection exists between the surface and the sub-surface. Due to the rural nature of the study area, there are few opportunities for groundwater testing using pre-existing water wells. However, seven domestic wells, located along a 2.2 km segment of the escarpment, were monitored by Dyck et al. (2019). The investigation focused on changes in hydraulic head, specific conductance, and O and H isotopic ratios, as they may indicate a high-permeability connection.

A time-series profile showing hydraulic head and specific conductance data from one of the seven wells monitored by Dyck et al. (2019) is presented in Figure 1-11. The data display a consistent inverse relationship between hydraulic head and specific conductance. It is also reported that the maximum change in both parameters occurs within 24 to 72 hours following a precipitation event (Dyck et al., 2019). These observations demonstrate that the changes in hydraulic head and specific conductance are closely coupled, and that an increase in hydraulic head is caused by rapid infiltration of meteoric water into the aquifer following a precipitation event.

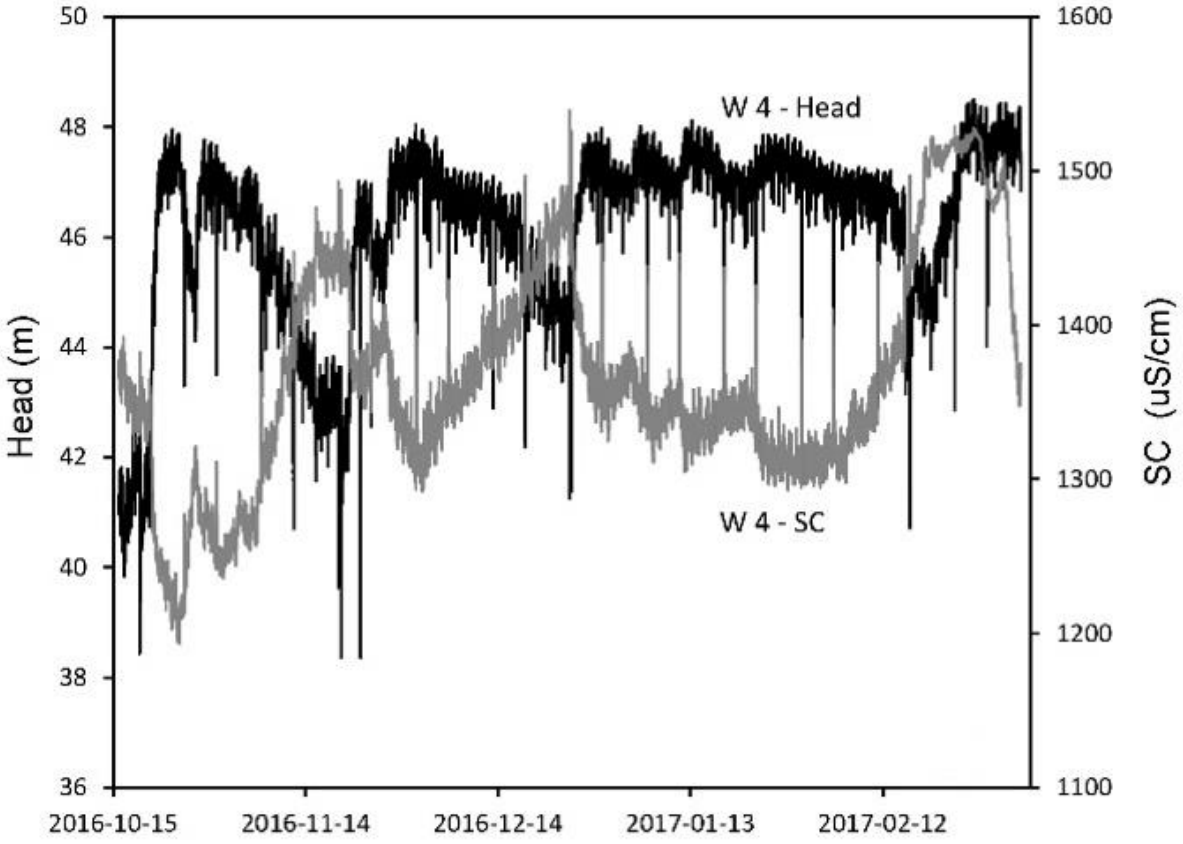

Figure 1-11. Hydraulic head and specific conductance data recorded in wells located in a vulnerable karst terrain in the Township of Alfred and Plantagenet (from Dyck et al., 2019).

The isotopes of O and H in the water molecules of precipitation, surface, and groundwater represent another tool that can be used to identify rapid infiltration and flow through fractured and karst bedrock terrains. Dyck et al., (2019) monitored time series of O and H isotopic ratios in precipitation and groundwater in an effort to identify high-permeability and rapid-transit-time connections between surface and groundwater. Figure 1-12 shows $\delta^{18}O$ profiles for samples collected over a two-month period from precipitation and from groundwater that discharges into a quarry adjacent to one of the seven monitored wells. Most notably, the precipitation and groundwater profiles show a coincidental decline in $\delta^{18}O$ following a two-day 55 mm precipitation event, in mid-late October. This event produced a signal, marked in the red box, which indicates a near-simultaneous link between the isotopic composition of meteoric water and groundwater, suggesting a high-permeability connection between surface water and

groundwater. The relatively low magnitude for the signal in the groundwater $\delta^{18}O$ profile is due to dispersion and mixing (Dyck et al., 2019).

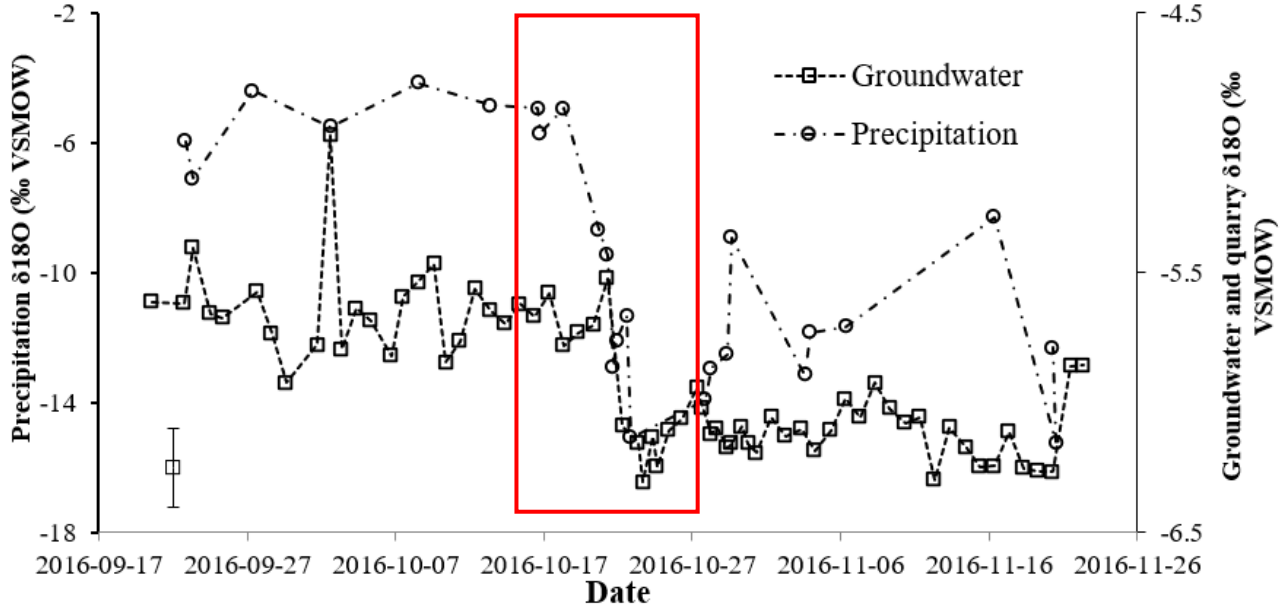

Figure 1-12. $\delta^{18}O$ time-series from samples of precipitation and from groundwater collected from karst fractures at the base of a quarry (from Dyck et al., 2019).

Within the West Rural Ottawa study area, thin soils and the presence of karst features suggest the potential for groundwater vulnerability. The presence of thin soils, defined as less than two meters of overburden, has been mapped over more than 60% of the study area. (Figure 1-13). This was determined following a regional characterization of groundwater geochemistry, which identified distinct groundwater quality issues associated with thin to absent overburden (Colgrove, 2016). In addition, known, inferred or potential karst features have been mapped over approximately 50% of the study area (Figure 1-14). Known karst is mapped where karst features have been observed directly, inferred karst is mapped where features are presumed from known karst, and potential karst is mapped where the terrain may be susceptible to karstification (Brunton and Dodge, 2008). However, direct observation of surficial karst features in the study areas is limited due to glacial erosion and/or overburden cover on bedrock. As such, buried karst systems may be far more extensive than mapped (Hamilton et al., 2017).

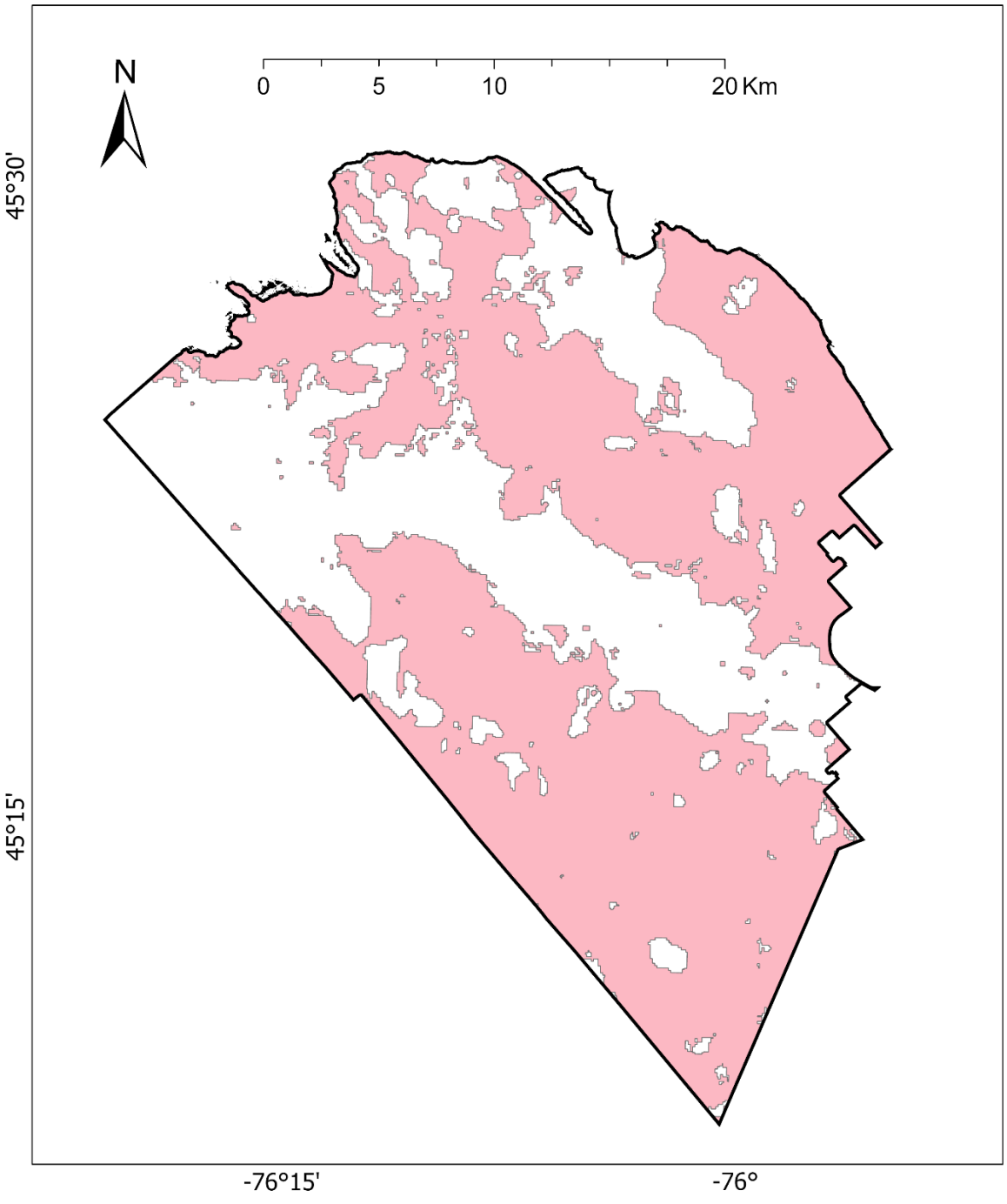

Figure 1-13. Areas mapped with less than two metres of overburden in West Rural Ottawa.

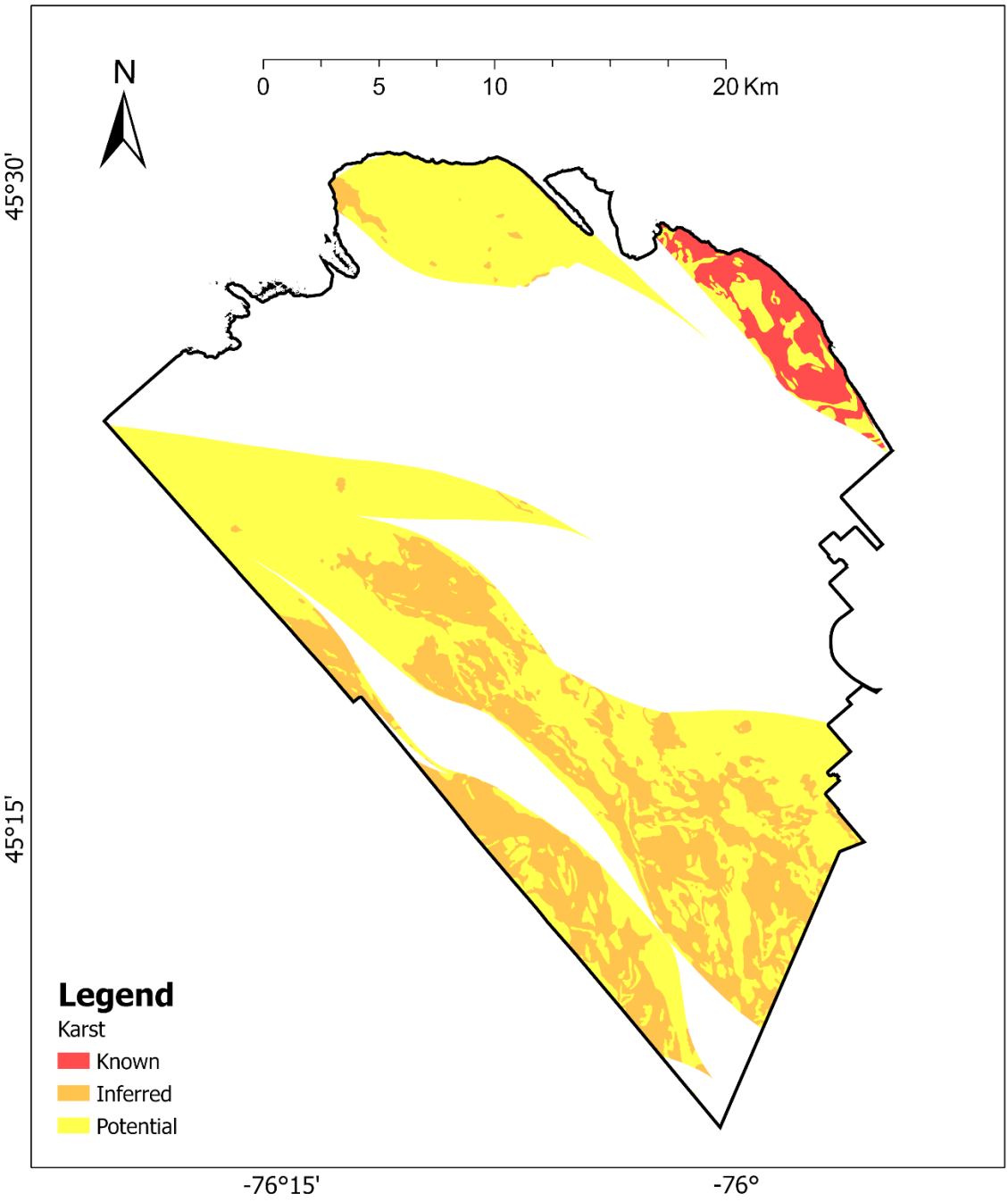

Figure 1-14. Distribution of known, potential, and inferred karst in West Rural Ottawa (GRS005, Brunton and Dodge, 2008).

2. Methods

2.1. Selection of Sampling Points

The sites identified for vulnerability testing in the Township of Alfred and Plantagenet were pre-selected based on the information presented in Section 1.3. The sites identified for vulnerability testing in West Rural Ottawa were selected based on data collected as part of the 2019 Ontario Groundwater Geochemistry Program (OAGGP). A brief description of relevant aspects of the OAGGP sampling program is given below, followed by a description of the vulnerability identification process.

The 2019 West Rural Ottawa Groundwater Study area was overlaid with a 2 × 2 km^2 uniform grid with the intent to collect a bedrock groundwater sample from each cell and an overburden groundwater sample from cells in areas without thin soils. Of the 307 groundwater samples that were collected, 263 were from wells finished in bedrock and 44 were from wells finished in overburden material (Figure 2-1). Data gaps exist where grid cells did not contain wells and in those with low population density, typical of areas that are predominantly agricultural, heavily forested, or overlain by wetlands. In most instances the wells tested were pre-existing private wells, which allow for rapid and relatively inexpensive testing. This sample selection method may introduce bias because domestic wells are generally intended to provide a good quality source of water, so it is probable that wells in aquifers with poor water quality are not represented proportionately. Additional information on the sampling biases inherent to the OAGGP protocol is provided by Hamilton and Lee, 2012.

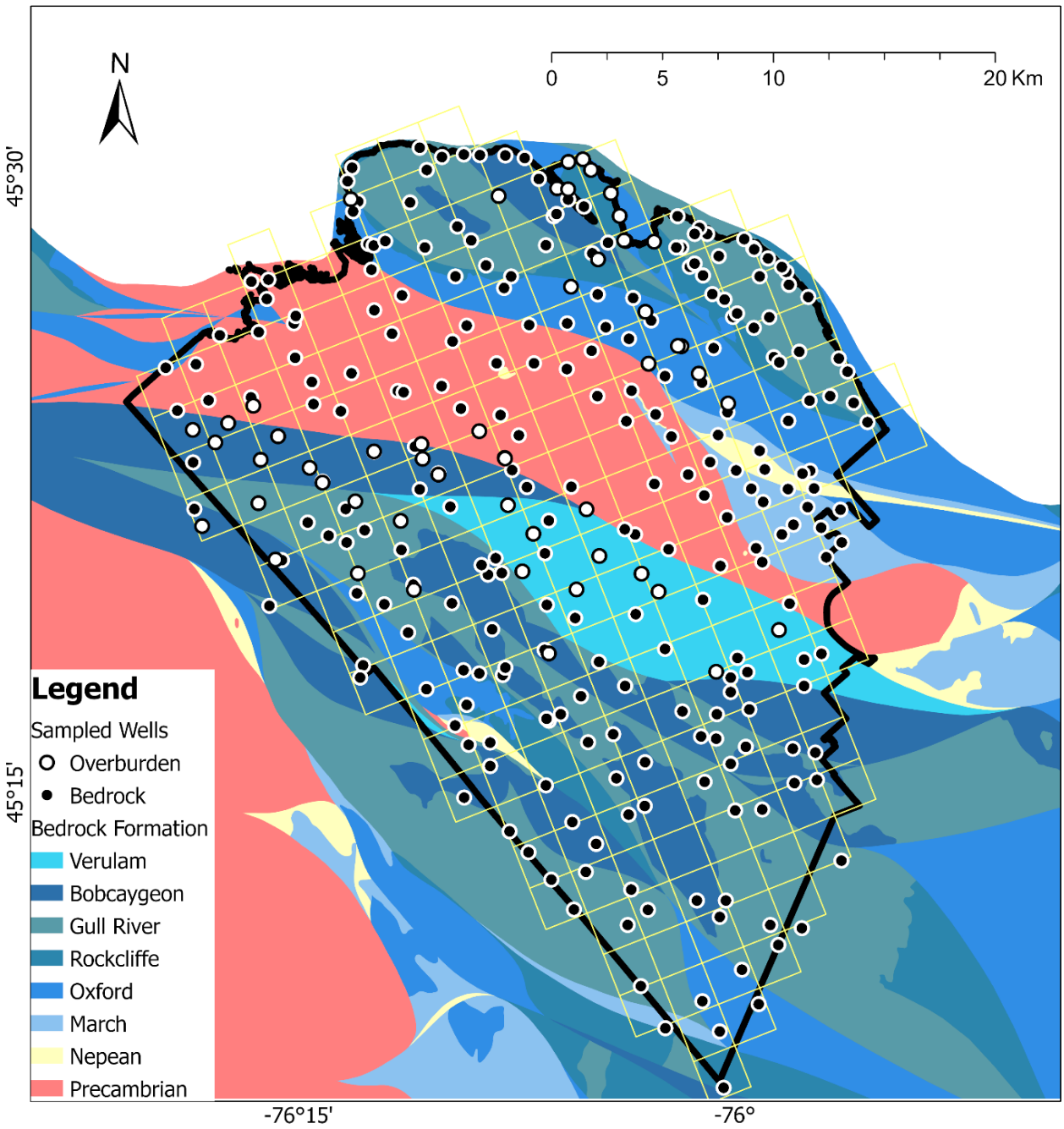

Figure 2-1. Location of groundwater samples obtained in West Rural Ottawa (n=307). Black circles represent samples from wells finished in bedrock (n=263) and white circles (n=44) represent wells finished in overburden material. Universal Transverse Mercator (UTM) co-ordinates provided using North American Datum 1983 (NAD83) in Zone 18N. Data obtained from OGS Miscellaneous Data Release 219.

At each site interviews were conducted with homeowners to gather details about the construction of the well, the use of the water, the presence of any treatment systems, and any historical water quality or quantity issues. Following this, a visual inspection of the well head was conducted, GPS coordinates were recorded, and the well collar stick-up and static water level were measured. Where the well depth could not be confirmed with a Ministry of the Environment (MOE) well record or pump installation record, the depth of the well was also measured. Water drawn from an untreated tap was then purged through a polyvinyl chloride supply hose and manifold with outlets to a 120L purging bucket, a sampling hose, and a flow through cell containing a YSI (YSI EXO 1) multi-parameter probe (Figure 2-2). This probe measured and logged temperature, pH, specific conductance, oxidation-reduction potential (ORP), dissolved oxygen, and turbidity. Samples were only collected once the temperature reading was stable within 0.1°C, typically after the purging bucket had been filled twice (~240L).

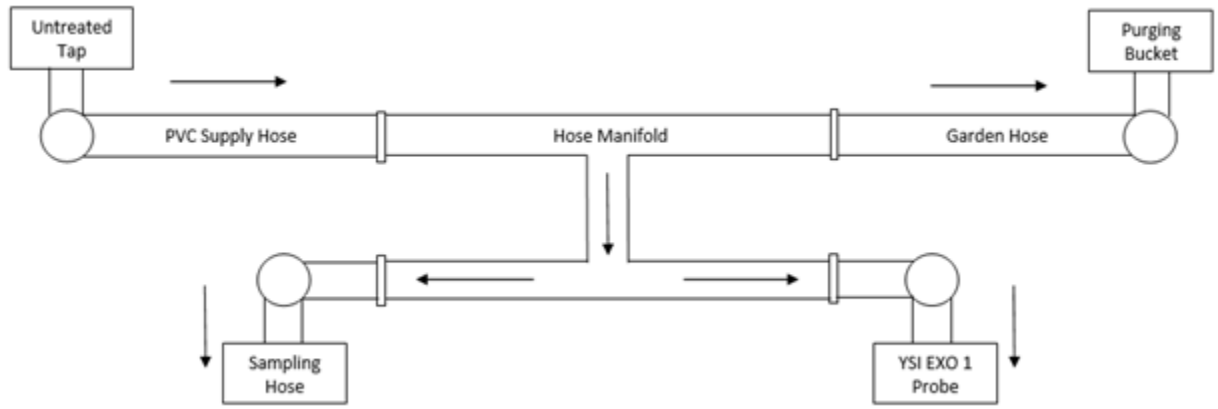

Figure 2-2. Schematic of sampling and measurement apparatus used when collecting OAGGP groundwater samples. Diagram not to scale.

The YSI EXO 1 was calibrated daily for pH and dissolved oxygen. The pH probe was calibrated with a three-point calibration at pH 4, 7, and 10. The dissolved oxygen probe was calibrated to a zero-oxygen standard solution and a water sample with 100% oxygen. The YSI EXO 1 was checked daily for electrical conductivity and turbidity. The specific conductance probe was tested with a 1413 µS/cm solution and calibrated when required. The turbidity probe was

tested with a 0 NTU standard and a 126 NTU standard and calibrated when required. The ORP probe was checked weekly against a standard solution of +250 mV.

Methane (CH_4) and carbon dioxide (CO_2) measurements were made within 24 hours by measuring the dissolved gas content in the headspace of temperature-equilibrated sample bottles. Methane measurements were made using two sensors. The low-level sensor measured methane between 0 and 25 000 ppmV and the high-level sensor measured up to 50 volume % CH_4. The low-level sensor was checked daily and calibrated when required using a 25 000 ppmV CH_4 gas standard. The high-level sensor was checked weekly and calibrated when required using a 50 volume % CH_4 gas standard. Carbon dioxide measurements were made with a single sensor that was checked daily and calibrated when required using a 2.5 volume % CO_2 gas standard and fresh air as 0%. The concentration of dissolved gas was then estimated using Henry's Law and the measured temperature and headspace gas concentrations (McIntosh et al., 2014). Hydrogen sulfide (H_2S) content was measured in the field using the methylene-blue method and a HACH colour disc test kit. A blank of deionized water was compared through a rotating colour wheel to a prepared sample of the groundwater. No measurements were made at sites where free oxygen was present and ORP was positive or where H_2S wasn't detected by smell.

The selection of sites identified for inclusion in the study to test the use of excess ^{210}Pb and ^{137}Cs as tracers for identifying vulnerable aquifers in West Rural Ottawa followed a process of hierarchical elimination illustrated in Figure 2-3. Only groundwater samples with a complete geochemical data set and which were collected in wells finished in bedrock were considered. Wells treated with an aerator were eliminated as aeration is typically applied ahead of the pressure tank tap without a bypass, making it impossible to obtain an untreated sample. The remaining wells were divided into one of two groups of potentially vulnerable or non-vulnerable sampling sites based on whether or not there was more than 2 m of overburden. This was determined using the GPS measurements recorded at the well head and the City of Ottawa's overburden ArcGIS layer.

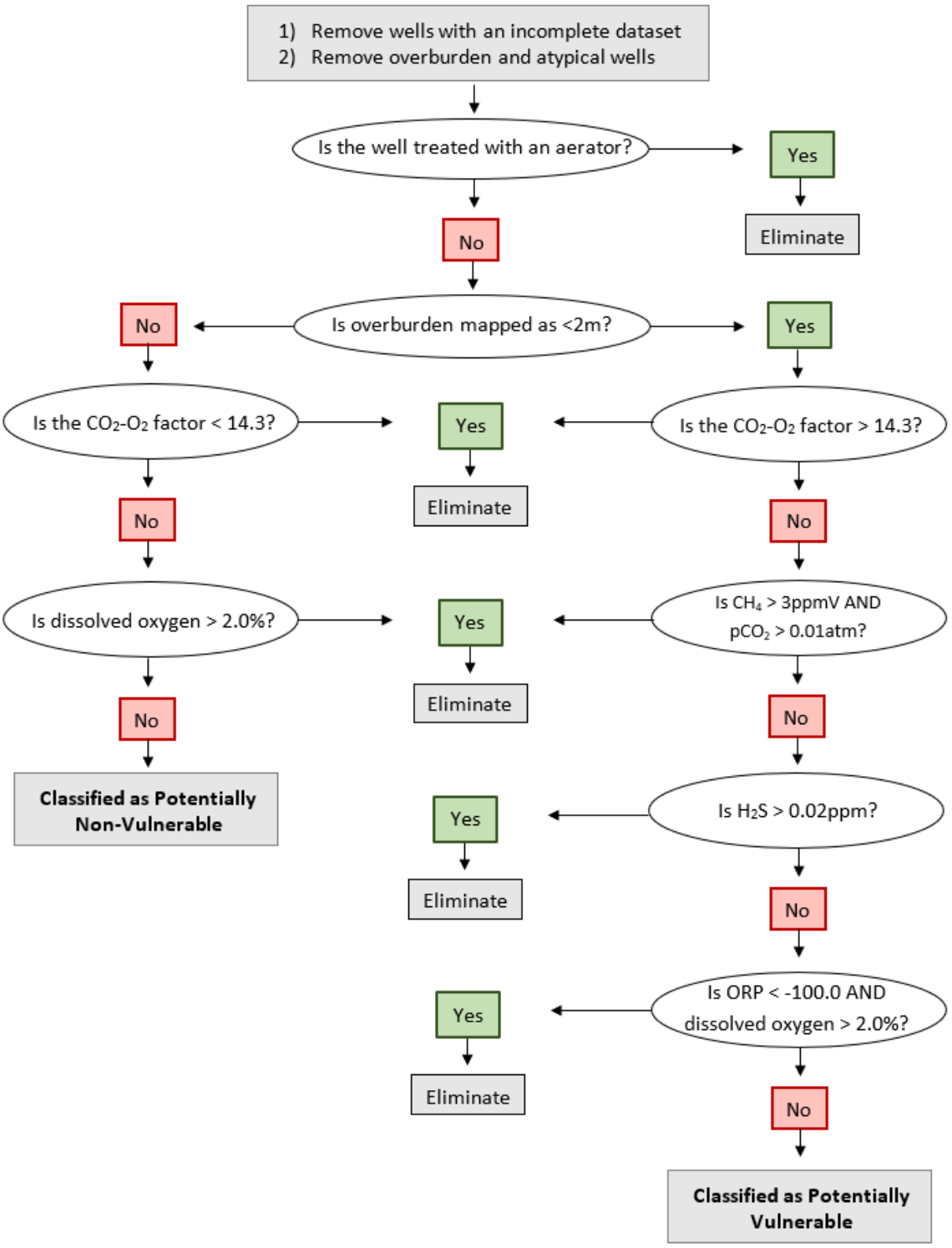

Figure 2-3. Flow chart showing site selection methodology for vulnerable and non-vulnerable sites.

Within the two groups, the presence of dissolved oxygen and carbon dioxide were used to evaluate the connectivity to the ground surface (atmosphere). As the only available source of dissolved oxygen is the atmosphere, recently recharged groundwater should be near saturation with respect to dissolved oxygen. Elevated levels of carbon dioxide likely occur when recharge occurs through a soil zone and therefore are also used to indicate recently recharged groundwater. As per Hamilton et al., (2017) the carbon dioxide and dissolved oxygen parameters were combined, with equal weighting, into a single CO_2-O_2 factor. This factor supported the identification of areas subject to rapid recharge where there is a strong connection between the surface and the subsurface. The third quartile of the CO_2-O_2 factor (14.3) was used as a threshold to identify potentially vulnerable regions. Those samples with an overburden thickness greater than 2 m and a CO_2-O_2 factor less than 14.3 were eliminated as potential sampling locations. The final elimination step in selecting potentially non-vulnerable sampling sites was to eliminate sites with dissolved oxygen values that were greater than 2.0%, as anything below that could be reasonably explained by calibration error but anything above that was not consistent with a potentially non-vulnerable environment.

Those samples with an overburden thickness less than 2 m and a CO_2-O_2 factor greater than the third quartile were eliminated as potentially vulnerable sampling locations. It is important to note that unlike dissolved oxygen, carbon dioxide in groundwater has more than one source. Examples include dissolution of calcite or dolomite and oxidation of organic matter and methane. In most instances either carbon dioxide or methane will be the dominant gas in the system, and they are present in oxidizing and reducing environments, respectively (Hamilton et al., 2017). However, in cases where they co-exist at significant levels it is likely a result of (1) a methanotrophic environment leading to partial oxidation of methane or (2) both gases being produced from fermentation of hydrogenous organic matter (Hamilton et al., 2017). In these instances (Figure 2-4), the presence of carbon dioxide has no relationship with recharge timing or groundwater movement. Any remaining samples that were not classified as potentially non-vulnerable that had a partial pressure of carbon dioxide (PCO_2) greater than 0.01 atm and methane greater than 3 ppmv were eliminated. Samples with hydrogen sulfide greater than

0.02 ppm and samples with the presence of any dissolved oxygen and anomalously low ORP were also removed, as these geochemical characteristics are indicative of reducing environments.

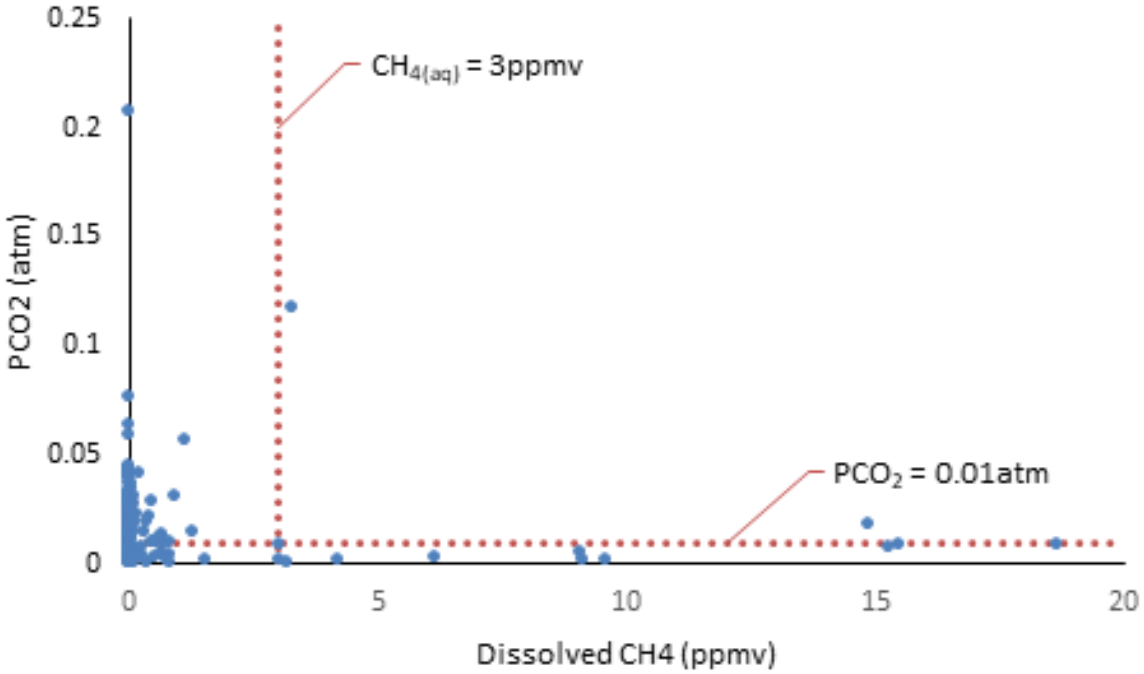

Figure 2-4. PCO_2 as a function of dissolved CH_4 in all bedrock wells sampled in West Rural Ottawa (n=263). Red dashed lines show thresholds above which samples were eliminated from the site selection process.

2.2. Sediment Sampling and Preparation

2.2.1. Suspended Sediment

Samples of suspended sediment were collected by attaching the polyvinyl chloride supply hose to the previously identified untreated tap at each site. The sampling apparatus was modified to include a Geotech Polycarbonate In-Line Filter Holder (Figure 2-5). The filter holder contained a 0.45 µm cellulose acetate filter paper (142 mm diameter), through which approximately 20 L of water was passed. Once the sample was collected, each filter membrane was stored in a plastic Petrie dish and then dried in a field glove box for 48 hrs.

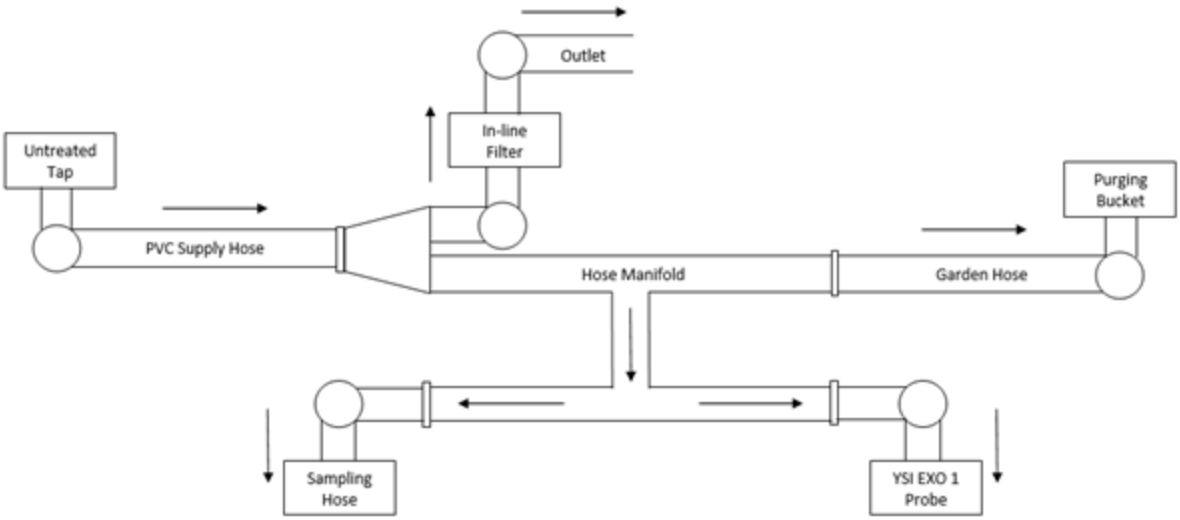

Figure 2-5. Schematic of hose and in-line filter set up used to collect sediment samples. Diagram not to scale.

2.2.2. Surface Soils

Samples of surface soil were collected from nine locations across the two study areas indicated in Figure 2-6 and Figure 2-7. Sample locations were chosen in forest covered areas where the surface soil was likely undisturbed for at least several decades. Two samples were collected from the top layer of soil at each location, after the removal of surficial detritus, and were stored in plastic Zip-loc bags. Leaves, twigs, and stones were separated from the sample and then the samples were dried at 100°C for 12 hrs. After drying, the samples were sieved to < 37 µm and prepared for gamma spectroscopy analysis.

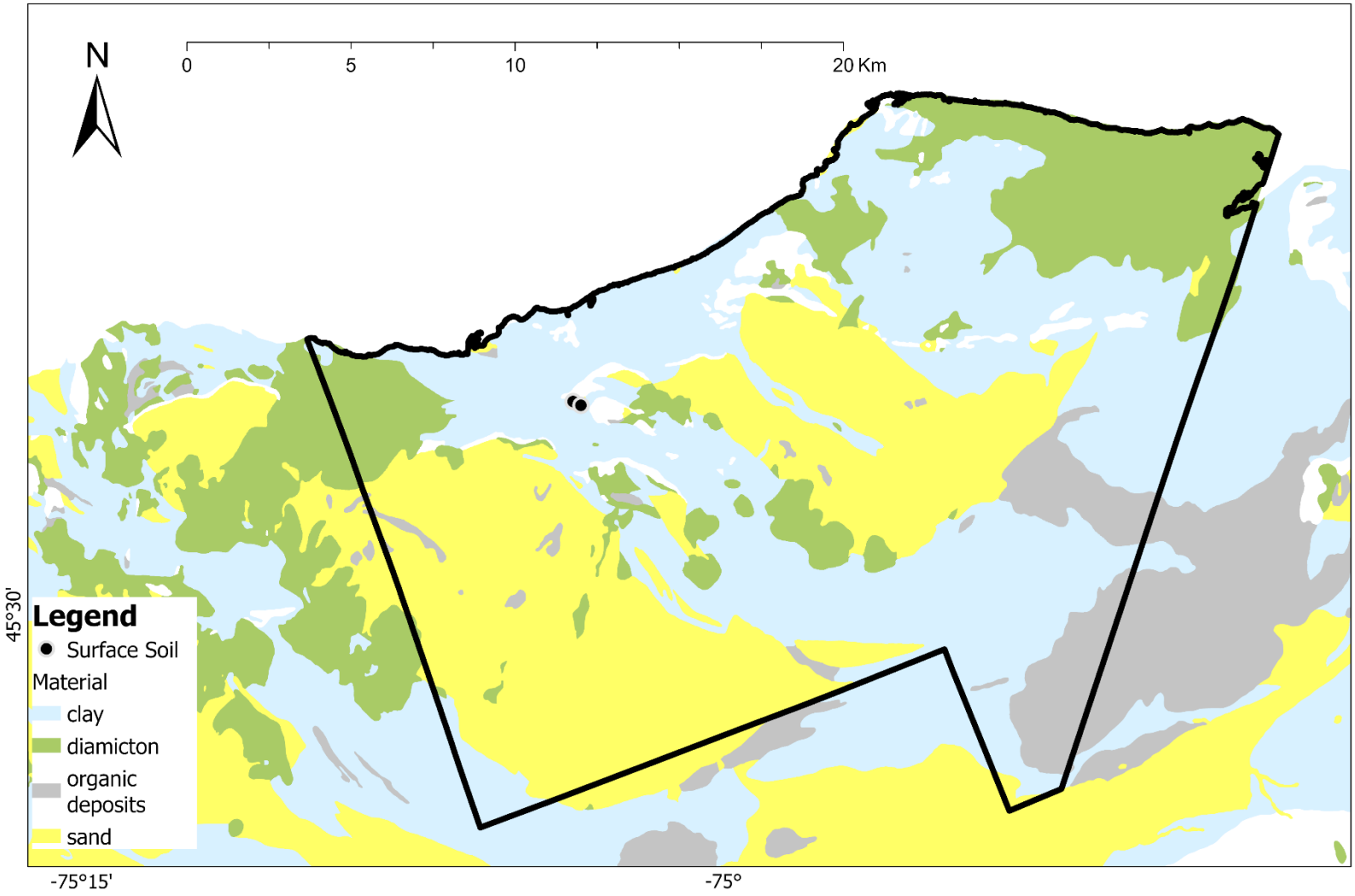

Figure 2-6. Sampling locations for surface soil samples in the Township of Alfred & Plantagenet. Universal Transverse Mercator (UTM) co-ordinates provided using North American Datum 1983 (NAD83) in Zone 19. Data obtained from OGS Miscellaneous Data Release 128.

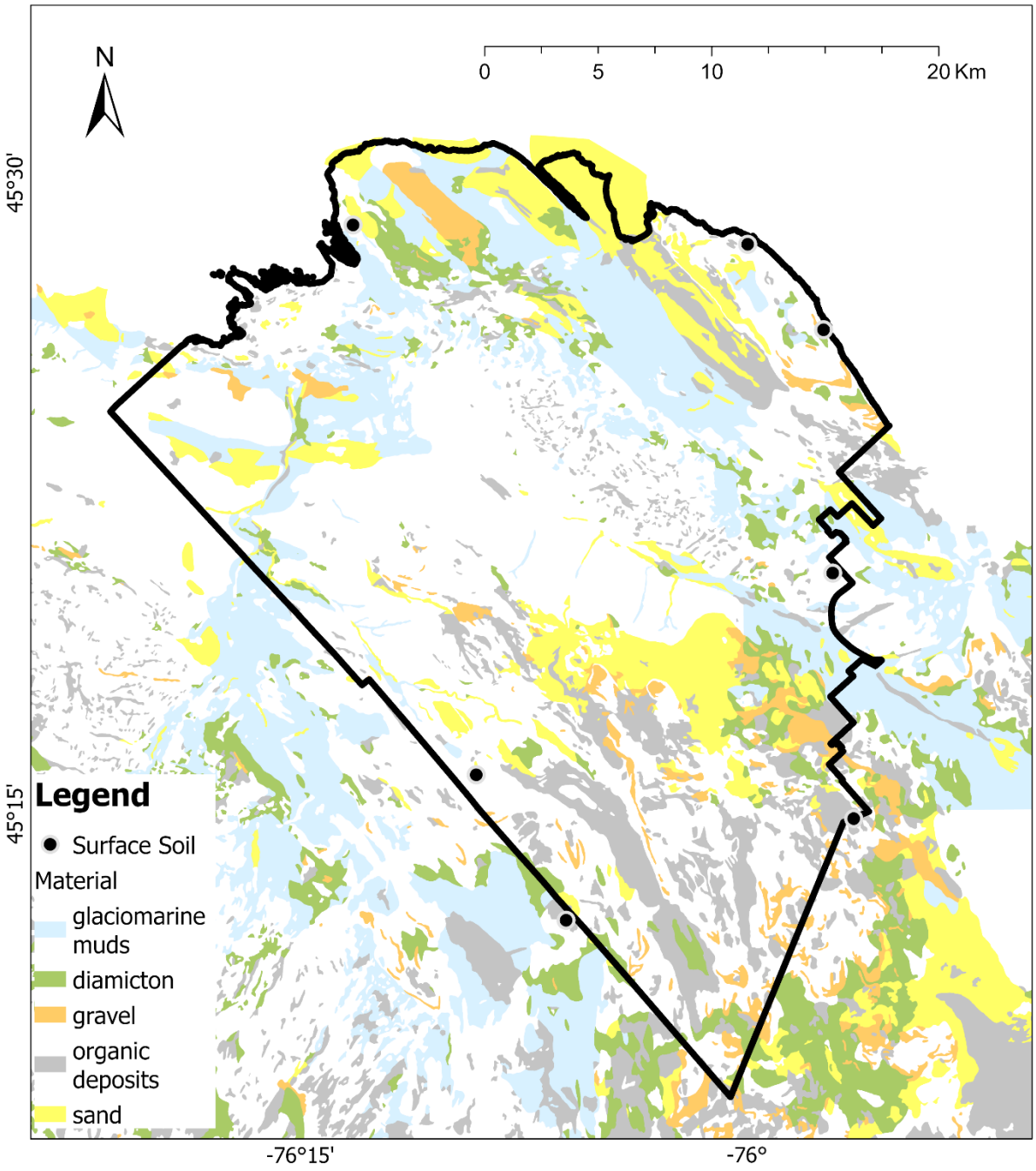

Figure 2-7. Sampling locations for surface soil samples in West Rural Ottawa. Universal Transverse Mercator (UTM) co-ordinates provided using North American Datum 1983 (NAD83) in Zone 18N. Data obtained from OGS Miscellaneous Data Release 128.

2.2.3. Well-bottom Sediment

Samples of sediment from the bottoms of the wells were also collected from sites identified as potentially vulnerable and non-vulnerable. To collect these samples, a 12.7 mm copper tube, with a ball valve fitted to the end, was lowered on aircraft cable to the bottom of the well (Figure 2-8). Once at the bottom of the well, the probe was raised and lowered several times to fill the tube with a sediment slurry. The probe was then carefully pulled to the surface and the contents were emptied in a sample bottle. This process was repeated as necessary to collect a substantial sample from each well. After allowing the sediment in the samples to settle to the bottom of the bottle, the excess water was decanted to isolate the sediment slurry. The sample was then dried at 100°C for 4 hrs. After drying, the samples were sieved to < 105 µm and prepared for gamma spectroscopy analysis.

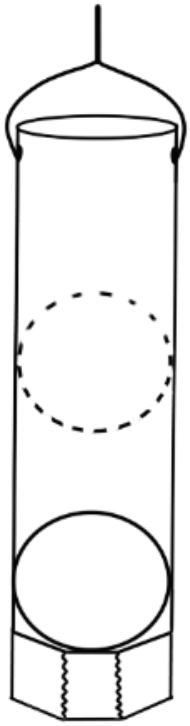

Figure 2-8. Schematic of the probe used to collect sediment from the bottom of wells. Diagram not to scale.

2.2.4. Sample Preparation for Analysis

Suspended sediment samples: The dried papers were folded and rolled in an identical manner, to maintain consistent geometry, and then inserted into scintillation vials. The vials were capped and then inserted in the gamma spectrometer for analysis.

Soil and Well-bottom Sediments: Each of the surface soil and well-bottom sediment samples were weighed, placed in vials and prepared for gamma counting following a simple and non-destructive technique that allows for the simultaneous analysis of ^{137}Cs, total ^{210}Pb and other photo peaks used to estimate supported ^{210}Pb activity. Using a method modified from Manolopoulou et al. (2003), each sample was mixed with 2% by weight activated carbon, which is an adsorbent of ^{222}Rn. The vials were centrifuged for 15 min at 4000 rpm to ensure consistent geometry. All of the vials were then sealed with 12.7 mm of epoxy resin and capped. The epoxy seal traps and retains the ^{222}Rn produced by ^{226}Ra decay (Putyrskaya et al., 2015; Schelske et al., 1994). All of the vials were then stored for 28 days to establish secular equilibrium between ^{226}Ra, ^{222}Rn, and their progenies.

2.3. Gamma Spectroscopy

Activities of gamma-emitting radionuclides were determined using data collected from an Ortec High Purity Germanium Gamma Spectrometer (Model LS-1116) at the University of Ottawa and data were analyzed using MAESTRO version 6.08 software. Samples were counted in scintillation vials for 24 hrs (86400 s), consistent with previously reported methods (Joel et al., 2017; Nisti et al., 2009). To confirm that a longer counting time would not result in a significant difference in radionuclide activities, a paper blank and a suspended sediment sample were each counted three times for 48 hrs. It was determined that, for each of ^{137}Cs and ^{210}Pb, the average gross counts observed over 48 hrs were approximately double the average gross counts observed over 24 hrs. Therefore, it was concluded that a longer counting time did not yield a significant benefit. A two-point energy calibration was conducted using high purity potassium chloride and calibrated using the ^{40}K 1460 keV γ-emission and the 511 keV annihilation peak.

No corrections were made for detector efficiency and self absorption as it was decided that these corrections would result in relatively small changes in radionuclide activities and would not alter the interpretation of the results.

For analysis of the suspended sediment samples, the activities of ^{137}Cs and ^{210}Pb were measured from the 661.66 keV and 46.65 keV γ-emissions. The region of interest for ^{137}Cs was defined as nine channels centered on the 661.66 keV peak and nine background channels at low- and high-energy positions adjacent to the photo peak (Figure 2-10). The region of interest for ^{210}Pb was defined as eleven channels centered on the 46.65 keV peak and eight background channels at low- and high-energy positions adjacent to the photo peak. The differences in the widths of the photo peaks were chosen to give a reasonably good fit to the Gaussian shape in the region of interest. Similarly, the difference in the widths of the background regions were chosen to minimize error in the subtraction of underlying background radiation.

Additional photo peaks were considered in the analysis of surface soil and well-bottom sediment samples to differentiate between supported and unsupported ^{210}Pb. Using gamma spectroscopy, supported ^{210}Pb activity can be estimated by analyzing one of the several γ-emissions of ^{226}Ra, ^{214}Pb, or ^{214}Bi. Unsupported ^{210}Pb activity can then be obtained by subtracting the estimated supported activity from total activity. The use of the ^{226}Ra peak is difficult because, although gamma emissions occur at five discrete energies during the decay of ^{226}Ra, only the 186.2 keV γ-emission has a sufficiently high branching ratio (3.64%) (IAEA, 2009) to be measurable. However, without additional corrections this peak is unresolvable from the ^{235}U 185.7 keV γ-emission, which is present in all natural samples (Patricio & Bonotto, 2021; Putyrskaya et al., 2015).

Alternatively, supported ^{210}Pb can be determined from one of several γ-emissions of the daughter radionuclides ^{214}Bi or ^{214}Pb. Given the low radioactivity of the samples and higher detector efficiency at lower energies, ^{214}Pb was used to estimate supported ^{210}Pb activity. The two most abundant ^{214}Pb γ-emissions occur at 295.2 keV (18.4%) and 351.9 keV (35.6%) (IAEA,

2009). When considering the impact of unresolved interference from other peaks, it is expected that the ^{234}Pa 293.7 keV γ-emission may contribute about 7.9% of the total counts in the 295.2 keV photopeak, while the ^{211}Bi 351.1 keV γ-emission may contribute only about 1.6% of the total counts in the 351.9 keV photopeak (Joshi, 1987). Therefore, because of the lower level of interference and the higher branching ratio, the 351.9 keV photopeak was used to derive concentrations of ^{226}Ra and estimate the activity of supported ^{210}Pb. The region of interest for ^{214}Pb was defined as eleven channels centered on the 351.9 keV photo peak and eight background channels at low- and high-energy positions adjacent to the photo peak (Figure 2-10).

For each radionuclide measured in the samples, the counts, corrected for Compton scattering, were determined using a method modified from Schelske et al. (1994). In each instance, the average counts in the two shoulder regions were subtracted from the average counts in the photo peak region, and then multiplied by the number of channels in the photo peak region (Figure 2-10). The average background counts in the photo peak region for the blanks were determined in the same way. Net counts for each radionuclide were then found by subtracting Compton corrected background counts in the blanks from Compton corrected sample counts.

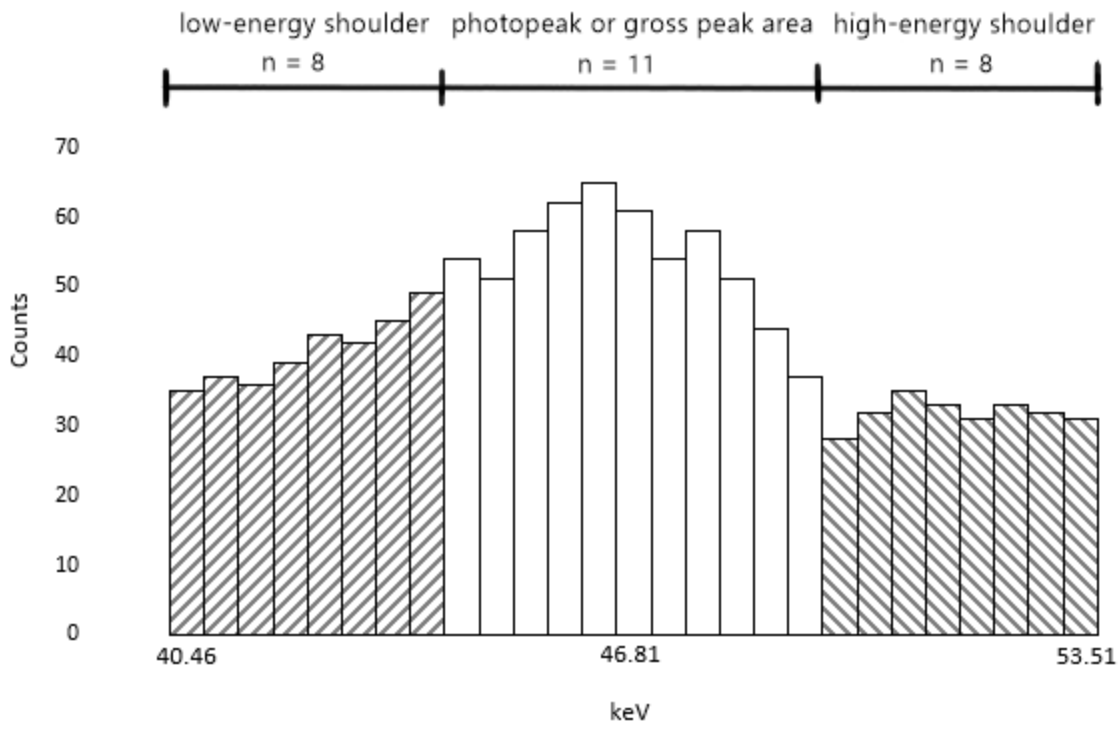

Figure 2-9. Components of an idealized ^{210}Pb region of interest used to determine count rates.

Prior to interpretation, each of the radionuclide net count values were corrected to a counting duration of exactly 1 day (86400 s) and their respective branching ratios (Table 2-1). The net count values for the soils and well-bottom sediments were also corrected to the sediment mass. To evaluate a signal measured using gamma spectroscopy methods, limits of detection must be determined (Figure 2-11). Following Currie (1968), the critical level (L_C) was determined *a posteriori* to delineate the level above which a signal is detected. This value was calculated as $1.64\sigma_B$, where σ_B is the standard deviation of the mean net signal of the blank. For the suspended sediment analysis, the L_C was found to be 25 cps for ^{137}Cs and 41 cps for ^{210}Pb (Table 2-1). For the surface soil and well-bottom sediment analysis the L_C was found to be 17 cps/g for ^{137}Cs and 65 cps/g for ^{210}Pb. The detection limit (L_D) was determined *a priori* and denotes the level above which the analytical procedure can produce reliable detection (Currie, 1968). This value was calculated as $2L_C$. For the suspended sediment analysis, the L_D was found to be 50 cps for ^{137}Cs and 82 cps for ^{210}Pb. For the surface soil and well-bottom sediment analysis the L_D was found to be 34 cps/g for ^{137}Cs and 130 cps/g for ^{210}Pb.

Table 2-1. Critical level (L_C) and Detection Limit (L_D) determined for ^{137}Cs and ^{210}Pb

Radionuclide	Critical Level (L_C)	Detection Limit (L_D)
Suspended Sediment Analysis (cps)		
^{137}Cs	25	50
^{210}Pb	41	82
Surface Soil and Well-bottom Sediment Analysis (cps/g)		
^{137}Cs	17	34
^{210}Pb	65	130

Table 2-2. γ-emission energies, central energy channels, and branching ratios for selected radionuclides (IAEA, 2009)

Radionuclide	γ-emission Energy (keV)	Branching Ratio (%)
^{210}Pb	46.65	4.25
^{235}U	185.7	57.0
^{226}Ra	186.2	3.64
^{234}Pa	293.7	7.9
^{214}Pb	295.2	18.4
^{211}Bi	351.1	1.6
^{214}Pb	351.9	35.6
^{137}Cs	661.66	85.1

2.3.1 Preparation and Analysis of Blanks

Suspended Sediment Analysis: Blanks were prepared prior to sample analysis. Initially, two paper blanks were prepared for the suspended sediment analyses, along with two drying blanks, and two empty scintillation vials. Each was counted on the gamma spectrometer for 24 hrs. The paper blanks were filter papers removed from their packaging and inserted immediately into empty scintillation vials. The drying blanks were filter papers left in the field glove box for 48 hrs and then inserted into empty scintillation vials. Using the average counts for each of the regions of interest, it was determined that the empty scintillation vials produced the majority of the signal, with negligible contribution from the paper. Therefore, an additional

six empty scintillation vials were counted for 24 hrs, for a total of eight blanks, in order to quantify the background radiation in the regions of interest for all samples.

Soils and Well-bottom Sediment: Blanks were prepared for analysis of the soils and well-bottom sediment using five scintillation vials, each with approximately 0.0160 g of activated carbon, a septum, 13mm of epoxy resin seal, and a cap – as for the samples. These were counted on the gamma spectrometer for 24 hrs.

3. Results and Discussion

3.1 Results of Hierarchical Elimination

The locations of the suspended sediment sampling sites are shown in Figure 3-1 and Figure 3-2, where there are 20 potentially vulnerable and 4 potentially non-vulnerable locations. The final sampling sites were selected by prioritizing those with associated MOE well records. Additionally, the potentially vulnerable sampling sites were selected by prioritizing those with high dissolved oxygen over those with high carbon dioxide, as the former must be sourced at the point of infiltration. Suspended sediment samples were collected from sampling sites where the well depth ranged from 13.9 m to 90.9 m below ground surface (bgs) and were found in areas where the deepest unit penetrated was one of either the Gull River, Lindsay, Rockcliffe, or Nepean formations or the Precambrian basement. In wells classified as potentially vulnerable, the overburden thickness ranged from 0 m to 3.6 m bgs with an average of 1.4 m, while in wells classified as potentially non-vulnerable the overburden thickness ranged from 0 m to 18.3 m bgs with an average of 8.7 m.

The locations of the well-bottom sediment sampling sites are shown in Figure 3-3 and 3-4, where there are 9 potentially vulnerable and 10 potentially non-vulnerable locations. The final sampling sites were selected using data that had been updated through quality assurance and quality control procedures, and by prioritizing those with associated MOE well records. Additionally, the potentially vulnerable sampling sites were selected by prioritizing those with higher dissolved oxygen than carbon dioxide, those with thin soil cover, and where total coliforms were recorded above 5 MPN/100mL. Well-bottom sediment samples were collected from sampling sites where the well depth ranged from 16.4 m to 83.2 m bgs and were found in areas where the deepest unit penetrated was one of either the Gull River, Lindsay, Oxford, Bobcaygeon, or Verulam formations or the Precambrian basement. In wells classified as potentially vulnerable the overburden thickness ranged from 0 m to 3.7 m bgs and an average of 1.0 m, while in wells classified as potentially non-vulnerable the overburden thickness ranged from 0 m to 36.6 m bgs with an average of 13.1 m. The single potentially non-vulnerable well

with no overburden cover was included because it had also been included in the suspended sediment sampling, so it was useful as a replicate.

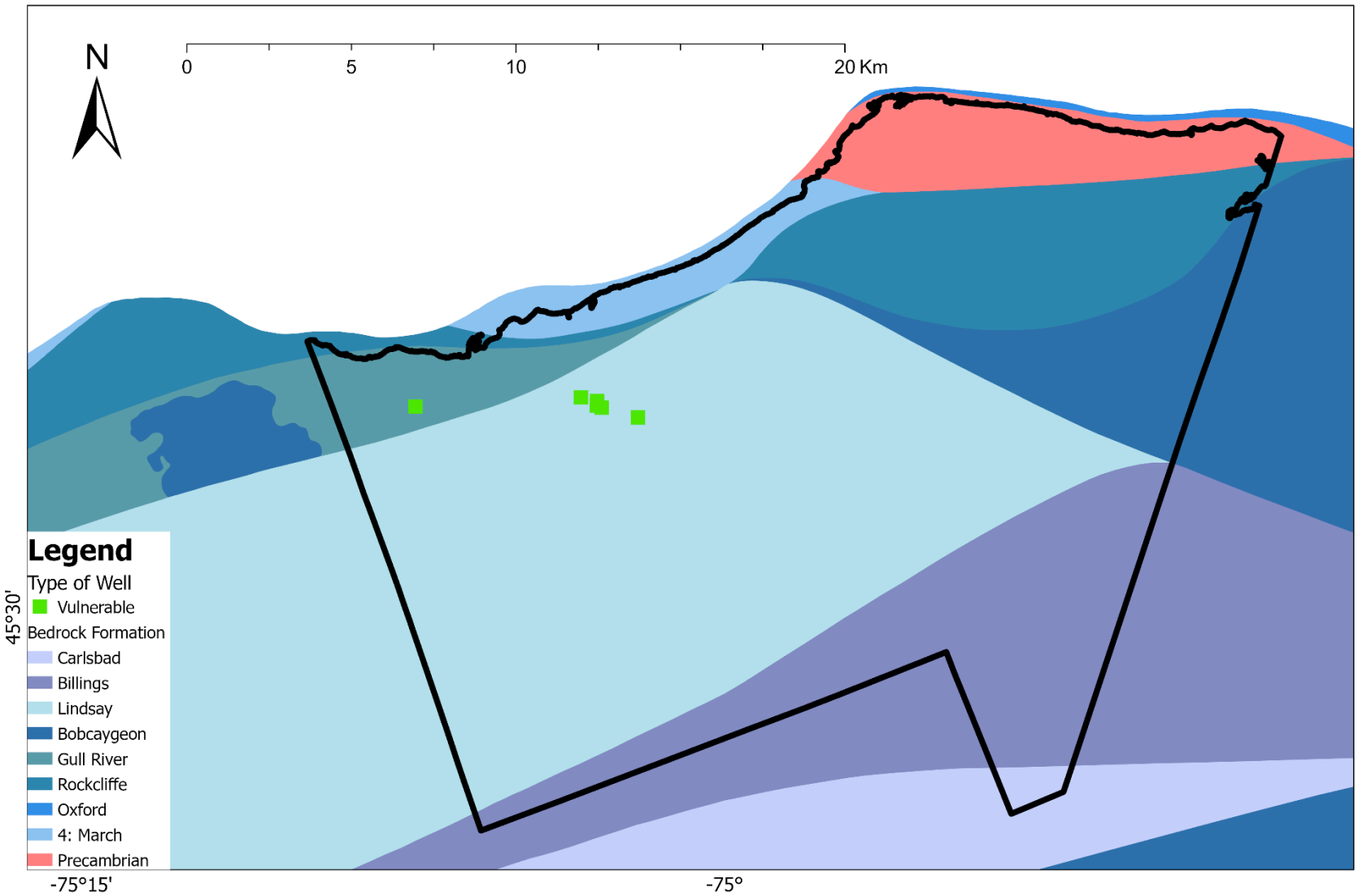

Figure 3-1. Sampling locations for suspended sediment samples in the Township of Alfred & Plantagenet. Universal Transverse Mercator (UTM) co-ordinates provided using North American Datum 1983 (NAD83) in Zone 18N. Geologic data obtained from OGS Miscellaneous Data Release 219.

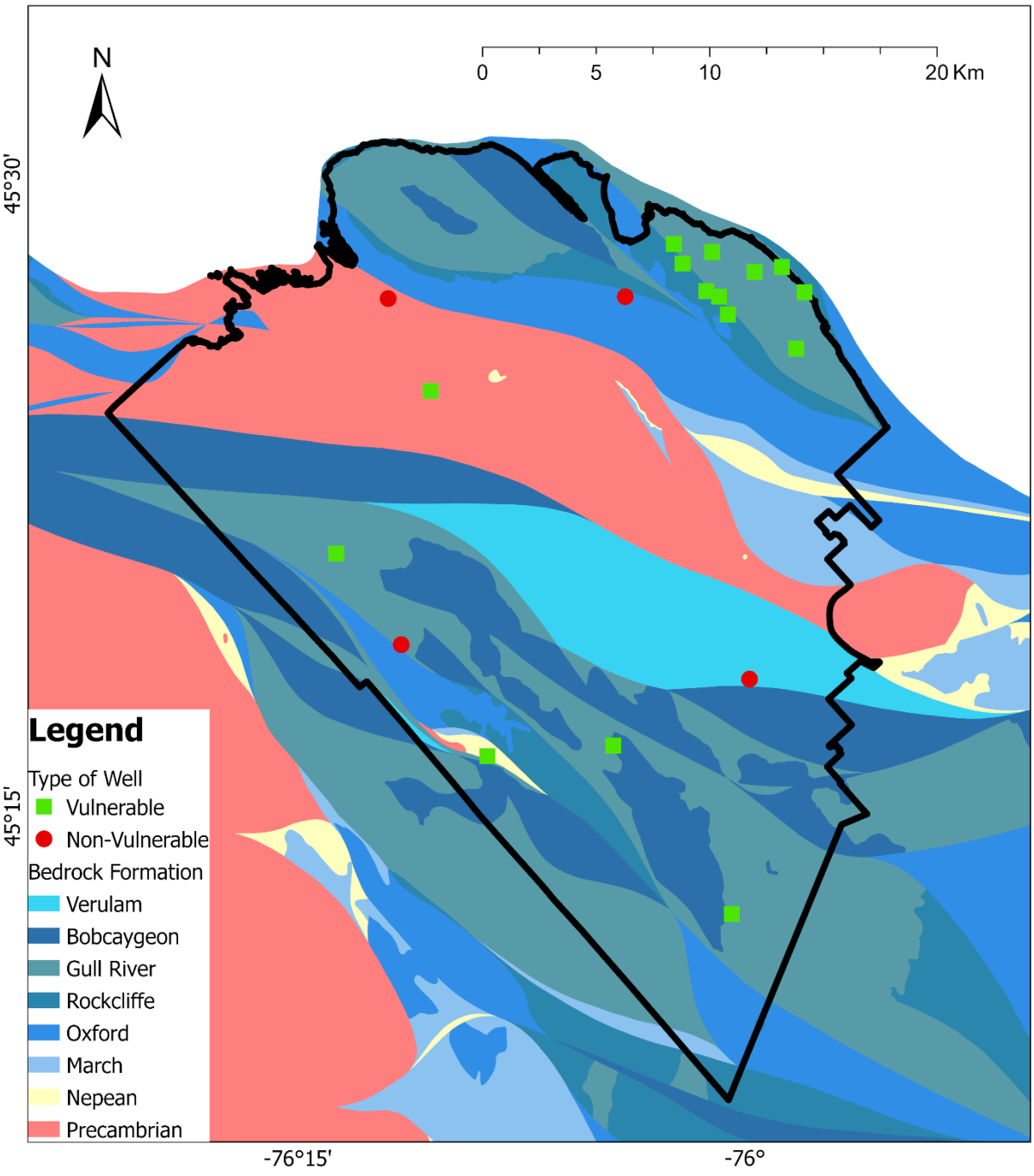

Figure 3-2. Sampling locations for suspended sediment samples in West Rural Ottawa. Universal Transverse Mercator (UTM) co-ordinates provided using North American Datum 1983 (NAD83) in Zone 18N. Geologic data obtained from OGS Miscellaneous Data Release 219.

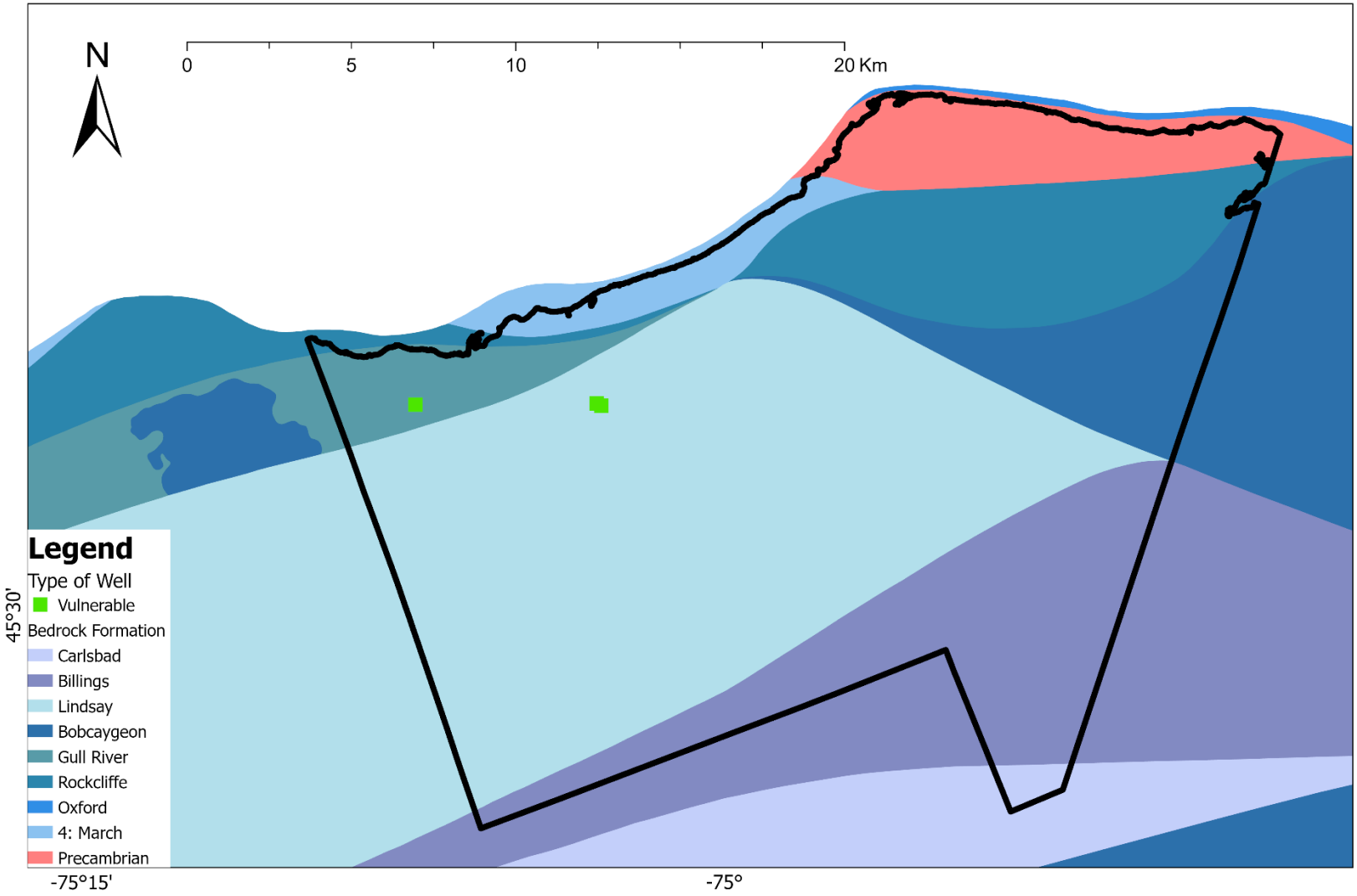

Figure 3-3. Sampling locations for well-bottom sediment samples in the Township of Alfred & Plantagenet. Universal Transverse Mercator (UTM) co-ordinates provided using North American Datum 1983 (NAD83) in Zone 18N. Geologic data obtained from OGS Miscellaneous Data Release 219.

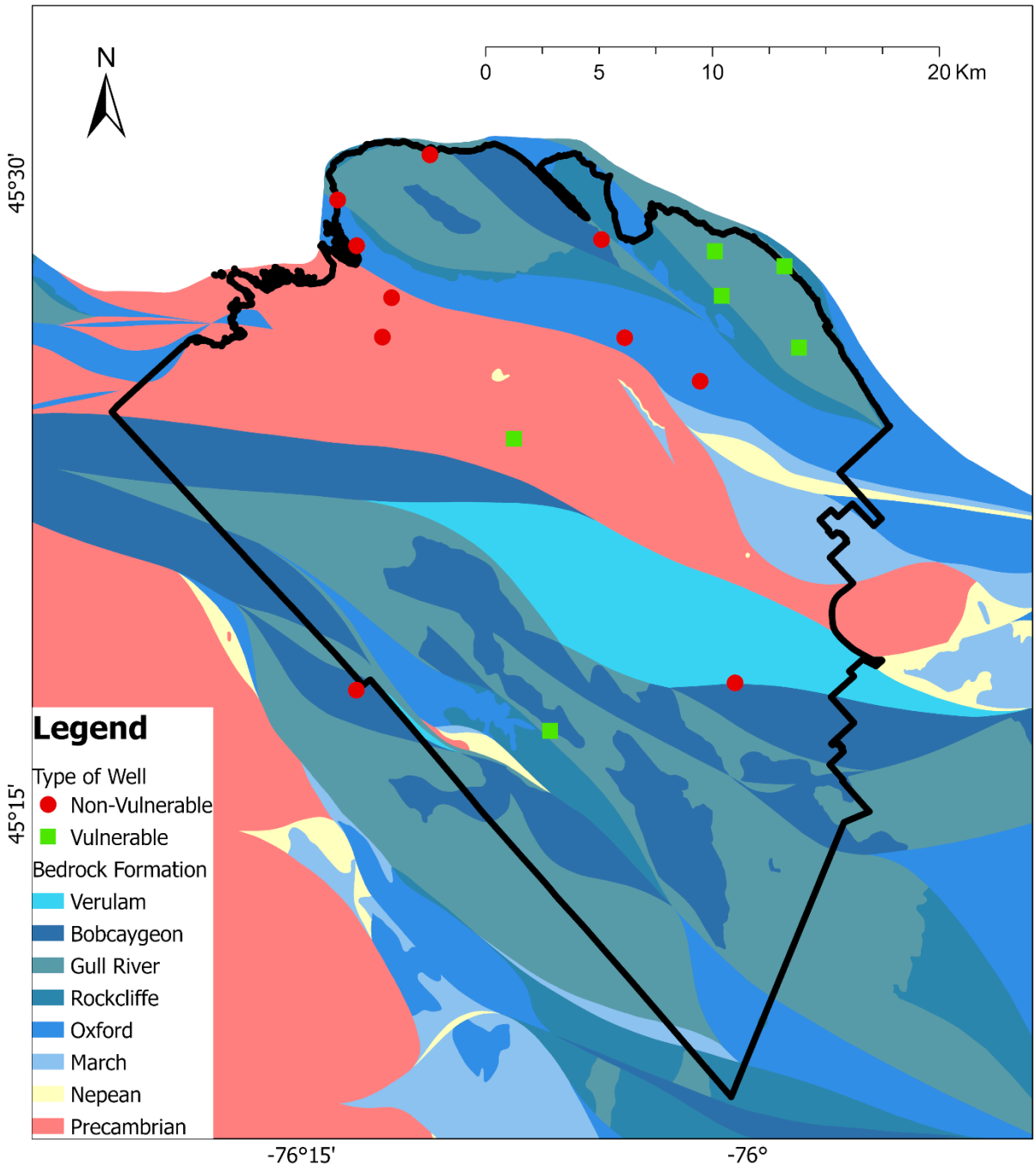

Figure 3-4. Sampling locations for well-bottom sediment samples in West Rural Ottawa. Universal Transverse Mercator (UTM) co-ordinates provided using North American Datum 1983 (NAD83) in Zone 18N. Geologic data obtained from OGS Miscellaneous Data Release 219.

3.2 Suspended Sediment

Measurements of ^{137}Cs range from -36 cps to 42 cps (Figure 3-5A) with data points from all wells falling below the L_D of 50 cps. Negative values in this dataset, and all other ^{137}Cs datasets, result from subtracting the established background values from samples that were detected in such low quantities that they cannot be reliably distinguished from the background. There is no apparent relationship between the depth of the wells (Figure 3-6A) or the overburden thickness and the measurements of ^{137}Cs activity (Figure 3-6A). However, positive values were only found in those wells where the Lindsay or the Gull River Formations were the deepest unit penetrated. As previously mentioned, these formations contain repeating beds of highly fossiliferous interbedded limestone and shale units, which may be susceptible to karstification. The results indicate that measurements of ^{137}Cs cannot be reliably distinguished from the background, so this analytical procedure is not effective at distinguishing between potentially vulnerable and non-vulnerable wells.

Measurements of total ^{210}Pb range from -72 cps to 227 cps and all except one of the values that are greater than the L_D (82 cps) are from potentially vulnerable wells (Figure 3-5B). Negative values in this dataset, and all other ^{210}Pb datasets, result from subtracting the established background values from samples that were detected in such low quantities that they cannot be reliably distinguished from the background. There is no apparent relationship between the depth of the wells (Figure 3-7A) and the measurements of ^{210}Pb, but higher measurements appear to be associated with thinner overburden cover (Figure 3-7B). In those wells where the Lindsay Formation is the deepest unit penetrated, all of the values are above the L_D while values from wells that end in the Gull River, Rockcliffe, and Nepean formations or the Precambrian basement, range widely from -69 cps to 227 cps. These results indicate that the measurements of ^{210}Pb in the samples can be reliably distinguished from the background in some instances and that higher ^{210}Pb values occur in wells that are designated as vulnerable, due to thin overburden. However, since the ^{210}Pb measurements from the suspended sediment did not distinguish between supported and excess ^{210}Pb, it is not possible to determine if the

elevated values in the areas of thin overburden are a result of infiltration of surface-derived, excess ^{210}Pb.

The outcome from the analysis of the suspended sediment samples demonstrates that the total counts are very low which leads to unsatisfactorily high counting error. As a result, methodological improvements were implemented to increase the sediment mass, and thereby total counts, and to distinguish between supported and excess ^{210}Pb.

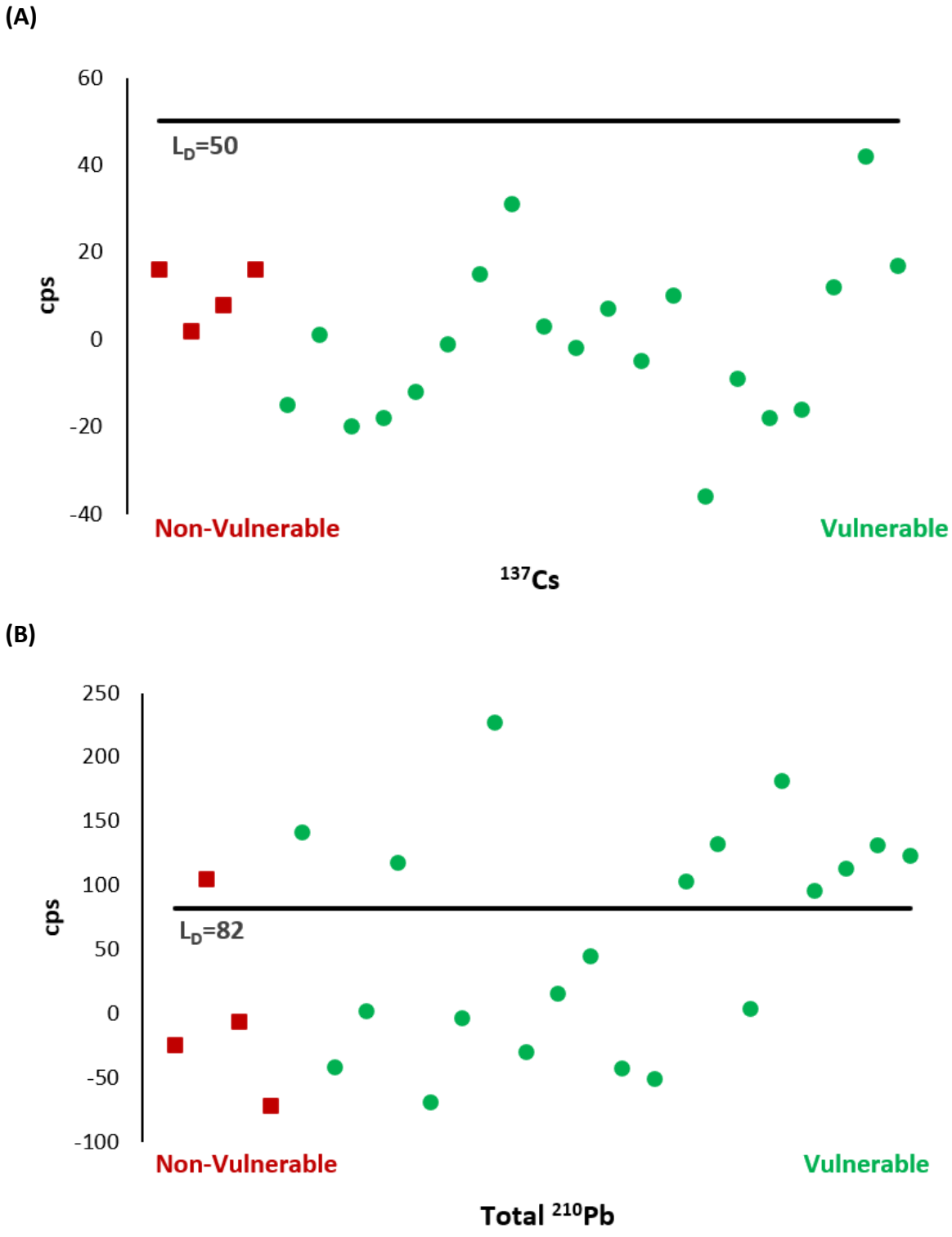

Figure 3-5. Measurements of (A) ^{137}Cs and (B) total ^{210}Pb in suspended sediment samples collected from potentially vulnerable (green circle) and non-vulnerable wells (red square). Black lines indicate the detection limit (L_D) calculated.

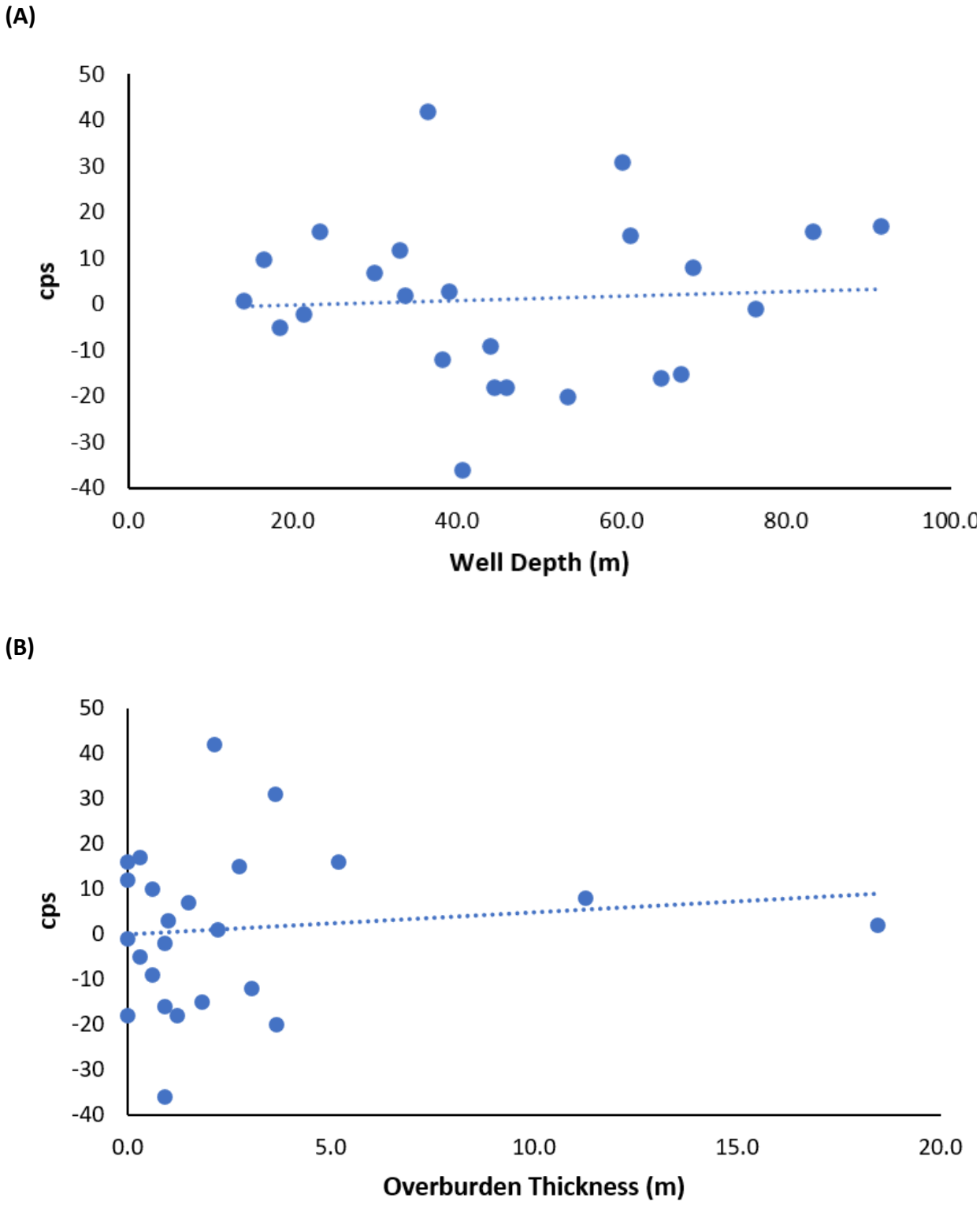

Figure 3-6. Measurements of ^{137}Cs in suspended sediment samples collected from all wells compared to (A) well depth and (B) overburden thickness.

(A)

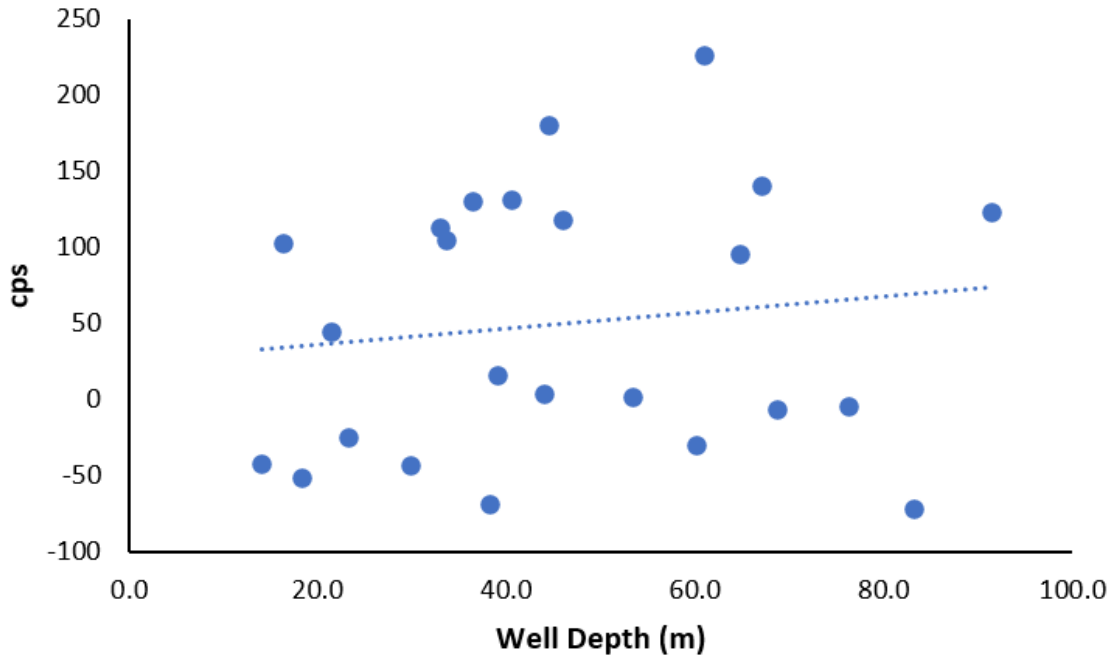

(B)

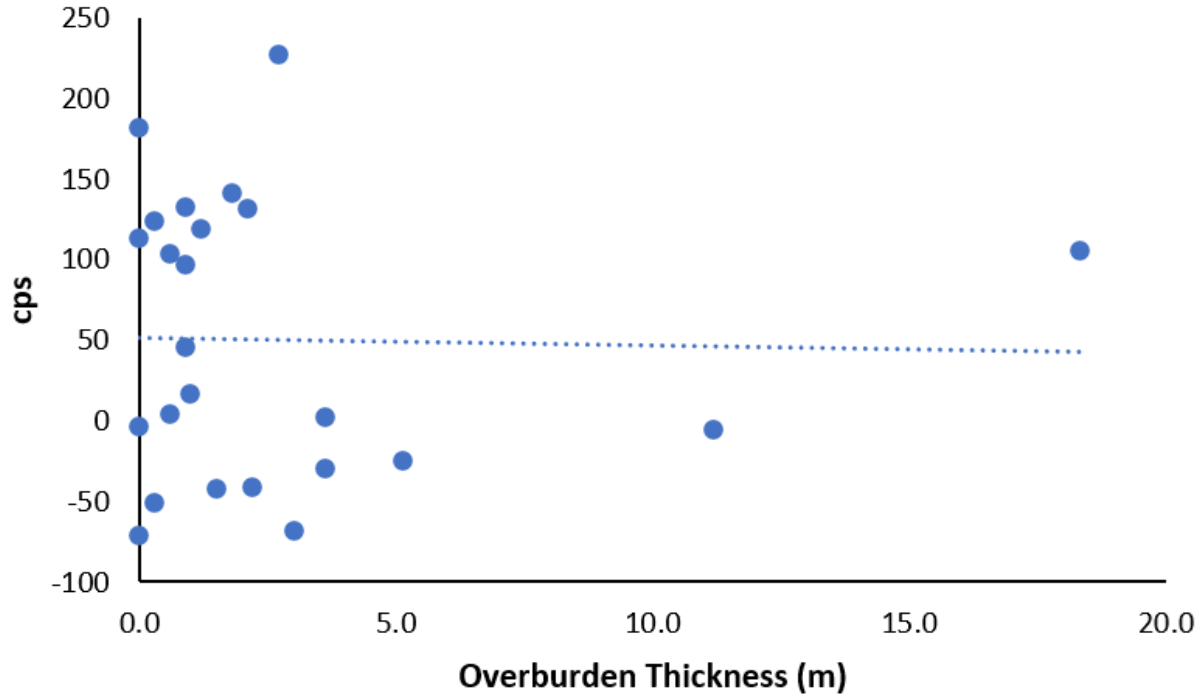

Figure 3-7. Measurements of total ^{210}Pb in suspended sediment samples collected from all wells compared to (A) well depth and (B) overburden thickness.

3.3 Surface Soils and Well-bottom Sediment

Measurements of ^{137}Cs in surface soil samples range from 102 cps to 377 cps (Figure 3-8A). All of the data from the surface soil samples are above the L_D (34 cps). Measurements of ^{137}Cs in well-bottom samples range from -31 cps to 162 cps (Figure 3-8A). The data in Figure 3-8 are not corrected for mass as this presentation allows for the assessment of the measured values with respect to the detection limit. Values for one sample from each of the wells designated as potentially vulnerable and non-vulnerable are also above the L_D. There is no apparent relationship between ^{137}Cs and the depth of the wells (Figure 3-9A) or the overburden thickness (Figure 3-9B). The single detectable data point in a well classified as potentially vulnerable was from a well where the Gull River Formation was the deepest unit penetrated. As previously mentioned, this formation contains repeating beds of highly fossiliferous interbedded limestone and shale units, which may be susceptible to karstification. However, the inability to detect ^{137}Cs in the remainder of the wells suggests that sediment with adsorbed ^{137}Cs is not being transported into the aquifers in sufficient quantities to allow for quantification with this sampling and analytical procedure.

The data in Figure 3-10 are corrected for mass and presented in cps/g, herein referred to as activities. The mean of each population is indicated by the horizontal line. While many of the data points fall below the L_D, a one-way ANOVA was used to test the null hypothesis that all three groups have the same mean value, and that random variation explains the observed differences. The p-value of the one-way ANOVA is 0.019. Therefore, at a threshold of p-value $\leq$ 0.05, the null hypothesis is rejected, suggesting that not all population means are equal. A Tukey's multiple comparison test is used to identify which of the population means differs significantly from the others. The difference in the population means, 95% confidence intervals, and p-values adjusted for multiple comparisons are shown in Figure 3-11. A statistically significant result (p-value $\leq$ 0.05) was only found in the comparison between potentially vulnerable wells and surface soil samples. Therefore, the results suggest that this analytical procedure is not effective at distinguishing between potentially vulnerable and non-vulnerable wells.

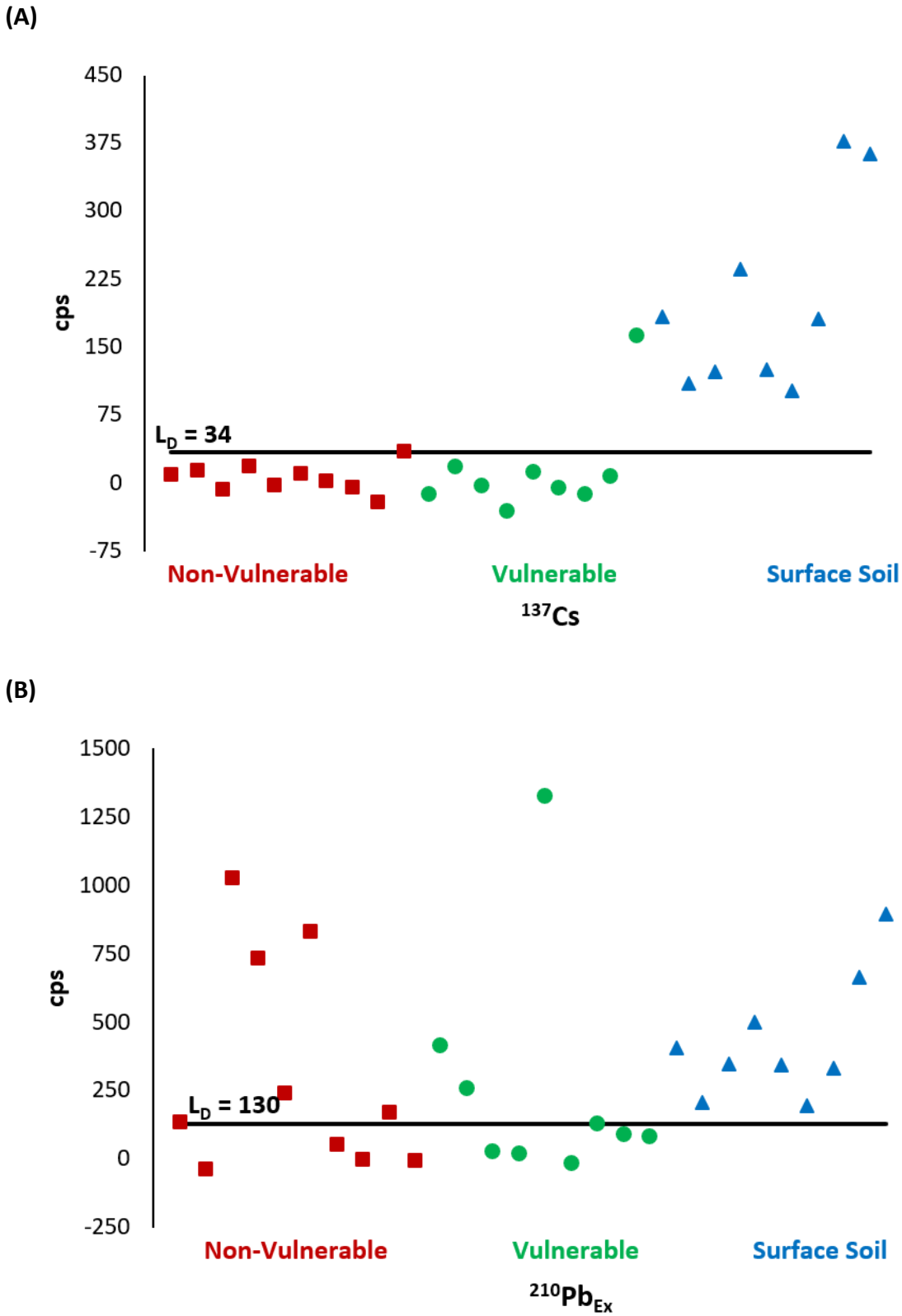

Figure 3-8. Measurements of (A) ^{137}Cs and (B) $^{210}Pb_{Ex}$ in surface soil (blue triangle) and well-bottom sediment samples collected from potentially vulnerable (green circle) and non-vulnerable wells (red square). Black lines indicate the detection limit (L_D) calculated.

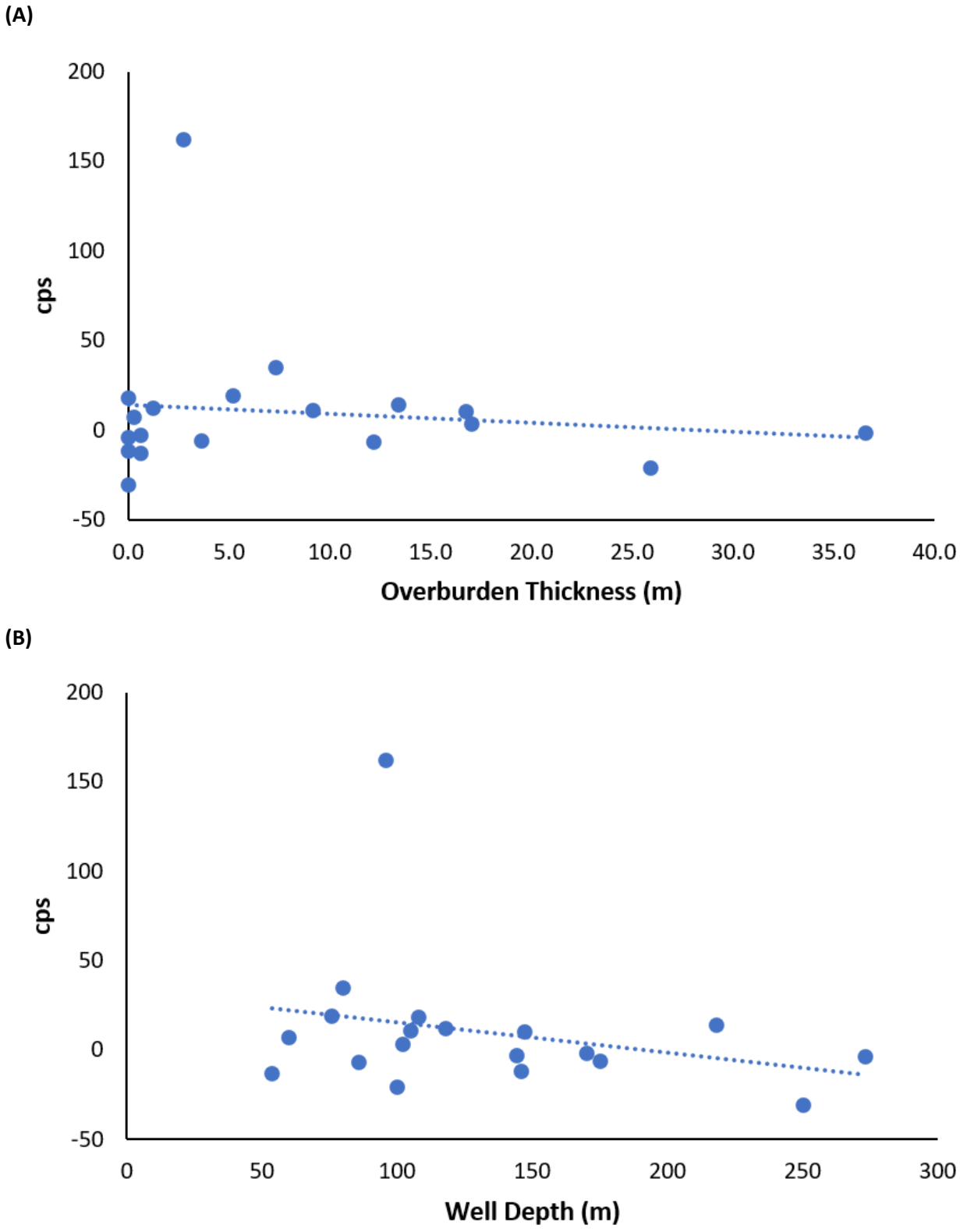

Figure 3-9. Measurements of ^{137}Cs in well-bottom sediment samples collected from all wells compared to (A) well depth and (B) overburden thickness.

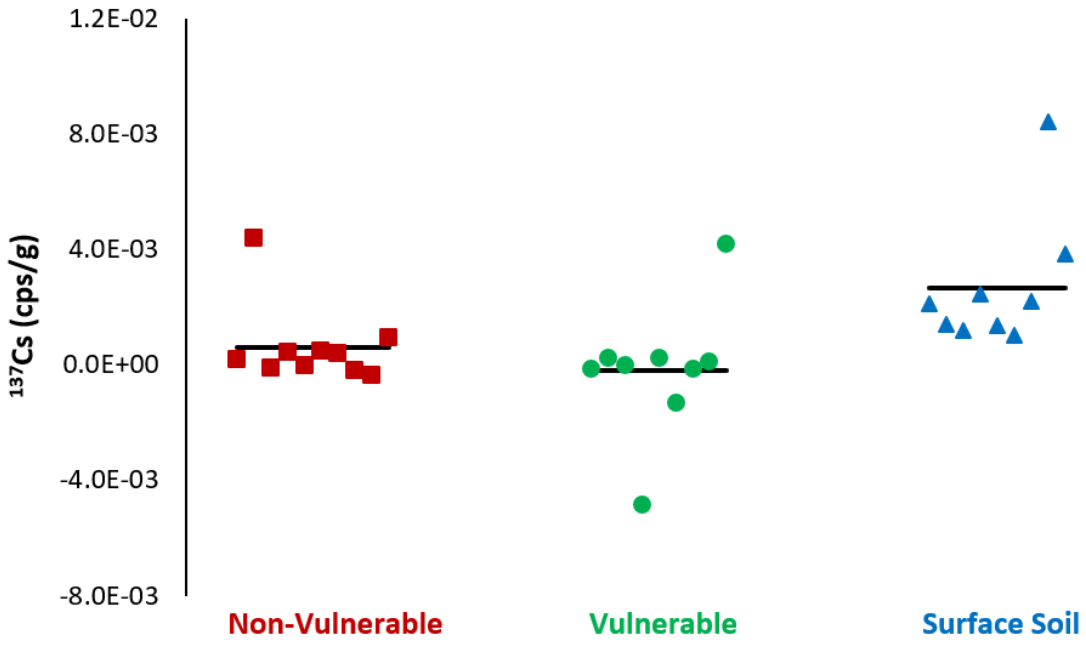

Figure 3-10. Activities of ^{137}Cs in surface soil (blue triangle) and well-bottom sediment samples collected from potentially vulnerable (green circle) and non-vulnerable wells (red square). Black lines indicate the sample mean.

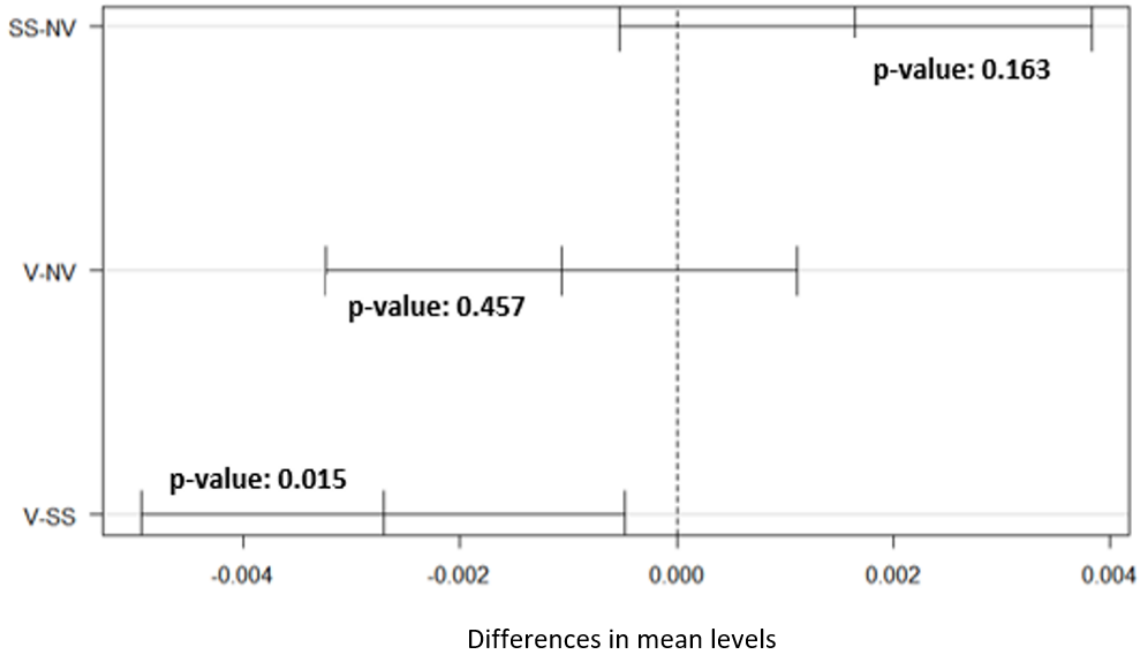

Figure 3-11. Difference in mean levels of ^{137}Cs and 95% confidence intervals for Tukey's multiple comparisons test. "SS" refers to surface soil samples, "NV" refers to potentially non-vulnerable well-bottom sediment samples, and "V" refers to potentially vulnerable well-bottom sediment samples.

Measurements of $^{210}Pb_{Ex}$ in surface soil samples range from 196 cps to 895 cps (Figure 3-8B). All of the data from the surface soil samples are above the L_D (130 cps). Measurements of $^{210}Pb_{Ex}$ in well-bottom samples range from -36 cps to 1324 cps (Figure 3-8B). Most of the data points from the wells classified as potentially vulnerable and non-vulnerable fall below the L_D. The results suggest a relationship with well depth (Figure 3-12A); with elevated activity of $^{210}Pb_{Ex}$ associated with relatively shallow wells, but there is no apparent relationship between $^{210}Pb_{Ex}$ activity and the overburden thickness (Figure 3-12B). In those wells where the Precambrian basement was the deepest unit penetrated, all of the data points are substantially above the L_D. Other data points that are substantially above the L_D include those in wells where the deepest unit penetrated was the Lindsay or Gull River formation. All of the surface soil data points are above the L_D, which demonstrates that $^{210}Pb_{Ex}$ is present at the surface in quantities that are detectable using this analytical procedure. However, the inability to distinguish between vulnerable and non-vulnerable wells on the basis of $^{210}Pb_{Ex}$ activity suggests that the influx of ^{210}Pb with surface-derived suspended sediment cannot be distinguished from $^{210}Pb_{Ex}$ generated from decay of ^{222}Rn that is sourced and transported in the aquifer and subsequently accumulated in the well-bottom sediment.

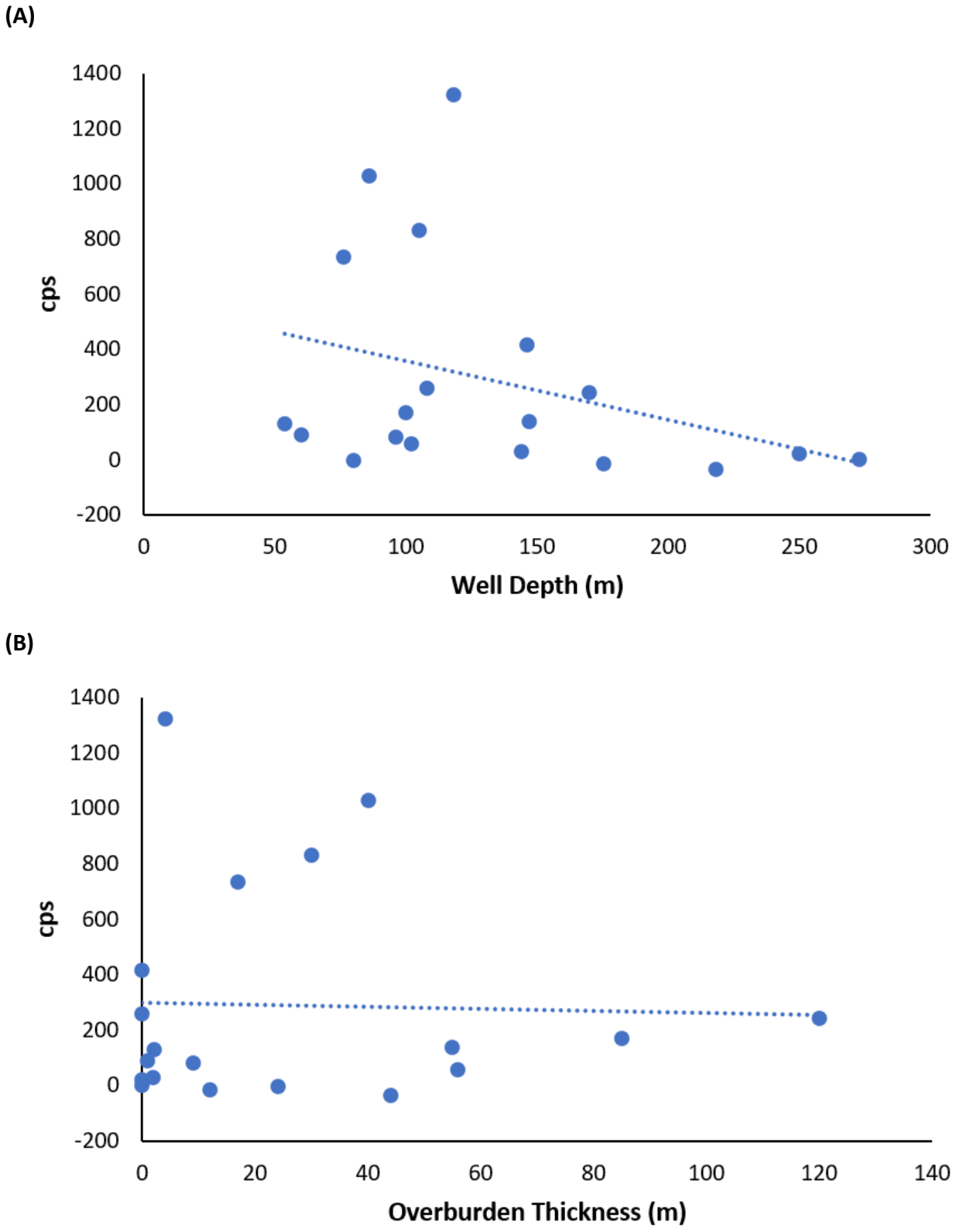

Figure 3-12. Measurements of $^{210}Pb_{Ex}$ in well-bottom sediment samples collected from all wells compared to (A) well depth and (B) overburden thickness.

The data in Figure 3-13 are corrected for mass and presented in cps/g, herein referred to as activities. The mean of each population is indicated by the horizontal line. A one-way ANOVA is used to test the null hypothesis that all three groups have the same mean value of $^{210}Pb_{Ex}$ and random variation explains the difference between the means. The p-value of the one-way ANOVA is 0.433. Therefore, the null hypothesis is not rejected, and the population means are considered to be equal. The results suggest that this analytical procedure is not effective at distinguishing between potentially vulnerable and non-vulnerable wells.

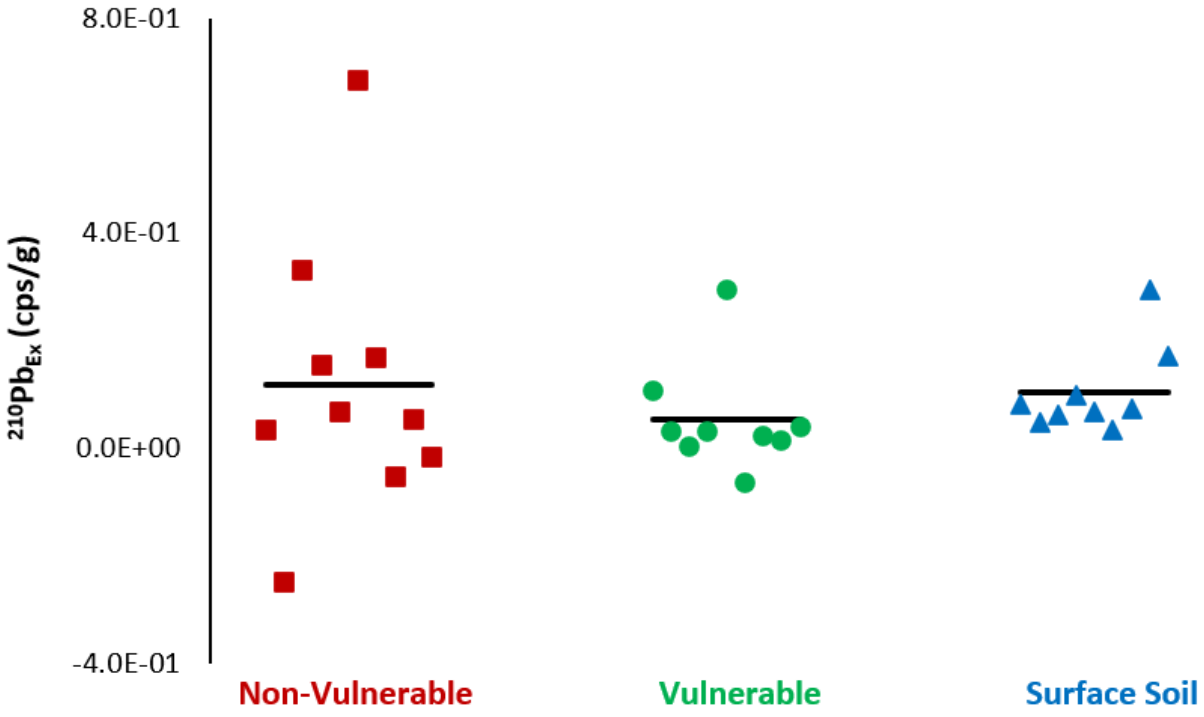

Figure 3-13. Activities of $^{210}Pb_{Ex}$ in surface soil (blue triangle) and well-bottom sediment samples collected from potentially vulnerable (green circle) and non-vulnerable wells (red square). Black lines indicate the sample mean.

3.4 Mobility of Radionuclides

3.4.1 ^{137}Cs

The contrast between activity of ^{137}Cs in the well-bottom sediment samples versus the surface soil samples indicates that the low levels of ^{137}Cs activity reported in the well-bottom sediment samples result from ineffective transport from the surface to the depths of the aquifers. Since the origin of ^{137}Cs in overburden material is exclusively from atmospheric fallout, it is expected that the first barrier in downward infiltration results from characteristics of the soil profile.

It may be that even in areas with thin overburden cover, there is not adequate physical redistribution of soil particles to facilitate the movement of ^{137}Cs adsorbed to particulate fractions into the underlying aquifer. Jagercikova et al. (2015) compiled ninety-nine vertical ^{137}Cs soil profiles sampled from varying locations in the Northern hemisphere between 1992 and 2007. It was found that the depth of the ^{137}Cs activity peak was between 0 cm and 12 cm, while the maximum depth at which ^{137}Cs was detectable ranged from 12 cm to 60 cm (Jagercikova et al., 2015). This is consistent with Abraham et al. (2018) who reported that at a site with high-infiltration in Germany, the peak of ^{137}Cs activity in the soil profile was found between 6 cm and 9 cm, and the maximum detectable activity at a depth of 84 cm. A third study that considered forty-five Hungarian soil monoliths ranging from 0 cm to 150 cm in depth, reported that detectable activities of ^{137}Cs were only present in the upper 30 cm of the profiles (Szabo et al., 2012). These studies support the explanation that where overburden material covers vulnerable fractured or karst bedrock aquifers, ^{137}Cs may not migrate to a depth where infiltration to underlying aquifers can occur.

In areas where there is no overburden cover, it may be that ^{137}Cs migration is inhibited by other physical factors. For instance, the mobile colloidal and particulate fractions may accumulate within the irregularities of fracture surfaces, terminal flow paths, or other void spaces. Factors related to well construction such as the depth of the well casing or the length of the screen may also impact migration of fine particulates into the well-bottom. Additionally, even though preferential flow paths exist in fractured bedrock and karst aquifers, it may be that the

adsorbed ^{137}Cs on fine particulates is not transported along these high permeability fractures to the extent that measurable amounts can accumulate in the well-bottom.

3.4.2 ^{210}Pb

The results demonstrate that the measured net counts of $^{210}Pb_{Ex}$ are not an effective indicator of potentially vulnerable and non-vulnerable wells. The low levels of ^{210}PbEx reported in the potentially vulnerable well-bottom samples and the statistically insignificant difference between the potentially non-vulnerable well-bottom samples suggest that this may be due to the mobility of the parent ^{222}Rn in the aquifer system. As shown in Figure 1-4, ^{222}Rn gas is released from the decay of a ^{226}Ra atom. Though ^{226}Ra does not easily diffuse, a significant activity of ^{226}Ra can accumulate along fracture surfaces, due to its long half-life of 1600 years, where it adsorbs onto ion exchange minerals (Wood et al., 2004). When the ^{226}Ra in the mineral matrix decays to the daughter ^{222}Rn it becomes more readily diffusible and is released to the groundwater and to fracture voids in the unsaturated zone. Also, when the ^{226}Ra atom decays to ^{222}Rn, the energy generated can carry the ^{222}Rn recoil nucleus approximately 40 nm, resulting in one of three scenarios (Figure 3-14): (1) it can travel this distance and remain embedded within the same grain; (2) it can migrate into an adjacent grain; or (3) it can be released into an open pore space (Tanner, 1980; Schumann, 1993; Krupp et al., 2017). As such, a distance of only a few millimeters from the fracture's edge can reasonably contribute to the total ^{222}Rn concentration within the aquifer void space or groundwater (Skeppström and Olofsson, 2007). The ratio of the number of radon atoms that remain embedded within a radium-bearing grain to the number of radon atoms emitted is called the radon emanation coefficient (REC).

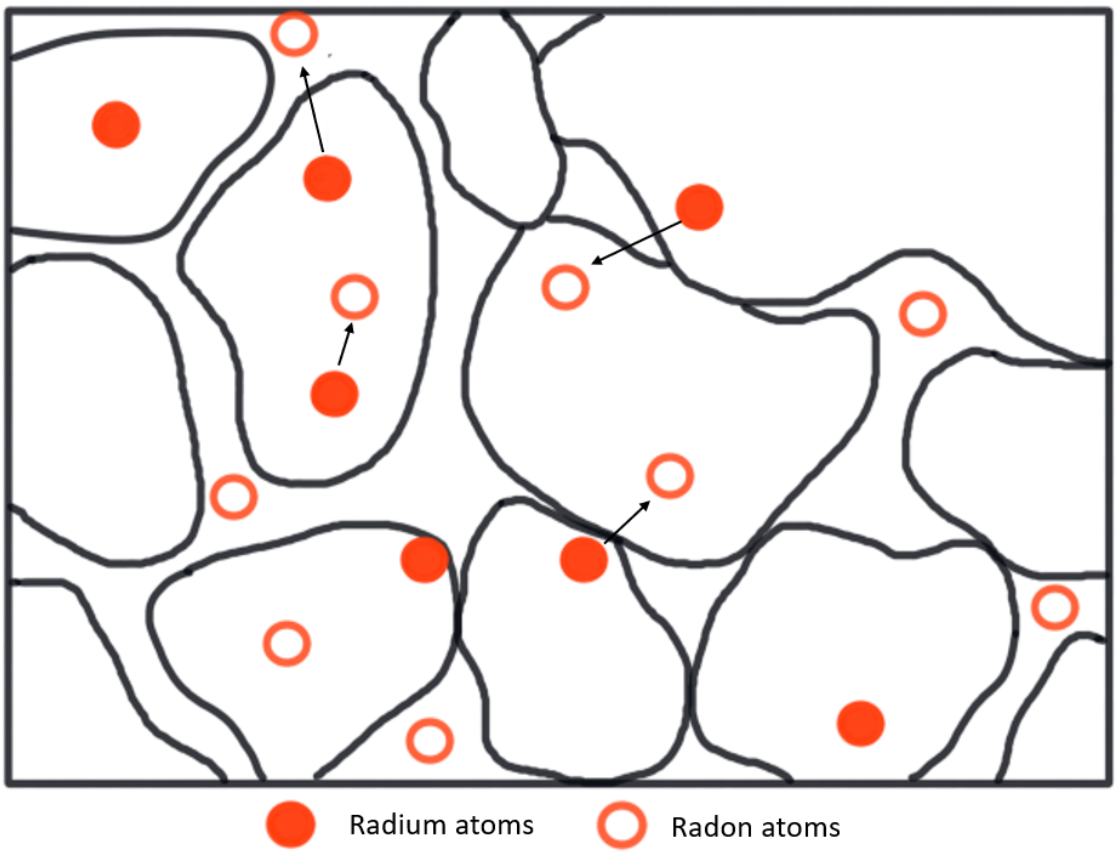

Figure 3-14. Conceptual diagram depicting three possible scenarios resulting from radium decay (modified from Tanner, 1980).

The emitted radon atoms can then dissolve into flowing groundwater or partition into an available gas phase, such as in void spaces, fractures, or the well bore. Radon-222 gas can be carried short distances by diffusion and to longer distances by advection (Skeppström and Olofsson, 2007; Gregoric et al., 2013). As the concentration of radon in groundwater is many orders of magnitude too small to migrate independently by advection, it is suggested that radon becomes mixed with a primary carrier gas such as CO_2, CH_4 or N_2 during transport (Somogyi and Lenart 1986; Malmqvist et al., 1989; Etiope and Martinelli, 2002). This mode of transport may be limited as it requires a relatively fast-moving advective fluid (Etiope and Martinelli, 2002). Advective transport may be further limited in recharge areas where the upflow of gases is inhibited by the movement of water (Gascoyne et al., 1992). Taken together, it is likely that in some instances ^{222}Rn is unable to penetrate the overburden material and escape into the atmosphere. Instead, it is transported from the source region, but remains

trapped in the subsurface, such as in the well bore, where it decays in the sub-surface gas phases and creates a source for $^{210}Pb_{Ex}$ (Figure 3-15). This makes it impossible to distinguish between the $^{210}Pb_{Ex}$ generated in this manner from that which has been transported into the aquifer as atmospheric fallout. This proposed mechanism may account for the similarity between the $^{210}Pb_{Ex}$ group means in potentially vulnerable and non-vulnerable well samples. The $^{210}Pb_{Ex}$ population mean in the surface soils may be attributable to a variety of factors that impact RECs. Two important factors that control the soil's REC are grain size and grain shape, as they influence the concentration of ^{226}Ra close enough to the grain's surface to allow for ^{222}Rn emanation (Schumann, 1993). Other factors include the concentration and distribution of ^{226}Ra, the internal porosity of the grain, and the presence of impurities in the crystal lattice (Krupp et al., 2017).

The low activities reported in all of the samples may be due to a combination of low RECs and low concentrations of ^{226}Ra in the areas sampled. The latter view is supported by the fact that the three potentially non-vulnerable data points found above the L_Q were all collected from wells where the deepest unit penetrated was the Precambrian Formation. Due to its metamorphic and igneous nature, it is likely that this formation contains more ^{238}U, and thus ^{226}Ra, than the other formations found within the study areas. The analytical procedure may also be responsible for the low activities of $^{210}Pb_{Ex}$ reported in the samples. As previously mentioned, self-adsorption of γ-emissions by the sample is a principal difficulty in low energy gamma spectroscopy and no corrections were made to the data to account for this. Further, the low branching yield for ^{210}Pb at the 46.65 keV γ-emission and the relatively small sample mass, may have contributed to the procedure being insufficiently precise to yield an adequate quantitative estimate of excess ^{210}Pb activity.

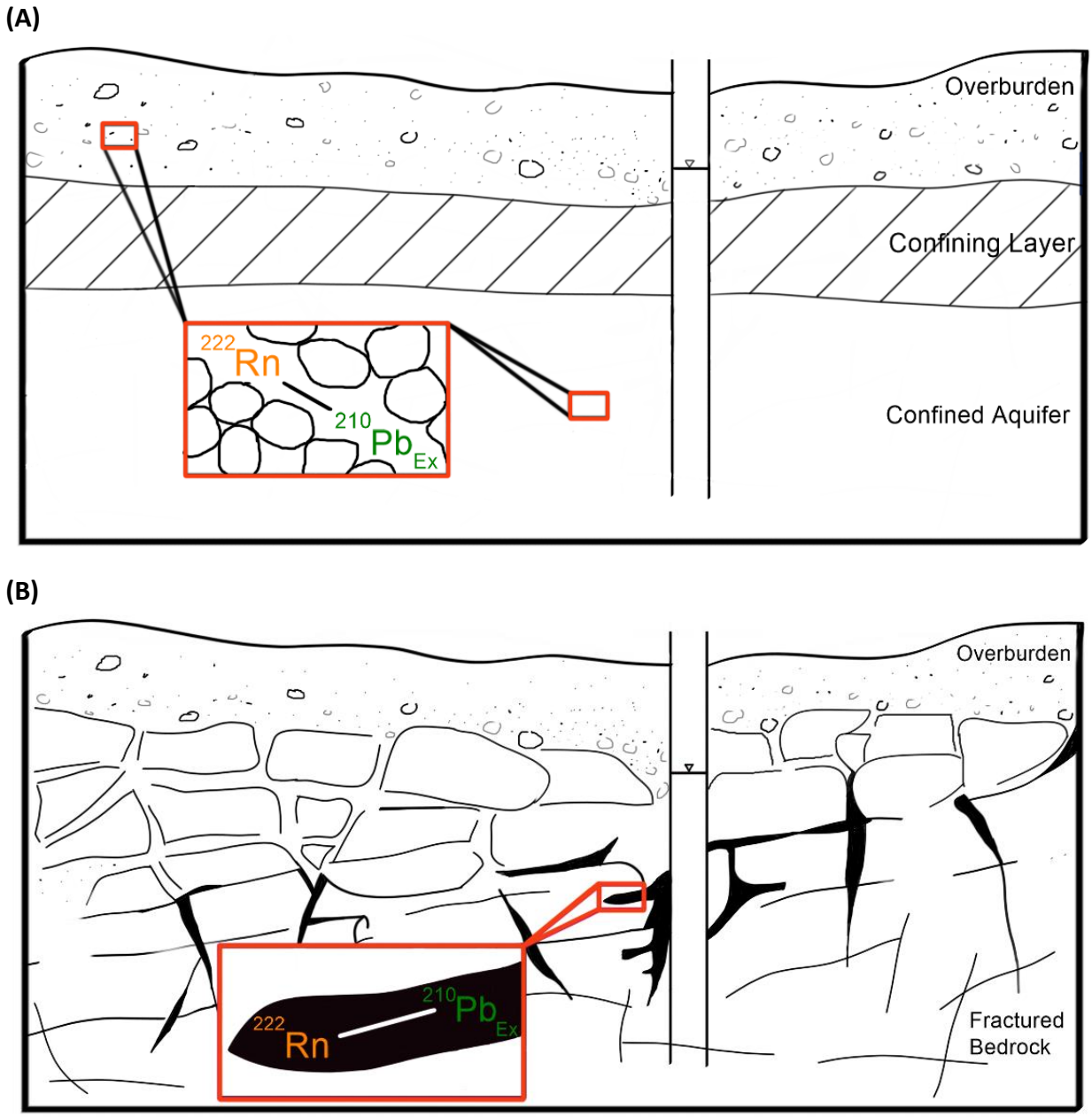

Figure 3-15. Conceptual model describing controls on the distribution of $^{210}Pb_{Ex}$ in vulnerable and non-vulnerable bedrock aquifers. Decay of ^{222}Rn occurring in (A) void space and (B) fractures. Diagrams are not to scale.

4. Conclusions

This study tested the potential for a novel geochemical method using ^{137}Cs and $^{210}Pb_{Ex}$ to assess aquifer vulnerability in fractured and karst bedrock aquifers. The long-term mobility of both ^{137}Cs and ^{210}Pb are predominantly associated with physical redistribution of soil particles, as both radionuclides have the tendency to strong and rapidly adsorb to clay minerals and organic matter.

Analysis of suspended sediment samples demonstrated low total counts and thus poor analytical precision. However, in some instances the measurements of total ^{210}Pb were reliably distinguished from the background and found to occur in wells in areas with thinner overburden over bedrock.

The methodology was improved by collecting larger masses of sediment from the bottom of wells, allowing better analytical precision. Analysis of surface soil samples demonstrated that both ^{137}Cs and $^{210}Pb_{Ex}$ are present at the surface in detectable quantities. However, the inability to detect ^{137}Cs in the well-bottom sediment samples indicates that sediment with adsorbed ^{137}Cs was not transported into the aquifers in sufficient quantities to allow for quantification. Additionally, the influx of ^{210}Pb with surface-derived suspended sediment cannot be distinguished from $^{210}Pb_{Ex}$ generated from the decay of ^{222}Rn that is sourced and transported in the aquifer. The results from the analysis by gamma spectroscopy suggest that the geogenic origin of $^{210}Pb_{Ex}$ and the hydrologic and geologic controls inhibiting downward mobility of ^{137}Cs prevent the use of these radionuclides as reliable indicators of aquifer vulnerability.

The results from the hierarchical elimination of domestic wells in West Rural Ottawa indicate potentially vulnerable wells in areas of fractured and karst bedrock aquifers with thin overburden. Future research may succeed in identifying and developing additional techniques to improve vulnerability assessment methods in these geologic settings.

References

Abbott, M. D., Lini, A., & Bierman, P. R. (2000). $\delta^{18}O$, δD and 3H measurements constrain groundwater recharge patterns in an upland fractured bedrock aquifer, Vermont, USA. *Journal of Hydrology*, 12.

Abraham, J., Meusburger, K., Waldis, J. K., Ketterer, M. E., & Zehringer, M. (2018). Fate of 137 Cs, 90 Sr and 239+240 Pu in soil profiles at a water recharge site in Basel, Switzerland. *Journal of Environmental Radioactivity*, *182*, 85–94. https://doi.org/10.1016/j.jenvrad.2017.11.019

Allen, M. J., & Morrison, S. M. (1973). Bacterial Movement Through Fractured Bedrock. *Ground Water*, *11*(2), 6–10. https://doi.org/10.1111/j.1745-6584.1973.tb02960.x

Aller, L., Bennett, T., Lehr, J. H., Petty, R. J., & Hackett, G. (1987). DRASTIC: A standardized system for evaluating ground water pollution using hydrogeological settings. *United States Environmental Protection Agency*, 641.

Armstrong, D.K. & Dodge, J.E.P. (2007). Paleozoic geology of southern Ontario: Project summary and technical document. *Ontario Geological Survey*, Miscellaneous Release – Data 219.

Auckenthaler, A., Raso, G., & Huggenberger, P. (2002). Particle transport in a karst aquifer: Natural and artificial tracer experiments with bacteria, bacteriophages and microspheres. *Water Science and Technology*, *46*(3), 131–138. https://doi.org/10.2166/wst.2002.0072

Benninger, L. K., Lewis, D. M., & Turekian, K. K. (1975). The Use of Natural Pb-210 as a Heavy Metal Tracer in the River—Estuarine System. In T. M. Church (Ed.), *Marine Chemistry in the Coastal Environment* (Vol. 18, pp. 202–210). AMERICAN CHEMICAL SOCIETY. https://doi.org/10.1021/bk-1975-0018.ch012

Berkowitz, B. (2002). Characterizing flow and transport in fractured geological media: A review. *Advances in Water Resources*, *25*(8–12), 861–884. https://doi.org/10.1016/S0309-1708(02)00042-8

Brunton, F.R. & Dodge, J.E.P. 2008. Karst of southern Ontario and Manitoulin Island; *Ontario Geological Survey*, Groundwater Resources Study 5, 99.

Buddemeier, R. W., & Hunt, J. R. (1988). Transport of colloidal contaminants in groundwater: Radionuclide migration at the Nevada test site. *Applied Geochemistry*, *3*(5), 535–548. https://doi.org/10.1016/0883-2927(88)90025-X

Catani, V., Zuzolo, D., Esposito, L., Albanese, S., Pagnozzi, M., Fiorillo, F., De Vivo, B., & Cicchella, D. (2020). A New Approach for Aquifer Vulnerability Assessment: The Case Study of Campania Plain. *Water Resources Management*, *34*(2), 819–834. https://doi.org/10.1007/s11269-019-02476-5

Chapman, L. J. & Putnam, D. F. (1984). *The Physiography of Southern Ontario*, (3rd ed., Vol 4). Ontario Geological Survey.

City of Ottawa. (2011). "Characterization of Ottawa's watersheds: an environmental foundation document with supporting information base". Retrieved online from: https://app06.ottawa.ca/calendar/ottawa/citycouncil/ec/2012/01-17/05-Document%201%20EN%20-%20watershed_report_en%5b1%5d.pdf on Nov 24, 2021.

Colgrove, L. M. (2016). *A Regional Chemical Characterization and Analysis of Groundwater in Eastern Ontario*. [Master's thesis, University of Western Ontario].

Conboy, M. J., & Goss, M. J. (2000). Natural protection of groundwater against bacteria of fecal origin. *Journal of Contaminant Hydrology*, *43*(1), 1–24. https://doi.org/10.1016/S0169-7722(99)00100-X

Currie, L. A. (1963). Limits for Qualitative Detection and Quantitative Determination. *Application to Radiochemistry*, 40(3), 586-593.

Dahlman, R.C., C.W. Francis, & T. Tamura. (1975). Radiocesium cycling in vegetation and soil. In F.G. Howell et al. (Eds.) *US ERDA Symposium Series CONF-740513,* 462-481.

Davis, J. J. (1963). Cesium and its relationship to potassium in ecology. In V. Schultz and A.W. Klement, Jr. (Eds.), *Radioecology*, 539-556.

Davis, R. B., Hess, C. T., Norton, S. A., Hanson, D. W., Hoagland, K. D., & Anderson, D. S. (1984). ^{137}Cs and ^{210}Pb dating of sediments from soft-water lakes in New England (U.S.A.) and Scandinavia, a failure of ^{137}Cs dating. *Chemical Geology*, *44*(1–3), 151–185. https://doi.org/10.1016/0009-2541(84)90071-8

Di Stefano, E., Clemenza, M., Baccolo, G., Delmonte, B., & Maggi, V. (2019). ^{137}Cs contamination in the Adamello glacier: Improving the analytical method. *Journal of Environmental Radioactivity*, *208–209*, 106039. https://doi.org/10.1016/j.jenvrad.2019.106039

Doerfliger, N., Jeannin, P.-Y., & Zwahlen, F. (1999). Water vulnerability assessment in karst environments: A new method of defining protection areas using a multi-attribute approach and GIS tools (EPIK method). *Environmental Geology*, *39*(2), 165–176. https://doi.org/10.1007/s002540050446

Dyck, A., Redmond, B., Al, T., Crowley, J.W., Silliker, R. J., & Brunton, F. (2019). *Karst Aquifers and Groundwater Vulnerability: A Natural-Tracer Case Study in Eastern Ontario, Canada*. [Unpublished undergraduate thesis]. University of Ottawa.

Einsiedl, F. (2005). Flow system dynamics and water storage of a fissured-porous karst aquifer characterized by artificial and environmental tracers. *Journal of Hydrology*, *312*(1–4), 312–321. https://doi.org/10.1016/j.jhydrol.2005.03.03.

Environment Canada. (2013). "Water sources: groundwater". Retrieved online from: https://www.canada.ca/en/environment-climate-change/services/water-overview/sources/groundwater.html on Nov 24, 2021.

Environment Canada. (2021). Canadian Climate Normals 1981-2010 Station Data: Ottawa CDA. Retrieved online from: https://climate.weather.gc.ca/climate_normals/index_e.html on Nover 24, 2021.

Etiope, G., & Martinelli, G. (2002). Migration of carrier and trace gases in the geosphere: An overview. *Physics of the Earth and Planetary Interiors*, *129*(3–4), 185–204. https://doi.org/10.1016/S0031-9201(01)00292-8

Flury, M., Mathison, J. B., & Harsh, J. B. (2002). In Situ Mobilization of Colloids and Transport of Cesium in Hanford Sediments. *Environmental Science & Technology*, *36*(24), 5335–5341. https://doi.org/10.1021/es025638k

Ford, D., & Williams, P. W. (2007). *Karst hydrogeology and geomorphology* (Rev. ed.). John Wiley & Sons.

Foster, S. (1987). Fundamental Concepts in Aquifer Vulnerability, Pollution Risk and Protection Strategy. In W. Van Van Duijevenboden and H.G. Van Waegeningh (Eds.), *TNO Committee on Hydrogeological Research Proceedings and Information*, 38(1), 69-86.

Foster, S., Hirata, R., & Andreo, B. (2013). The aquifer pollution vulnerability concept: Aid or impediment in promoting groundwater protection? *Hydrogeology Journal*, *21*(7), 1389–1392. https://doi.org/10.1007/s10040-013-1019-7

Freeze, R. A., & Cherry, J. A. (1979). *Groundwater*. Prentice-Hall.

Froidevaux, P., Steinmann, P., & Pourcelot, L. (2010). Long-Term and Long-Range Migration of Radioactive Fallout in a Karst System. *Environmental Science & Technology*, *44*(22), 8479–8484. https://doi.org/10.1021/es100954h

Fulton, R. J. (1987). *Quaternary geology of the Ottawa region, Ontario and Quebec* (No. 86–23). https://doi.org/10.4095/122374.

Gascoyne, M., Wuschke, D. M., & Durrance, E. M. (1993). Fracture detection and groundwater flow characterization using He and Rn in soil gases, Manitoba, Canada. *Applied Geochemistry*, *8*(3), 223–233. https://doi.org/10.1016/0883-2927(93)90037-H

Goldscheider, N., Klute, M., Sturm, S., & Hötzl, H. (2000). *The PI method – a GIS-based approach to mapping groundwater vulnerability with special consideration of karst aquifers*. 17.

Goldscheider, N., Meiman, J., Pronk, M., & Smart, C. (2008). Tracer tests in karst hydrogeology and speleology. *International Journal of Speleology*, *37*(1), 27–40. https://doi.org/10.5038/1827-806X.37.1.3

Gregoric, A., Vaupotic, J., Kardos, R., Horvath, M., Bujtor, T., & Kovacs, T. (2013). Radon Emanation of Soiles From Different Lithological Units. *Carpathian Journal of Earth and Environmental Sciences*, 8(2), 185-190.

Grolimund, D., Borkovec, M., Barmettler, K., & Sticher, H. (1996). Colloid-Facilitated Transport of Strongly Sorbing Contaminants in Natural Porous Media: A Laboratory Column Study. *Environmental Science & Technology*, *30*(10), 3118–3123. https://doi.org/10.1021/es960246x

Gustafsson, P. (1994). Spot Satellite Data For Exploration Of Fractured Aquifers In A Semi-Arid Area In Southeastern Botswana. *Hydrogeology Journal*, *2*(2), 9–18. https://doi.org/10.1007/s100400050246.

Hamilton, S. M., Brunton, F. R., & Priebe, E. H. (2017). *Regional-scale mapping of buried, surface-connected, karstic groundwater systems using dissolved CO2-O2 in groundwater*. 8.

Hamilton, S.M. & Lee, V.L. (2012). Summary of Fieldwork and Other Activities: Description and mitigation of domestic well sampling biases. *Ontario Geological Survey*, Open file report 6280. 36(1), 36-15.

Hirose, K., Igarashi, Y., & Aoyama, M. (2008). Analysis of the 50-year records of the atmospheric deposition of long-lived radionuclides in Japan. *Applied Radiation and Isotopes*, *66*(11), 1675–1678. https://doi.org/10.1016/j.apradiso.2007.09.019

International Atomic Energy Association (IAEA), 2019. Live Chart of Nuclides. Retried on Jul 04, 2022 from Nuclear Structure and Decay Data.

Iqbal, M. Z., & Krothe, N. C. (1995). Infiltration mechanisms related to agricultural waste transport through the soil mantle to karst aquifers of southern Indiana, USA. *Journal of Hydrology*, *164*(1–4), 171–192. https://doi.org/10.1016/0022-1694(94)02573-T

Jagercikova, M., Cornu, S., Le Bas, C., & Evrard, O. (2015). Vertical distributions of 137Cs in soils: A meta-analysis. *Journal of Soils and Sediments*, *15*(1), 81–95. https://doi.org/10.1007/s11368-014-0982-5

Joel, G. S. C., Penabei, S., Maurice, N. M., Gregoire, C., Jilbert, N. M. E., Didier, T. S., & David, S. (2017). *Optimal measurement counting time and statistics in gamma spectrometry analysis: The time balance*. 100001. https://doi.org/10.1063/1.4969040.

Johnson, M.D., Armstrong, D.K., Sandford, B.V., Telford, P.G., & Rutka, M.A. (1992). Geology of Ontario; Paleozoic and Mesozoic Geology of Ontario (2nd ed., Vol 4). Ontario Geological Survey.

Joshi, S. R. (1987). Nondestructive determination of lead-210 and radium-226 in sediments by direct photon analysis. *Journal of Radioanalytical and Nuclear Chemistry Articles*, *116*(1), 169–182. https://doi.org/10.1007/BF02037220

Karamanos, R. E., Bettany, J. R., & Rennie, D. A. (1975). Lead-210 Assay in Soil and Plant Material Using Cerenkov Radiation. *Canadian Journal of Soil Science*, *55*(4), 407–413. https://doi.org/10.4141/cjss75-048

Kersting, A. B., Efurd, D. W., Finnegan, D. L., Rokop, D. J., Smith, D. K., & Thompson, J. L. (1999). Migration of plutonium in ground water at the Nevada Test Site. *Nature*, *397*(6714), 56–59. https://doi.org/10.1038/16231

Kiss, J. J., Jong, E., & Martz, L. W. (1988). The Distribution of Fallout Cesium-137 in Southern Saskatchewan, Canada. *Journal of Environmental Quality*, *17*(3), 445–452. https://doi.org/10.2134/jeq1988.00472425001700030017x

Klimchouk, A. B., Ford, D. C., Palmer, A. N., & Dreybrodt, W. (2000). Speleogenesis: Evolution of Karst Aquifers. *Journal of Hydrology*, 240(1), 527.

Koarashi, J., Nishimura, S., Atarashi-Andoh, M., Muto, K., & Matsunaga, T. (2019). A new perspective on the ^{137}Cs retention mechanism in surface soils during the early stage after the Fukushima nuclear accident. *Scientific Reports*, *9*(1), 7034. https://doi.org/10.1038/s41598-019-43499-7

Krásný, J., & Sharp, J. M. (Eds.). (2007). *Groundwater in fractured rocks: Selected papers from the Groundwater in Fractured Rocks International Conference, Prague, 2003*. Taylor & Francis.

Kresic, N. (2013). *Water in Karst: Management, Vulnerability, and Restoration.* McGraw-Hill.

Krupp, K., Baskaran, M., & Brownlee, S. J. (2017). Radon emanation coefficients of several minerals: How they vary with physical and mineralogical properties. *American Mineralogist*, *102*(7), 1375–1383. https://doi.org/10.2138/am-2017-6017

Lapcevic, P. A., Novakowski, K. S., & Sudicky, E. A. (2017). Groundwater flow and solute transport in fractured media (3rd ed.). In J. H. Cushman & D. M. Tartakovsky (Eds.), *The Handbook of Groundwater Engineering*. CRC Press.

Levison, J. K., & Novakowski, K. S. (2012). Rapid transport from the surface to wells in fractured rock: A unique infiltration tracer experiment. *Journal of Contaminant Hydrology*, *131*(1–4), 29–38. https://doi.org/10.1016/j.jconhyd.2012.01.001

Lewis, D. M. (1977). The use of ^{210}Pb as a heavy metal tracer in the Susquehanna River system. *Geochimica et Cosmochimica Acta*, *41*(11), 1557–1564. https://doi.org/10.1016/0016-7037(77)90167-3

Machiwal, D., Jha, M. K., Singh, V. P., & Mohan, C. (2018). Assessment and mapping of groundwater vulnerability to pollution: Current status and challenges. *Earth-Science Reviews*, *185*, 901–927. https://doi.org/10.1016/j.earscirev.2018.08.009

Malard, F., Reygrobellet, J., & Soulié, M. (1994). Transport and Retention of Fecal Bacteria at Sewage-Polluted Fractured Rock Sites. *Journal of Environmental Quality*, *23*(6), 1352–1363. https://doi.org/10.2134/jeq1994.00472425002300060032x

Malmqvist, L., Isaksson, M., & Kristiansson, K. (1989). Radon migration through soil and bedrock. *Geoexploration*, 26(1), 135-144.

Manolopoulou, M., Stoulos, St., Mironaki, D., & Papastefanou, C. (2003). A new technique for the accurate measurement of ^{226}Ra by gamma spectroscopy in voluminous samples. *Nuclear Instruments and Methods in Physics Research Section A: Accelerators, Spectrometers, Detectors and Associated Equipment*, *508*(3), 362–366. https://doi.org/10.1016/S0168-9002(03)01701-7

Massei, N., Lacroix, M., Wang, H. Q., Mahler, B. J., & Dupont, J. P. (2002). Transport of suspended solids from a karstic to an alluvial aquifer: The role of the karst/alluvium interface. *Journal of Hydrology*, *260*(1–4), 88–101. https://doi.org/10.1016/S0022-1694(01)00608-4

McCormack, R. & Therrien, R. (2014.) *Canada's Groundwater Resources: St. Lawrence Lowlands Region – Chapter 13.* (A. Rivera, Ed.). Fitzhenry & Whiteside Ltd

Mizugaki, S., Nakamura, F., & Araya, T. (2006). Using dendrogeomorphology and ^{137}Cs and ^{210}Pb radiochronology to estimate recent changes in sedimentation rates in Kushiro Mire, Northern Japan, resulting from land use change and river channelization. *CATENA*, *68*(1), 25–40. https://doi.org/10.1016/j.catena.2006.03.014

Mudarra, M., Andreo, B., Marín, A. I., Vadillo, I., & Barberá, J. A. (2014). Combined use of natural and artificial tracers to determine the hydrogeological functioning of a karst aquifer: The Villanueva del Rosario system (Andalusia, southern Spain). *Hydrogeology Journal*, *22*(5), 1027–1039. https://doi.org/10.1007/s10040-014-1117-1

Neuman, S. P. (2005). Trends, prospects and challenges in quantifying flow and transport through fractured rocks. *Hydrogeology Journal*, *13*(1), 124–147. https://doi.org/10.1007/s10040-004-0397-2

Nisti, M. B., Santos, A. J. G., Pecequilo, B. R. S., Máduar, M. F., Alencar, M. M., & Moreira, S. R. D. (2009). Fast methodology for time counting optimization in gamma-ray spectrometry based on preset minimum detectable amounts. *Journal of Radioanalytical and Nuclear Chemistry*, *281*(2), 283–286. https://doi.org/10.1007/s10967-009-0102-y

Ontario Geological Survey. (2010). *Surficial geology of southern Ontario*. Ontario Geological Survey, Miscellaneous Release—Data 128 – Revised.

Ohtsuka, Y., Takebe, S., Yamamoto, T., & Wadachi, Y. (1988). Migration Behavior of Radionuclides (^{60}Co, ^{85}Sr and ^{137}Cs) in Aquifer. *Journal of Nuclear Science and Technology*, *25*(2), 165–168. https://doi.org/10.1080/18811248.1988.9733572

O'Shaughnessy, V. & Garga, V. K. (1994). The hydrogeological and contaminant-transport properties of fractured Champlain Sea clay in Eastern Ontario. Part 1. Hydrogeological properties. *Canadian Geotechnical Journal*, 31(6): 885-901.

Patricio, M. L. V., & Bonotto, D. M. (2021). Natural radium isotopes in waters determined with gamma-ray spectrometry using a HPGe detector. *Journal of Radioanalytical and Nuclear Chemistry*, *327*(1), 403–416. https://doi.org/10.1007/s10967-020-07517-7

Penrose, W. R., Polzer, W. L., Essington, E. H., Nelson, D. M., & Orlandini, K. A. (1990). Mobility of plutonium and americium through a shallow aquifer in a semiarid region. *Environmental Science & Technology*, *24*(2), 228–234. https://doi.org/10.1021/es00072a012

Personne, J. C., Poty, F., Vaute, L., & Drogue, C. (1998). Survival, transport and dissemination of Escherichia coli and enterococcci in a fissured environment. Study of a flood in a karstic aquifer. *Journal of Applied Microbiology*, *84*(3), 431–438. https://doi.org/10.1046/j.1365-2672.1998.00366.x

Pirson, S. J. (1953). Performance of Fractured Oil Reservoirs. *Bulletin of the American Association of Petroleum Geologists*, 37(2): 232-244.

Plummer, L. N., Vacher, H. L., Mackenzie, F. T., Bricker, O. P., & Land, L. S. (1976). Hydrogeochemistry of Bermuda: A case history of ground-water diagenesis of biocalcarenites. *Geological Society of America Bulletin*, *87*(9), 1301. https://doi.org/10.1130/0016-7606(1976)87<1301:HOBACH>2.0.CO;2

Putyrskaya, V., Klemt, E., Röllin, S., Astner, M., & Sahli, H. (2015). Dating of sediments from four Swiss prealpine lakes with 210 Pb determined by gamma-spectrometry: Progress and problems. *Journal of Environmental Radioactivity*, *145*, 78–94. https://doi.org/10.1016/j.jenvrad.2015.03.028

Putyrskaya, V., Klemt, E., Röllin, S., Corcho-Alvarado, J. A., & Sahli, H. (2020). Dating of recent sediments from Lago Maggiore and Lago di Lugano (Switzerland/Italy) using 137Cs and 210Pb. *Journal of Environmental Radioactivity*, *212*, 106135. https://doi.org/10.1016/j.jenvrad.2019.106135

Quigley, R. M., Gwyn, Q. H. J., White, O. L., Rowe, R. K., Haynes, J. E., & Bohdanowicz, A. (1983). Leda clay from deep boreholes at Hawkesbury, Ontario. Part I: Geology and geotechnique. *Canadian Geotechnical Journal*, *20*(2), 288–298. https://doi.org/10.1139/t83-032

Ravbar, N., Engelhardt, I., & Goldscheider, N. (2011). Anomalous behaviour of specific electrical conductivity at a karst spring induced by variable catchment boundaries: The case of the Podstenjšek spring, Slovenia. *Hydrological Processes*, *25*(13), 2130–2140. https://doi.org/10.1002/hyp.7966

Ritchie, J. C., & McHenry, J. R. (1990). Application of Radioactive Fallout Cesium-137 for Measuring Soil Erosion and Sediment Accumulation Rates and Patterns: A Review. *Journal of Environmental Quality*, *19*(2), 215–233. https://doi.org/10.2134/jeq1990.00472425001900020006x

Ritchie, J. C., McHenry, R. J., & Gill, A. C. (1973). Dating Recent Reservoir Sediments. *Limnology and Oceanography*, *18*(2), 254–263. https://doi.org/10.4319/lo.1973.18.2.0254

Rossi, P., Dorfliger, N., Kennedy, K., Muller, I., & Aragno, M. (1998). Bacteriophages as surface and ground water tracers. *Hydrology and Earth System Seciences*, 2(1): 101-110.

Rumynin, V. G., & Nikulenkov, A. M. (2016). Geological and physicochemical controls of the spatial distribution of partition coefficients for radionuclides (Sr-90, Cs-137, Co-60, Pu-239,240 and Am-241) at a site of nuclear reactors and radioactive waste disposal (St. Petersburg region, Russian Federation). *Journal of Environmental Radioactivity*, *162–163*, 205–218. https://doi.org/10.1016/j.jenvrad.2016.05.030

Saiers, J. E., & Hornberger, G. M. (1996). The Role of Colloidal Kaolinite in the Transport of Cesium through Laboratory Sand Columns. *Water Resources Research*, *32*(1), 33–41. https://doi.org/10.1029/95WR03096

Sanford, B. V. (1993). Sedimentary cover of the craton in Canada: St. Lawrence Platform - Chapters 10 & 11. In D.F Stott and J.D. Aitken JD (Eds.), *Geological Survey of Canada*, 5(1), 709-722.

Sankar, M., Green, S. M., Mishra, P. K., Snoalv, J. T. C., Sharma, N. K., Karthikeyan, K., Somasundaram, J., Kadam, D. M., Dinesh, D., Kumar, S., & Kasthuri Thilagam, V. (2018). Nationwide Soil Erosion Assessment in India Using Radioisotope Tracers ^{137}Cs and ^{210}Pb: The Need for Fallout Mapping. *Current Science*, *115*(3), 388. https://doi.org/10.18520/cs/v115/i3/388-390

Schelske, C. L., Peplow, A., Brenner, M., & Spencer, C. N. (1994). Low-background gamma counting: Applications for ^{210}Pb dating of sediments. *Journal of Paleolimnology*, *10*(2), 115–128. https://doi.org/10.1007/BF00682508

Sidle, W. (2009). Vulnerability of headwater catchment resources to incidences of ^{210}Pb excess and ^{137}Cs radionuclide fallout. *Environmental Geology*, *57*(2), 377–388. https://doi.org/10.1007/s00254-008-1306-0.

Singer, S. N., Cheng, C.K., & Scafe, M.G. (2003). The Hydrogeology of Southern Ontario 2nd Edition. *Ontario Ministry of the Environment*, 213.

Singhal, B. B. S., & Gupta, R. P. (2010). *Applied Hydrogeology of Fractured Rocks*. Springer Netherlands. https://doi.org/10.1007/978-90-481-8799-7

Smith, P. A., & Degueldre, C. (1993). Colloid-facilitated transport of radionuclides through fractured media. *Journal of Contaminant Hydrology*, *13*(1–4), 143–166. https://doi.org/10.1016/0169-7722(93)90055-W

Skeppström, K., & Olofsson, B. (2007). *Uranium and radon in groundwater—An overview of the problem*. 12.

Somogyi, G. & Lenart, L. (1986). Time-integrated radon measurements in spring and well waters by track technique. *International Journal of Radiation and Applied Instruments*, Part D, 12(1-6), 731-734.

Spezzano, P., Bortoluzzi, S., Giacomelli, R., & Massironi, L. (1994). Seasonal variations of ^{137}Cs activities in the Dora Baltea River (Northwest Italy) after the chernobyl accident. *Journal of Environmental Radioactivity*, *22*(1), 77–88. https://doi.org/10.1016/0265-931X(94)90037-X

Streltsova, T, D. (1976). Hydrodynamics of Groundwater Flow in a Fractured Formation. *Water Resources Research*, 12(3): 405-414.

Sudicky, E. A., & Frind, E. O. (1982). Contaminant transport in fractured porous media: Analytical solutions for a system of parallel fractures. *Water Resources Research*, *18*(6), 1634–1642. https://doi.org/10.1029/WR018i006p01634

Szabó, K. Z., Udvardi, B., Horváth, Á., Bakacsi, Z., Pásztor, L., Szabó, J., Laczkó, L., & Szabó, C. (2012). Cesium-137 concentration of soils in Pest County, Hungary. *Journal of Environmental Radioactivity*, *110*, 38–45. https://doi.org/10.1016/j.jenvrad.2012.01.023

Tang, X. & Weisbrod, N. (2010). Dissovled and Colloidal Transport of Cesium in Natural Discrete Fractures. Journal of Environmental Quality, 39(1): 1066-1076.

Tanner, A. B. (1980). Radon Migration in the Ground: A Supplementary Review. In Gesell, T.F. and Lowder, W.M., (Eds.), *The Natural Radiation Environment III*, National Technical Information Services. United States Department of Energy.

Tran, E. L., Teutsch, N., Klein-BenDavid, O., & Weisbrod, N. (2018). Uranium and Cesium sorption to bentonite colloids under carbonate-rich environments: Implications for radionuclide transport. *Science of The Total Environment*, *643*, 260–269. https://doi.org/10.1016/j.scitotenv.2018.06.162

Turner, N. B., Ryan, J. N., & Saiers, J. E. (2006). Effect of desorption kinetics on colloid-facilitated transport of contaminants: Cesium, strontium, and illite colloids: Cesium and Strontium Colloid-facilitated transport. *Water Resources Research*, *42*(12). https://doi.org/10.1029/2006WR004972

van Beynen, P. E., Niedzielski, M. A., Bialkowska-Jelinska, E., Alsharif, K., & Matusick, J. (2012). Comparative study of specific groundwater vulnerability of a karst aquifer in central Florida. *Applied Geography*, *32*(2), 868–877. https://doi.org/10.1016/j.apgeog.2011.09.005

Vesper, D. J., Loop, C. M., & White, W. B. (2013). Contaminant transport in karst aquifers. *Theoretical and Applied Karstology,* 13(14): 101-111.

Vilks, P., & Baik, M.-H. (2001). Laboratory migration experiments with radionuclides and natural colloids in a granite fracture. *Journal of Contaminant Hydrology*, *47*(2–4), 197–210. https://doi.org/10.1016/S0169-7722(00)00149-2

Wallbrink, P. J., & Murray, A. S. (1993). Use of fallout radionuclides as indicators of erosion processes. *Hydrological Processes*, *7*(3), 297–304. https://doi.org/10.1002/hyp.3360070307

Walling, D. E., & He, Q. (1999). Using Fallout Lead-210 Measurements to Estimate Soil Erosion on Cultivated Land. *Soil Science Society of America Journal*, *63*(5), 1404–1412. https://doi.org/10.2136/sssaj1999.6351404x

White, W. B. (2017). Groundwater Flow in Karstic Aquifers (3rd ed.). In J. H. Cushman & D. M. Tartakovsky (Eds.), *The Handbook in Groundwater Engineering*. CRC Press.

Wood, W. W., Kraemer, T. F., & Shapiro, A. (2004). Radon (^{222}Rn) in Ground Water of Fractured Rocks: A Diffusion/Ion Exchange Model. *Groundwater*, 42(4), 552-567.

Yan, D., Zhang, X., Wen, A., He, X., & Long, Y. (2012). Assessment of sediment yield in a small karst catchment by using ^{137}Cs tracer technique. *International Journal of Sediment Research*, *27*(4), 547–554. https://doi.org/10.1016/S1001-6279(13)60012-8

Zapata, F., & Nguyen, M.-L. (2009). Chapter 7 Soil Erosion and Sedimentation Studies Using Environmental Radionuclides. *Radioactivity in the Environment,* 16(1): 295-322. https://doi.org/10.1016/S1569-4860(09)01607-6

Zhang, W., Tang, X., Weisbrod, N., & Guan, Z. (2012). A review of colloid transport in fractured rocks. *Journal of Mountain Science*, *9*(6), 770–787. https://doi.org/10.1007/s11629-012-2443-1

Zhang, Y., Long, Y., Yu, X., & An, J. (2014). A comparison of measured ^{137}Cs and excess ^{210}Pb levels in the cultivated brown and cinnamon soils of the Yimeng Mountain area. *Chinese Journal of Geochemistry*, *33*(2), 155–162. https://doi.org/10.1007/s11631-014-0671-5

Appendices

Appendix A: ^{137}Cs and ^{210}Pb Dataset for Suspended Sediment

Sample ID	^{137}Cs (cps)	^{210}Pb (cps)	Well Depth (m)	Overburden Thickness (m)	Deepest Unit Penetrated	Easting	Northing
18-AG-836	16	-25	23.0	5.2	Precambrian	406360	5034119
18-AG-893	2	105	33.0	18.3	Rockcliffe	416787	5034007
18-AG-684	8	-6	68.2	11.2	Verulam	421935	5017119
18-AG-752	16	-72	82.7	0.0	Bobcaygeon	404476	5016877
18-AG-776	-15	141	66.7	1.8	Precambrian	408148	5030031
18-AG-771	1	-42	13.9	2.2	Gull River	403865	5022970
19-AG-903	-20	2	53.1	3.6	Gull River	420900	5033930
19-AG-902	-18	118	45.6	1.2	Rockcliffe	420356	5034188
19-AG-901	-12	-69	38.0	3.0	Rockcliffe	421281	5033149
19-AG-898	-1	-4	75.8	0.0	Gull River	424267	5031584
19-AG-935	15	227	60.6	2.7	Gull River	422494	5034985
18-AG-706	31	-30	59.7	3.6	Gull River	420967	5006823
18-AG-674	3	16	38.8	1.0	Gull River	415887	5014318
18-AG-734	-2	45	21.2	0.9	Nepean	410344	5013953
19-AG-915	7	-43	29.7	1.5	Gull River	424674	5034052
19-AG-897	-5	-51	18.2	0.3	Gull River	423696	5035184
19-AG-971	10	103	16.3	0.6	Gull River	420639	5035900
19-AG-891	-36	132	40.3	0.9	Gull River	418963	5036284
19-AG-986	-9	4	43.7	0.6	Gull River	490603	5044940
19-AG-987	-18	181	44.2	0.0	Lindsay	496261	504907
19-AG-988	-16	96	64.3	0.9	Lindsay	496124	5045110
19-AG-990	12	113	32.7	0.0	Lindsay	496113	5044972
19-AG-991	42	131	36.2	2.1	Lindsay	497364	5044605
19-AG-992	17	123	90.9	0.3	Lindsay	495629	5045220

Appendix B: ^{137}Cs and ^{210}Pb Dataset for Surface Soils and Well-bottom Sediment

Sample ID	^{137}Cs (cps/g)	^{210}Pb (cps/g)	Well Depth (m)	Overburden Thickness (m)	Deepest Unit Penetrated	Easting	Northing
Surface Soil Sediment							
SS1	183	407	-	-	-	425175	5032697
SS2	110	207	-	-	-	422235	5035993
SS3	123	347	-	-	-	404861	5038167
SS4	236	502	-	-	-	409965	5013069
SS5	125	345	-	-	-	423459	5021220
SS6	102	196	-	-	-	426815	5011356
SS7	181	331	-	-	-	497481	5044553
SS8	377	665	-	-	-	495936	5045373
SS9	363	895	-	-	-	496087	5044733
Well-bottom Sediment							
19-AG-999	10	138	44.8	16.8	Oxford	419883	5030195
19-AG-868	14	-36	66.4	13.4	Gull River	408168	5040370
18-AG-837	-7	1029	26.2	12.2	Gull River	404057	5038466
18-AG-836	19	735	23.2	5.2	Precambrian	406360	5034119
19-AG-880	-2	244	51.8	36.6	Bobcaygeon	415652	5036510
18-AG-826	11	832	32.0	9.1	Precambrian	405914	5032400
18-AG-831	3	56	31.1	17.1	Oxford	404854	5036443
18-AG-752	-4	0	83.2	0.0	Bobcaygeon	404476	5016877
19-AG-905	-21	171	30.5	25.9	Oxford	416598	5032161
18-AG-682	35	-2	24.4	7.3	Verulam	421177	5016882
19-AG-987	-12	414	44.5	0.0	Lindsay	496261	5044907
19-AG-990	18	260	32.9	0.0	Lindsay	496113	5044972
19-AG-986	-3	29	43.9	0.6	Gull River	496603	5044940
19-AG-898	-31	19	76.2	0.0	Gull River	424267	5031584
18-AG-764	12	1324	36.0	1.2	Precambrian	411626	5027808
19-AG-903	-6	-15	53.4	3.7	Gull River	420900	5033930